

National technical University of Athens
School of Civil Engineering
Department of Structural Engineering
Institute of Structural Analysis & Antiseismic Research



SIMULATION OF HUMAN AORTA AND ISOGEOMETRIC FLUID ANALYSIS



ELENI MICHAEL

SUPERVISORS

Minolis Papadtrakakis - Professor NTUA
Panagiotis Karakitsios - PhD Candidate NTUA

Acknowledgements

I would like to thank everyone that help me reach this point. First of all, I would like to thank Professor Manolis Papadrakakis for giving me the opportunity to work on such an interesting topic, the one of the combination of Isogeometric Analysis and Bioengineering. Also, I can't leave out the contribution of PhD Candidate Panagiotis Karakitsios in all stages of this thesis. Also, I wish to thank the doctors at the hospital "Hygeia", who gave me valuable advices. Last but not least, I would like to thank my parents for giving me the opportunity to study, but also for the constant guidance.

Ευχαριστίες

Θα ήθελα να ευχαριστήσω όλους όσους με βοήθησαν να φτάσω σε αυτό το σημείο. Πρώτα απ' όλα, θα ήθελα να ευχαριστήσω τον καθηγητή Μανώλη Παπαδρακάκη που μου έδωσε την ευκαιρία να δουλέψω πάνω σε αυτό το τόσο ενδιαφέρον θέμα, αυτό του συνδυασμού της Ισογεωμετρικής Ανάλυσης και της Εμβιομηχανικής. Ακόμα, δε μπορώ να παραλείψω τη συμβολή του υποψήφιου διδάκτορα Παναγιώτη Καρακίτσιου σε όλα τα στάδια αυτής της εργασίας. Επίσης, θέλω να ευχαριστήσω τους γιατρούς στο νοσοκομείο «Υγεία» που μου έδωσαν πολύτιμες συμβουλές. Τέλος, θα ήθελα να ευχαριστήσω τους γονείς μου που μου έδωσαν την ευκαιρία να σπουδάσω, αλλά και για τη συνεχή καθοδήγησή τους.

Abstract

The scope of this thesis is the investigation of aneurysms in thoracic and abdominal aorta with the help of Isogeometric Analysis. This method was chosen, as it is innovative, integrates CAD/ CAE and describes complex geometries with zero geometrical error. Heart disease (including aneurysms) is one of the leading causes of death in the world, especially in USA. Aneurysms in particular are very dangerous as they are asymptomatic and in high risk of rupture. The routines, which have been used for the analysis of the presented applications, were developed in the high-level language and interactive environment “MATLAB”, which can produce an exact geometry model of the patient’s aorta, analyze it and compute the values of flow’s velocity and pressure at every point.

Σύνοψη

Στόχος της παρούσας διπλωματικής είναι η μελέτη των ανευρυσμάτων στην θωρακική και κοιλιακή αορτή με τη βοήθεια της Ισογεωμετρικής Ανάλυσης. Αυτή η μέθοδος επιλέχθηκε, επειδή είναι καινοτόμος, ενώνει τις τεχνολογίες CAD/ CAE και περιγράφει πολύπλοκες γεωμετρίες με μηδενικό γεωμετρικό σφάλμα. Οι καρδιακές παθήσεις (συμπεριλαμβανομένων και των ανευρυσμάτων) είναι μία από τις κύριες αιτίες θανάτων στον κόσμο, ειδικά στις ΗΠΑ. Τα ανευρύσματα συγκεκριμένα είναι πολύ επικίνδυνα λόγω της ασυμπτωματικής τους φύσης και του υψηλού κινδύνου ρήξης. Οι ρουτίνες, οι οποίες χρησιμοποιήθηκαν για την ανάλυση των εφαρμογών, αναπτύχθηκαν στην υψηλού επιπέδου γλώσσα προγραμματισμού και το διαδραστικό περιβάλλον “MATLAB”, οι οποίες μπορούν να παράγουν ακριβές γεωμετρικό μοντέλο της αορτής του ασθενούς, να το αναλύουν και να υπολογίζουν τις τιμές της ταχύτητας ροής και της πίεσης σε κάθε σημείο.

Prologue

The last two years were very interesting. I was called to work on the challenging and intriguing topic of Bioengineering with Isogeometric Analysis. Challenging, as there were so many parameters to consider, not only for the bio part but for the engineering too. Intriguing, as this is a serious health issue that troubles many people, but also made me think that civil engineering and everything that I learned the last five years don't necessarily apply only on buildings and constructions.

Through this dissertation I hope to eliminate the number of deaths caused by unexpected ruptures of aneurysms. With the application of isogeometric analysis the idea of finding a way to prevent this is finally close to become real. Advanced computational methods hold the answer to many of our everyday problems and it is our duty, as tomorrow's scientists to take advantage of them.

Even at this difficult time for Greece, National Technical University of Athens, and especially the Institute of Structural Analysis and Antiseismic Research at School of Civil Engineering, gives the opportunity to its students to broaden their minds and the hope that we can reborn from this economic crisis and become even better.

Michael Eleni

Athens, July 2015

Table of Contents

Acknowledgements	i
Abstract	iii
Prologue	v
Table of Contents	vii
1. The concept of Isogeometric Analysis.....	11
1.1 Finite Element Method	11
1.1.1 Historical Overview	11
1.1.2 Basic Idea of Finite Element Method.....	16
1.1.3 Drawbacks.....	17
1.2 Computer Aided Design	20
1.2.1 Historical Overview	20
1.3 Isogeometric Analysis.....	23
2. Basic Ingredients of Isogeometric Analysis.....	25
2.1 Introduction.....	25
2.2 Index, Parameter and Physical Space	26
2.2.1 Index Space	27
2.2.2 Parameter Space	28
2.2.3 Physical Space.....	29
2.3 B-SPLine Geometries	30
2.3.1 B-SPLine Basis Functions.....	30
2.3.2 Knot Value Vector as Boundary of Basis Functions Support	31
2.3.3 Control Points as the Center of the Support	32
2.3.4 Full Tensor Product as a characteristic of B-SPLine Basis Functions ...	32
2.3.5 B-SPLine Basis Function Properties	33
2.3.6 B-SPLine Basis Function Derivatives.....	52
2.3.7 B-SPLine Curves, Surfaces and Solids	53
2.3.8 B-SPLine Curve Properties	54

2.4	Non-Uniform Rational B-SPLines.....	67
2.4.1	Basic Idea.....	67
2.4.2	NURBS Shape Functions.....	68
2.4.3	NURBS Shape Function Derivatives.....	69
2.4.4	NURBS Entities.....	70
2.4.5	NURBS Examples.....	71
2.5	Patches.....	75
3.	Fluid Analysis.....	77
3.1	CFD-Computational Fluid Dynamics.....	77
3.1.1	Introduction to CFD.....	77
3.1.2	Comparison with EFD.....	77
3.1.3	CFD Analysis Process.....	78
3.1.4	Applications of CFD.....	79
3.2	Navier Stokes Equations.....	81
4.	Geomiso Bio.....	87
4.1	Introduction.....	87
4.2	Element Types.....	89
4.3	Piola Transformation.....	91
4.4	Stiffness Matrix.....	93
4.5	Parameterization.....	97
4.5.1	Introduction.....	97
4.6	External Load.....	104
4.7	Boundary Conditions.....	106
5.	Human Circulatory System.....	107
5.1	Real geometry of aorta.....	107
5.1.1	Thoracic aorta.....	107
5.1.2	Abdominal Aorta.....	110
5.2	Aneurysms.....	111
5.3	Medical Imaging.....	114
5.3.1	Axial Tomography.....	115
5.3.2	Magnetic Tomography.....	118
5.3.3	Geomiso Bio.....	119

5.4	Constitutive Law	121
5.4.1	Introduction	121
5.4.2	Aortic wall.....	122
5.4.3	Blood Properties	126
6.	Applications	129
6.1	Bent Pipe.....	129
6.2	Annulus.....	133
Appendix	151
References	157

1. The concept of Isogeometric Analysis

1.1 Finite Element Method

1.1.1 Historical Overview

Isogeometric Analysis as a historic evolutionary computational mechanics achievement

Isogeometric Analysis is an innovative method, which integrates design and analysis in the greatest scale ever achieved. It was conceived by Thomas J.R. Hughes in 2003, Professor of Aerospace Engineering and Engineering Mechanics of the University of Texas at Austin.

Thomas J.R. Hughes is one of the greatest experts worldwide in Computational and Applied Mathematics. He began his career as a mechanical design engineer at Grumman Aerospace and then went on to General Dynamics as a research and development engineer. After receiving his Ph.D. from the University of California at Berkley, he joined the faculty and moved on to California Institute of Technology. Afterwards, he was hired by Stanford University before joining The University of Texas at Austin.



Figure 1.1
Thomas Joseph Robert Hughes.
(<http://users.ices.utexas.edu/~hughes/>)

Isogeometric Analysis is set to bridge the gap that exists between Computer-Aided Design and Computer-Aided Engineering. Thomas J.R. Hughes published a book in 2009, along with J.A. Cottrell and Y. Bazilevs, explaining the fundamentals of this new method. The book, “Isogeometric Analysis: Towards Integration of CAD and FEA” is the first book to be issued on this new field of study and a trustworthy guide to the researchers that want to invest in this method. It contains a vast number of applications of Isogeometric Analysis, potential resources for the new researcher, advantages of the new method and future fields of study. The application of Isogeometric Methods can lead to results and improvements in computational mechanics, structural statics and dynamics and biomechanics.

The need for Isogeometric Analysis

The compelling need for a new method had to be met; greater challenges in Finite Element Analysis were arising every day, demanding faster and more precise results. Even nowadays, although structures worldwide are designed using Finite Element Method instead of the traditional by-hand ways, design errors cannot be avoided. Since 2000, structural collapse cost humanity over 1500 lives; many of them could have been spared, had the engineer a more accurate tool for analysis and design. Unfortunately, present analysis technologies require a lot of man-hours for manual generation of approximated, FEM-suitable geometries and consequently they derive the engineer from his main task and force him to devote less time in result evaluation. The risk is even greater, considering the mistakes the engineer can make during this transformation. Furthermore, the approximation of the geometry sometimes is clearly not enough for the desired convergence. These are the gaps that Isogeometric Analysis is set to fill. In order to fully understand Isogeometric Analysis, one has to acknowledge the evolution of Analysis throughout its history and understand the principles this revolutionary method is based on. This introduction provides the historical review of the technologies and the requirements of structural analysis that led to the creation of this new method.

Before Finite Element Method

Engineers of the past had to meet the demands for structural analysis and representation of accurate results. Construction always needed the cost-efficiency provided by design. In the early years, the only weapon the engineer possessed was his mind. In order to solve a statically indeterminate structure, Equilibrium, Constitutive and Compatibility Laws had to be applied. Several methods existed in order to solve the problem.

The Force Method used the Betti-Maxwell Theorem in combination with virtual works in order to provide support forces and moments. The main idea is the preservation of Equilibrium and calculation of forces, in order to ensure Compatibility.

The Displacement Method, on the other hand, ensures Compatibility is maintained and Equilibrium is achieved via calculation of displacements.

The Moment Distribution Method, also known as the Cross Method, relies upon computational iteration cycles to an initial moment distribution, until the desired approximation is achieved. It only yields results for bending effects and ignores axial and shear tension, but its efficiency made it very popular among the engineers in the 1930s.

These methods had their limits; a vast amount of time was required for the solution and many errors would occur in the manual computational process. More complex problems could only be approximated and sometimes analysts had to solve differential equations by hand in order to obtain the solution.

Finite Element Method

Structural Analysis has been a major part of the engineering field of practice. The knowledge of a structure's reaction to certain loads enhances its safety and makes it cost-effective. It has a wide field of application, including buildings, bridges, airplanes, space shuttles, ships, satellites, nuclear stations and much more. At first, engineers used methods obtained from the solution of differential equations in order to evaluate the stress, strain and displacement conditions of the structure. Structural mechanics theorems were developed and used in order to solve the computational problem. These served their purpose well for relatively simple, everyday linear problems. However, new technologies emerged and the constant demand for faster, more accurate solutions to complicated problems had to be met.

Early computer models had made their appearance and engineering scientists were eager to use them in their problems. The birth of Finite Element Methods can be placed at the late stages of World War II. Structural Engineers working for the Royal Aeronautical Society of London had to design an innovative type of combat jet aircraft whose speed required swept-back wings. Unfortunately, none of the existing theories could fit to solve such a complex problem. The failure of the German ME262 was palpable proof of that matter.

This challenging task was assigned to one of the brightest minds of the Royal Aeronautical Society of London, John Argyris. Argyris was born in Greece, Volos in 1913 and had studied Civil Engineering at National Technical University of Athens.



Figure 1.2
John Argyris.
(<http://www.nae.edu/27953.aspx>)



Figure 1.3
City of Volos. Central Greece. John Argyris Birthplace.
(<http://www.greekscapes.gr/~landscapesatlas>)

John Argyris graduated from Technical University of Munich in 1936 and had begun to work in industrial applications of complex structures. He remained in Germany at the beginning of World War II and was accused of giving research info to the Allies, arrested and sent to a concentration camp when the Axis invaded Greece. He was rescued by a German Admiral, Kanaris, who was of Greek ancestry as well. After breaking out from the concentration camp, Argyris escaped to Switzerland by swimming through the Rhine river, in the middle of a raid holding his passport with his teeth. He finished his Doctoral Degree in Aeronautics from ETH, Zurich in 1942. Afterwards he moved to England and was engaged with the Royal Aeronautical Society of London, working as a technical officer. As a researcher, he was really skeptical with Cartesian coordinate systems and the way they were used in engineering. He believed that triangular and tetrahedral elements were far more suitable for engineering applications. John Argyris was not devoted to everyday problems, but would rather get busy with difficult, apparently unsolvable problems. His superiors quickly recognized this trait and he in return welcomed the challenges he was given, including the swept-back wings aircraft problem.

It seems he was the right man for the job. In August 1943, after 3 days and nights of devotion to the problem, he had a breakthrough. He used triangular elements to simulate the swept-back wings and solved the model in the electro-mechanical computing device the Society had recently acquired. The device was able to solve an equation with up to 64 unknowns. Analysis results were very close to the experimental results, with a deviation of approximately 8 %. This was the birth of the Finite Element Method (FEM). All relative papers were at once labeled “secret”. This innovative method included a different measurement of stresses and strains, diverging from the classical Cartesian field and was proving to be useful and easily generalized.

In the following years, the “Matrix Force and Displacement Method”, mostly known as “Finite Element Method” (or, as Ray Clough wrote in 1960, “The Argyris Method”) was developed by many researchers, including Turner, Clough, Zienkiewicz and Cheung. Argyris resumed his academic career with drastic contributions to the research and development of Finite Element Method as well as many other aspects of the Engineering field until he was 88 years old. He invented, among others, the triangular element TRIC and is also well known for the contribution to the solution of the heat protection problem for the NASA space shuttle during the entrance in the atmosphere. He passed away in April 2004.

Due to the swift evolution of computational speed and memory capacity, FEM became very popular within the engineering industry. Millions of dollars were invested in its development. New FEM technologies emerged, such as the isoparametric elements. These allowed for a more general approach and a better adaptation to complex geometries.

NTUA Professor Papadakis Manolis has devoted his career in the evolution and outspread of FEM technologies. Nowadays, in the middle of the financial crisis in Greece, NTUA's Institute of Structural Analysis and Antiseismic Research has a remarkable research portfolio to show, always being up to date with the latest technological trends. Bright young minds are given a chance to shine, in National Technical University of Athens, continuing and improving the cycle of expanding the boundaries of human knowledge.

In the dawn of 2000, the structural engineering field has changed drastically. Personal computers and a variety of FEM software are now available to engineers. All the hard work done so many years ago by hand is now avoided. Greater speeds and bigger rates of convergence are achieved every other month. Problems once thought to remain unsolved now seem common and relatively easy. Finite Elements are used in a wide range of computational analysis, such as structural and dynamic analysis, fluid mechanics, biomechanics, earthquake engineering and many more. The modern engineer does not need to solve complex mathematical equations by hand, but has to pursue a global and thorough understanding of his field of study as well as knowledge of the innovative computational methods.

The engineering software market consists of many products devoted to the analysis of FEM models. There are generalized and more theoretical software that can solve almost any type of structure. NASTRAN, a widely used FEM platform, was originally developed by NASA in the 1960s in order to cover the Agency's special needs. Simulia Abaqus, originally released in 1978, was developed using an open-source language, Python and was initially intended for non-linear problems. It is particularly popular due to its wide range of Modeling capabilities, both for linear and non-linear problems. ADINA (Automatic Dynamic Incremental Non-Linear Analysis) , first developed in 1974, is used in a wide range of non-linear problems. It has applications in static and dynamic analysis, heat transfer, compressible and incompressible flows and electromagnetic phenomena. FEMAP (Finite Element Modeling and Post-processing) is used as an input creation and output processing tool for the engineers. It cooperates with the solver routines from other platforms (e.g. NASTRAN) and focuses on the easy and accurate communication between software and user.

Specialized software is also available in the engineering market. The specific characteristics and complexity of today's structures require a more personal and delicate approach. ATENA, standing for Advanced Tool for Engineering Non-Linear Analysis, is specialized in everything to do with reinforced concrete structures. SOFiSTIK, first used in 1987, is directed towards bridge linear and non-linear analysis. Furthermore, there are platforms dedicated to the special needs of the Greek market. Designing structures in the country with the biggest seismic activity in Europe is not an easy task. StereoSTATIKA is suitable for reinforced concrete analysis in countries with dangerous seismic activity. FESPA is a Greek software dedicated to analysis and design of reinforced concrete and steel buildings.

1.1.2 Basic Idea of Finite Element Method

According to Analysis of Structures with the Finite Element Method (M. Papadrakakis - Papatiriou, 2001), the Basic Idea behind Finite Element Method is the approximation of the solution field via piecewise polynomial functions, called the shape functions N . Displacement values U at any internal point of the element can be computed from displacements at nodes d :

$$\left\{ U(X, Y, Z) \right\}_{(3 \times 1)} = \left[N(X, Y, Z) \right]_{(3 \times 3n_e)} \cdot \left\{ d \right\}_{(3n_e \times 1)}$$

where n_e is the number of the finite elements.

A generalization for the whole structure leads to

$$\left\{ U^S(X, Y, Z) \right\}_{(3 \times 1)} = \left[N^S(X, Y, Z) \right]_{(3 \times 3n)} \cdot \left\{ d^S \right\}_{(3n \times 1)}$$

The problem is directly downsized from infinite unknowns to a finite number of degrees of freedom. The next step is to define stress and strain matrices and their interconnection, which represents Hooke's Constitutive Law.

$$\left\{ \sigma \right\} = \begin{bmatrix} \sigma_X \\ \sigma_Y \\ \sigma_Z \\ \sigma_{XY} \\ \sigma_{YZ} \\ \sigma_{ZX} \end{bmatrix} \quad \left\{ \varepsilon \right\} = \begin{bmatrix} \varepsilon_X \\ \varepsilon_Y \\ \varepsilon_Z \\ \gamma_{XY} \\ \gamma_{YZ} \\ \gamma_{ZX} \end{bmatrix} \quad (3D \text{ case})$$

$$\left\{ \sigma \right\} = [E] \cdot \left\{ \varepsilon \right\}$$

Deformation Matrix $[B]$ evaluates strains anywhere in the model from nodal displacements.

$$\left\{ \varepsilon(X, Y, Z) \right\} = [B(X, Y, Z)] \cdot \left\{ d \right\}$$

Using internal and external virtual work equilibrium, we can evaluate the Stiffness Matrix $[k]$ for each element

$$\left[k \right]_{(3n_e \times 3n_e)} = \int_V \left[B \right]_{(3n_e \times 6)}^T \cdot \left[E \right]_{(6 \times 6)} \cdot \left[B \right]_{(6 \times 3n_e)} dV$$

In the same manner, distributed loads can be transformed into equivalent nodal loads.

$$\underbrace{\{\mathbf{r}\}}_{(3n_e \times 1)} = \int_V \underbrace{[\mathbf{N}]}_{(3n_e \times 3)}^T \cdot \underbrace{\{\mathbf{f}\}}_{(3 \times 1)} dV$$

The contribution of each element is added to the global matrices, producing the global Stiffness Matrix $[\mathbf{K}]$ and the Force Vector $\{\mathbf{R}\}$. The Displacement Matrix can now be calculated from:

$$\underbrace{\{\mathbf{R}\}}_{(3n \times 1)} = \underbrace{[\mathbf{K}]}_{(3n \times 3n)} \cdot \underbrace{\{\mathbf{D}\}}_{(3n \times 1)}$$

where n is the number of the nodes.

We can observe that (naturally) shape functions $[\mathbf{N}]$ and deformation matrix $[\mathbf{B}]$ depend on the Cartesian coordinates. This leads to iteration problems when complex geometries (e.g. circles or conic sections in general) are involved. The solution, which contributed to the further generalization of FEM, along with a more efficient iteration algorithm, is isoparametric elements. The basic idea is the existence of a parent element in the parameter space, which can be modeled as a regular shape (e.g. a cube, square or an equilateral triangle). Each element in the physical space (the “real” modeling space) can be described using a linear combination of the parent element’s shape functions. Hence, geometry can be approximated by the same functions used for the solution field. This explains the name “isoparametric”.

1.1.3 Drawbacks

Despite the evolution of FEM all this time, some problems have yet to be solved. For one, even isoparametric elements can only produce an approximation of geometry. The most challenging tasks of the day often require exact geometrical representation in order to achieve the necessary accuracy. After the meshing has been completed, the initial geometry plays no more role in the analysis procedure. This is intuitively worrying, to begin with. Furthermore, it produces a vast number of problems. The inevitable geometrical approximation means there will be convergence errors by definition, regardless of the solution methods and the available computational power. This affects the efficiency of the computational methods used for the solution.

If a finer mesh is required, refinement algorithms will return to the initial geometry and produce a different approximation. The new, fine mesh cannot be directly produced from the coarse mesh. Efficiency is certainly at a low, as procedures already completed have to be repeated in order for the new mesh to be created. Precious analysis time is required and the geometrical differences between the coarse and fine mesh make it difficult to compare the results. Hierarchical structures provide even greater challenges. Hierarchical refinement is considered an efficient refinement technique, as it focuses on the crucial areas of the model, but it is not easily applicable in FEM meshes.

The lack of integration between geometry and mesh generation is crucial. Computational geometry provides simply an input file for the meshing of the finite element model. Exact geometrical representation is not reflected in the new mesh, nor is the smoothness of the initial model, which leads to a slightly different model that analysis solves. Even for a small change in the geometrical model, reintegration and new mesh generation is required. This process is frustrating and pointless for the modern engineer; instead of devoting his time in creativity and design, he has to undergo the mundane task of regenerating a slightly different mesh over and over again. Many design errors are attributed to this task. In structural design, a vast amount of time is spent on these integration cycles between initial, preliminary and final design phases. The risk is even greater in complex and innovative structures, where the engineers cannot know beforehand what structural results to expect and have almost no way of checking the accuracy of the analysis.

Computational geometry has evolved since its birth; new and optimized geometrical structures are being used more often nowadays. Finite Element geometries fail to keep up with that pace and as a result, Computer-Aided Engineering is separated even more from Computer-Aided Design. Finite Elements cannot cooperate with the modern technologies of T-SPLines and Subdivision Surfaces. These problems had always been present throughout the history of Finite Elements. Complicated computational methods and algorithms have been developed in order to overcome them. The problem is that the nature of FEM does not allow for significant steps toward CAD-FEM integration. Improvements to the basic structure of Finite Elements are difficult and quite inefficient.

Figure 1.4 depicts a wine glass. In order to create this object, a designer has to define the following variables:

- degree of shape functions for each parametric axis
- knot value vector for each parametric axis
- control points (Cartesian coordinates and weights).

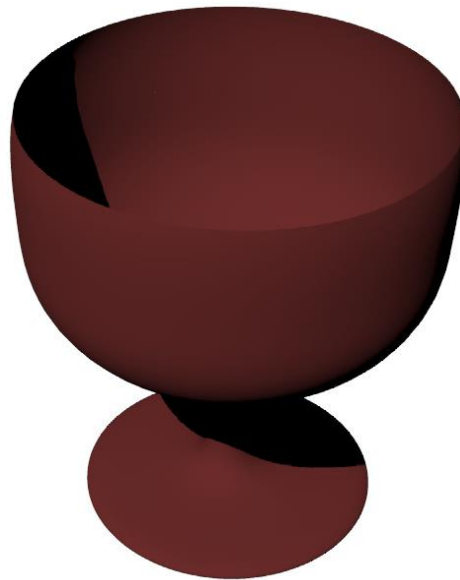


Figure 1.4
Wine glass. Geometry Design.

As a result, a mesh of finite elements is created, the “geometry mesh”, which surprisingly is not used by FEM software, which instead creates a new approximate one. Figure 1.5 represents the initial geometry mesh of the wine glass with the corresponding control net.

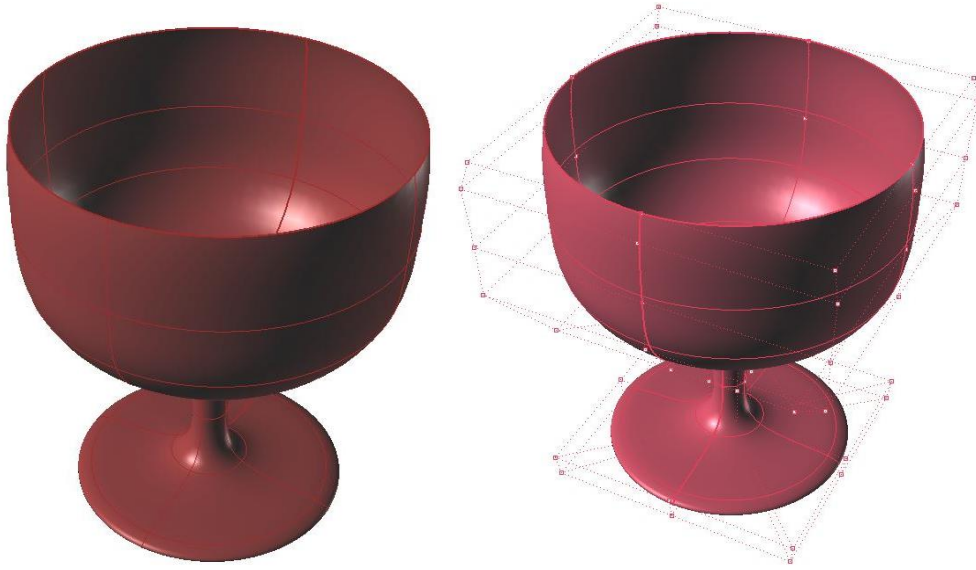


Figure 1.5
Wine glass. Geometry Initial Mesh.

With the previous initial mesh, a designer can represent exactly the wine glass, but an engineer cannot analyze it accurately and has to apply refinement in order to increase the accuracy of the solution field. Figure 1.6 shows a finer mesh of the wine glass for both cases. In FEA, the smooth surface of the cup participates only as input in FEM software and is thereafter replaced by quad finite elements. In IGA, the geometry remains intact and the mesh is the exact geometrical model.

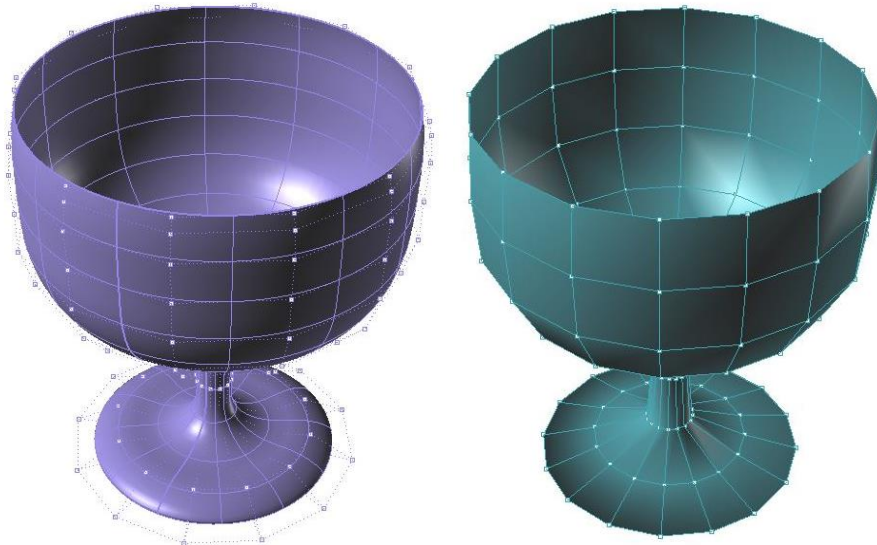


Figure 1.6.
Wine glass. Fine FEA Mesh (left one). Fine IGA Mesh.

1.2 Computer Aided Design

1.2.1 Historical Overview

Isogeometric Analysis as a historic evolutionary computational design achievement

The evolution of computing systems made the option to design on a platform very attractive. Drafts could be edited easily and data could be stored and transferred at much higher speeds. Computer Aided Design has many applications in today's world and a huge industrial support. Computer-generated imagery (CGI) is used in movies even more often; 3D and 2D cartoons are drafted and animated through computer software. Engineers draft complex designs such as cars, space shuttles, long span bridges and so on, one piece at a time in a computer. All the drafts can be edited and the escalation to optimized drafting is easier than ever. Designers' time is now being devoted to creative thinking and taking ideas to the next level, rather than useless drafting by hand for hours. However, there is still room for improvement. Computational geometry is involved in a vast number of engineering applications and should not be considered independently. Design entities are supposed to cooperate with Finite Element Methods. Reinventing and improving computational geometry structures is the first step in completing this task. In order to understand the modern and future world of Computer-Aided Design, one has to study the history, the creation and the necessities that led to the creation of computational geometry entities.

Computer Aided Design (CAD) emerged in the 1950s from the automotive, shipyard and aircraft industries. In those times, designers were able to produce accurate drafts by hand, but when ship cross sections had to be drafted in real-life size, pencils could not help anymore and things became a bit more complex. The main problem was the definition of a real-size curve, which smoothly interpolated several predetermined points in order to create the shell of the ship. This task was usually carried out in the loft of a building, due to the large amount of space needed. The loftsman, as he was called, used easy-to-bend pieces of steel or wood, the spline, in order to interpolate the points. In order to maintain the spline's shape, he usually put weights on them on certain points.



Figure 1.7
Original Splines and Weights (called Ducks).
(<http://www.boatdesign.net>)

The development of NURBS arose from the need to effectively represent freeform surfaces. Two engineers in France stood at the forefront of this approach, Pierre Bezier from Renault and Paul de Casteljaou from Citroen. Bezier's work was the first to reach publication, and soon after the CAD industry started using and enhancing Bezier curves. However, certain disadvantages of Bezier curves led to the search for more convenient forms of representation. Researchers finally introduced B-SPLines, which were similar to Bezier curves, meaning that the curve was defined by a set of points, called the "control points", but their number was independent of the polynomial order of the curve. B-SPLines were a generalization of Bezier curves, but they were also more convenient to edit; changing a point no longer changed the whole curve, but only part of it.

Another problem is that even B-SPLines cannot produce an exact representation of conic sections. This is where NURBS came along. Ken Versprille was the first to work with NURBS on his dissertation in 1975. Later, when he acquired a top position in Computervision, the company began to support NURBS. Boeing, in its ambitious project to create a single curve representation that included Bezier curves and conic sections, became the first to industrialize NURBS.

After that, NURBS began to spread across the CAD industry. They possessed a lot of interesting attributes. The parameterization of the whole curve was downsized to a few control points coordinates, numerically stable mathematical procedures and easy modification. Cartoon characters, videogame graphics, ships, cars, airplanes were designed using NUBRS. This led to major investments from research and industrial faculties. Graphic designers became accustomed to them and students were taught about the theory and implementation of NURBS in real-life problems. This cycle led to the increasing popularity of Non-Uniform Rational B-SPLines in the CAD industry .

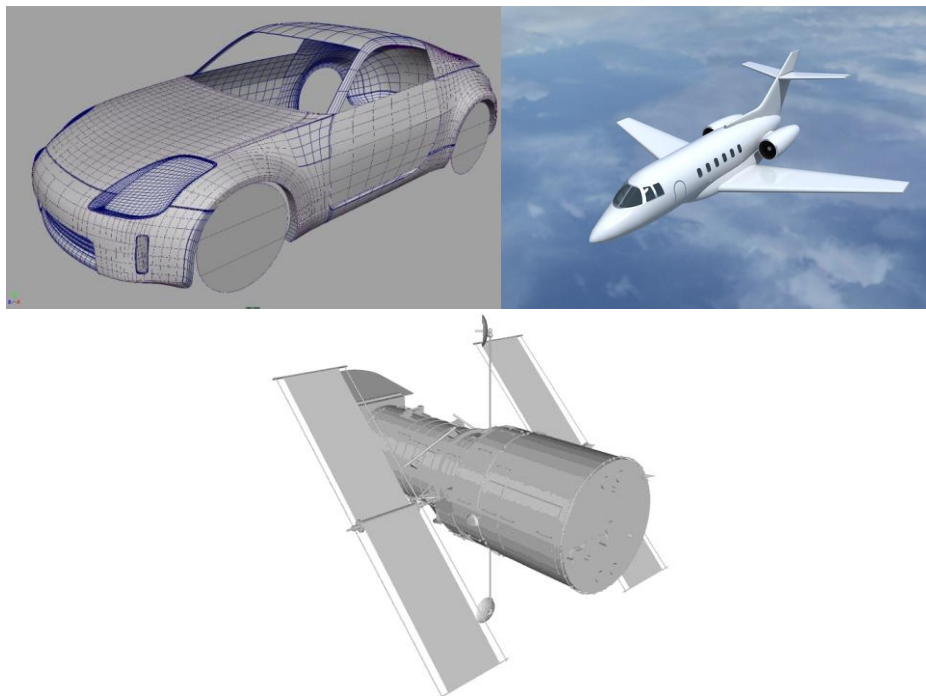


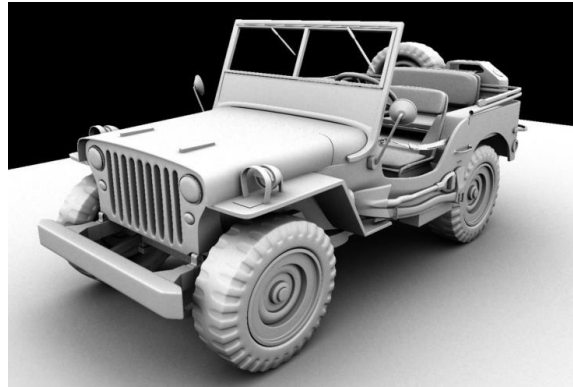
Figure 1.5

Entities created by NURBS.

(<http://www.smcars.net/threads>)(<http://www.turbosquid.com>)

Simulation of Human Aorta and Isogeometric Fluid Analysis

Today, even though many other forms of more suitable representations exist, such as T-SPLines, Polycube SPLines and Subdivision surfaces, NURBS still hold a large share of the market. Many platforms exist for NURBS and designers still find it easier to use them. Many handful tools have been developed over the years for them (knot insertion, order elevation, curve fitting, patching). This makes them more attractive and easy-to-use than newer techniques with less industry experience behind them.



Car (<http://asakomiyamori.blogspot.gr/>)



Castle (<http://asakomiyamori.blogspot.gr/>)



Motorbike (<http://kawasaki.turbosquid.com/3d-Models/3ds/max/xsi/c4d/obj>)

Figure 1.6
Entities created by Subdivision Surfaces.

1.3 Isogeometric Analysis

The usual design process requires both exact geometrical representation of the model and accurate engineering results. Unfortunately, computational geometry and Finite Element Method are represented in different file types and are not compatible to each other. The engineer has to create a model for FEM solution and the designer a model for CAD representation. Moreover, the typical design process is not straightforward. The designer produces CAD designs, which are transformed into FEM-compatible forms of representation by the analyst. After generating mesh and obtaining results, the analyst informs the designer of the appropriate changes in geometry. The designer then gives the new CAD model to the engineer, who has to regenerate the FEM model and the new mesh. This cycle of CAD/CAE interaction can go on multiple times. In complex projects each design consists of numerous CAD entities combined together and the integration process is estimated to take up at around 80% of the whole design time. Researchers around the world have been trying to achieve automatic CAD/CAE integration.

The main problem is that CAD and FEM, even though they refer to the same object, evolved differently. This incompatibility drove researchers into separate roads, building a wall between the two methods. Thomas J.R. Hughes, a Professor of Aerospace Engineering and Engineering Mechanics at the University of Texas at Austin, came up with a different point of view. Instead of trying to connect present CAD and CAE formulas, we should reinvent them in ways that enable the integration. This is the scope of Isogeometric Analysis.

The basic idea is to exploit the functions used for the exact geometrical representation in order to describe the solution field. Isogeometric Analysis extends, in essence, isoparametric elements, but the process of altering geometry for the sake of the solution approximation is reversed.

This leads to the creation of a single model, capable both of exact representation and analysis. Designers and engineers will be working on the same platform. Time for meshing and entity translation will be eliminated in an instant. This direct contact between analysis and geometry means that every single change can be integrated as soon as it happens, with no risk of errors or timely tasks involved. Most importantly, the designer has to follow the engineer's perspective and vice versa; the modern designer has to learn how to help the engineer and the modern engineer has to learn the methods the designer is using.

Isogeometric Analysis brings together two very different technologies, combining their best points to one. This leads to a better adaptation both from engineers and designers. In order to understand and improve Isogeometric Analysis, it simply needs to improve its counterparts. Finite element and computational geometry codes need not change drastically. This makes the new technology even more attractive. Understanding the basics of an innovation and implementation in the daily routine is usually a difficult and time-consuming task.

Simulation of Human Aorta and Isogeometric Fluid Analysis

There are many geometrical forms of representation suitable for analysis, such as NURBS, T-SPLines, Polycube SPLines and Subdivision surfaces. Each entity has its own advantages and drawbacks, but the variety provided ensures a vast number of alternatives to use, depending on the case. This ensures the generalization of Isogeometric Analysis method to even more complex geometries.

FEM's shape functions are defined only in the interior of the element. Each element has C^{-1} continuity in the edges. IGA's shape functions are not contained in one element. Most of the times, they are defined through many elements. This ensures a greater continuity and interconnectivity. This different approximation works better and leads to greater convergence than the classical methods.

Refinement by order elevation or knot insertion has always been important for computational geometry. Hierarchical adaptation has been developed for a vast number of entities. All these technologies can be exploited by IGA. Hierarchical structures can be easily developed, straight from the geometrical model. Meshing and refinement is also immediately accomplished.

2. Basic Ingredients of Isogeometric Analysis

2.1 Introduction

Until recently, the majority of CAD software users had not realized that by designing a model, they simultaneously created its corresponding mesh of finite elements. This information, although redundant for designers devoted to computational geometry, is a revolutionary remark for the engineering community. Before Thomas J.R. Hughes' idea, known as IsoGeometric Analysis (IGA), engineers used to create a new approximate mesh instead of taking advantage of the existing accurate one. The additional geometry error makes the process less accurate, though more time-consuming. This observation seems now very obvious, but it took years of research until 2003, when Thomas J.R. Hughes and his research team succeeded to cut the Gordian Knot of CAD – CAE integration.

The main idea is the elimination of the node mesh in the analysis process. The role and properties of the node mesh are inherited by two separate meshes, obtained directly from the geometrical representation:

- The Control Point mesh, which defines geometry and the finite number of degrees of freedom that form the problem equation.
- The Knot mesh, which provides appropriate discretization for numerical integration and boundaries for Shape function influence in the model.

For the scope of this thesis, I have worked exclusively with Non-Uniform Rational B-SPLines (NURBS), as they are the most commonly used computational geometry technology. Despite the fact that quite more advanced SPLines have emerged, CAD industry still invests in NURBS. Since 1970, billions of dollars have been directed towards the outspread and evolution of NURBS, establishing them as a common tool for graphic representation around the globe. Both professionals and amateurs still use NURBS despite their disadvantages, such as difficulties in Patch connection and local Refinement. The reason for this is that NURBS are not only much more simple in their definition and use, but also able to represent with accuracy smooth curves and all conic sections.

2.2 Index, Parameter and Physical Space

In most occasions, the exact solution of a natural problem is neither possible nor necessary. The actual objective is to find an accurate solution that satisfies a selected convergence criterion. The ultimate challenge for an engineer is to balance between accuracy and time. Design and analysis of extraordinary geometries is a powerful asset for modern engineers, who are capable of facing surprisingly more complicated problems. Accurate geometrical representations of the natural model are designed in the familiar Cartesian system, called Physical Space. Additionally, it is very helpful to envision a complex structure in an imaginary, basic space, where all geometries can be represented as lines, rectangles and cuboids. This is Parameter Space. This approach is far from new; it is already known from the isoparametric concept in Finite Element Methods. The Parameter Space utilized in Isogeometric Analysis, however, holds some major differences. Furthermore, Isogeometric Analysis also introduces the Index Space. This additional space plays an important role for some kinds of SPLines, but it is only auxiliary for NURBS.

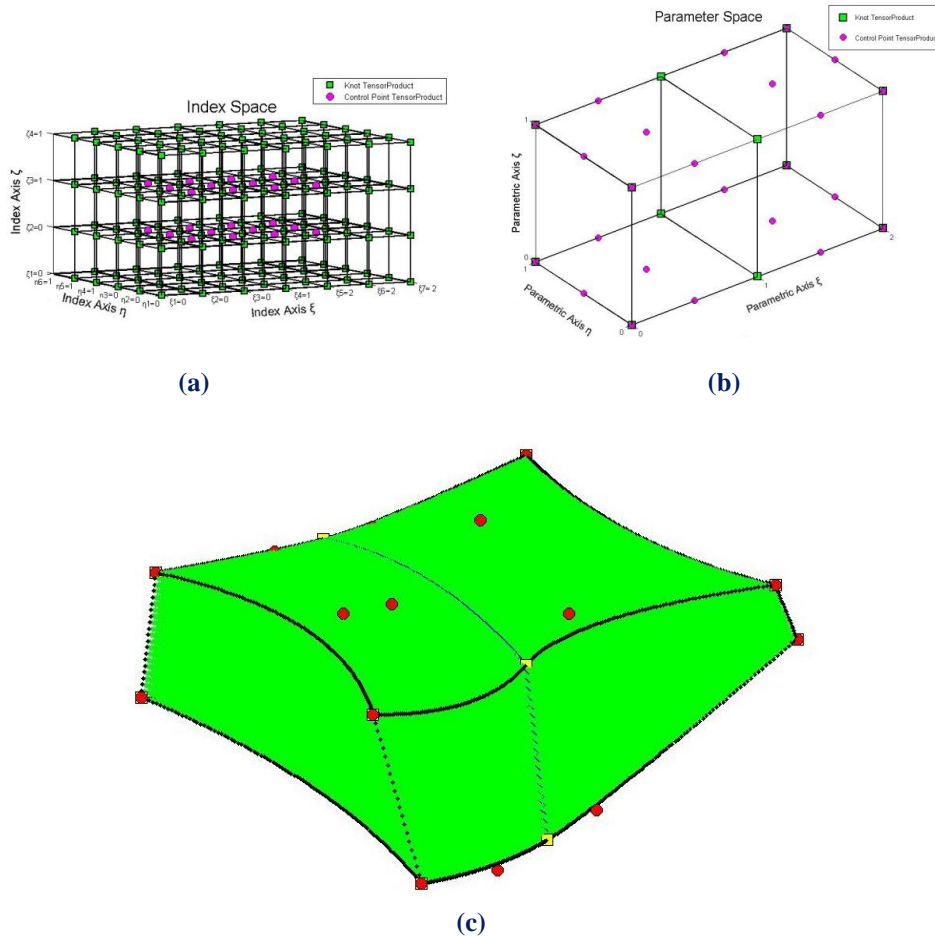


Figure 2.1
B-Spline solid.
(a) Index Space (b) Parameter Space
(c) Physical Space

2.2.1 Index Space

Index Space is a representation of the model with respect to Knot Values. It is a line in 1D, containing the corresponding Knot Values in equally spaced positions. This space focuses upon the sequence of Knot Values rather than their actual numerical content.

Index Space describes the contribution of each Knot Value to the creation of a certain B-Spline basis function. This helps identify the level of interconnection between basis functions and the Knot Value support of each function.

Control Points are also evaluated in the Index Space. In fact, Control Points are defined as the center of the support of Knot Value Spans.

Expansion to 2D or 3D leads to the creation of rectangles or cuboids respectively. Due to tensor product properties, everything mentioned about 1D extends and applies to both 2D and 3D. Thus, Index Space provides information that can contribute to the comprehension of a complex representation.

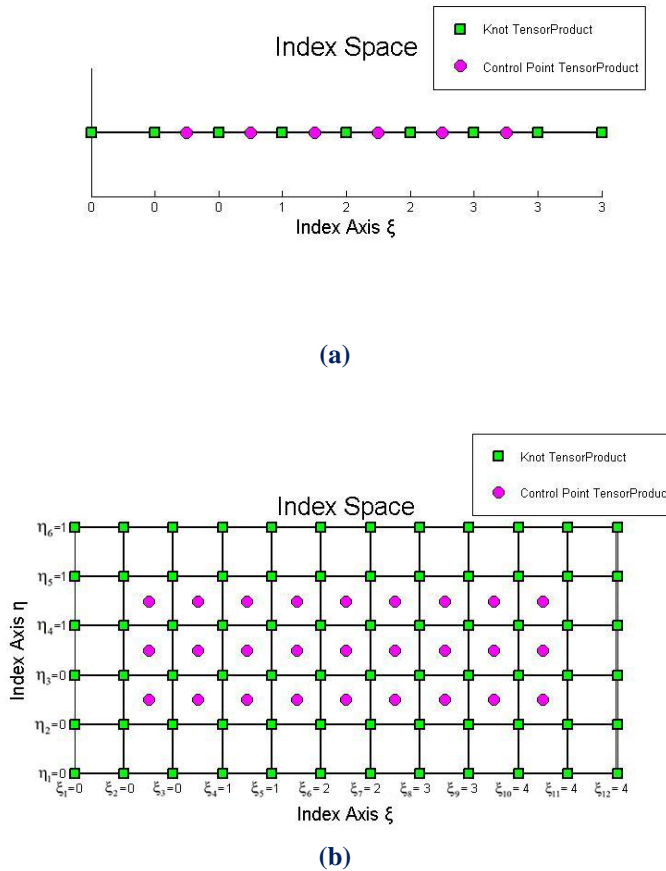
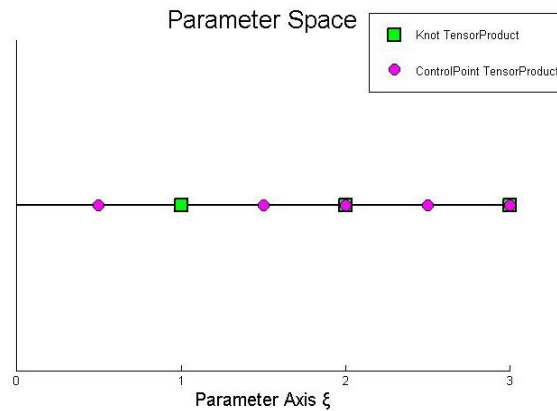


Figure 2.2
 (a) Curve and (b) Surface represented in Index Space

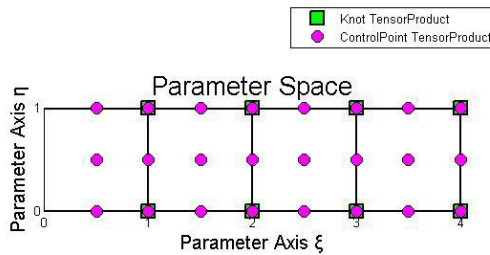
2.2.2 Parameter Space

Parameter Space is a representation of the model with respect to Knots. SPLine entities are always represented as orthogonal shapes in Parameter Space. Only lines, rectangles and cuboids exist here. In order to transform those simple patterns to virtually unlimited, complex geometries, the application of a mapping from Parameter to Physical Space is required. Hence, Parameter Space is a primitive, abstract representation of Physical Space. The mapping between Parameter Space and Physical Space is achieved through the Jacobian Matrix and its inverse. This is something widely utilized in FEM as well.

The illustration of basis functions in the Parameter Space allows for a better understanding of concepts such as support, Control Point coordinates and the role of Knots in basis function creation. Each Knot marks the beginning and the end of a basis function domain. By “domain” we mean the area in which the basis function is non-zero, as all basis functions are defined throughout the Parameter Space, but are non-zero only in specific Knot Spans. Basis functions sharing the same domain are overlapping in Parameter Space and controlling a common part of the entity in the Physical Space.



(a)



(b)

Figure 2.3
(a) Curve and (b) Surface represented in Parameter Space

2.2.3 Physical Space

Physical Space is the already known Cartesian Space, where the real model is represented. Simple orthogonal shapes from Parameter Space are transformed into complex entities in the Physical Space. Physical coordinates of the Control Points play a major role in the aforementioned mapping, but an equally drastic role is set upon basis functions. In fact, for a given set of Control Points, only a single set of basis functions can lead to the same geometry. We will examine this thoroughly later.

Control Points can often be seen outside the model in Physical Space in contrast to FEM's nodes which always belong to the mesh. It is one of the reasons NURBS and SPLine entities in general can accurately represent multiple types of geometries and the understanding of this peculiarity is one of the many challenges of Isogeometric Analysis.

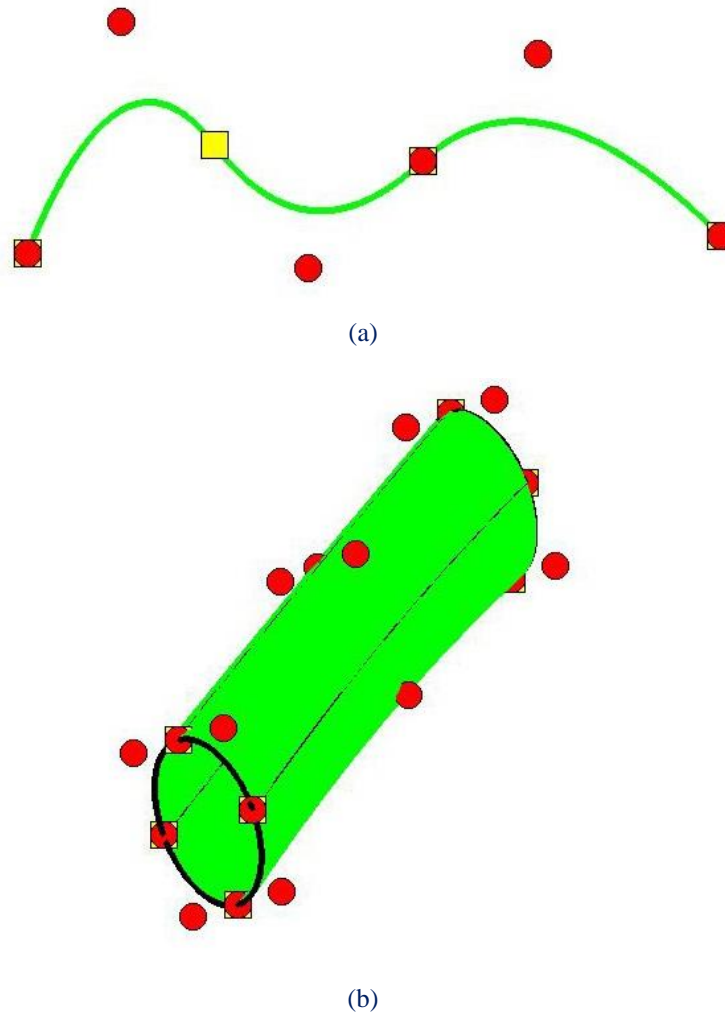


Figure 2.4
(a) Curve and (b) Surface represented in Physical Space

2.3 B-SPLine Geometries

2.3.1 B-SPLine Basis Functions

Given a sequence of non-decreasing numbers, $\Xi = \{ \xi_1 \ \xi_2 \ \dots \ \xi_{n+p} \ \xi_{n+p+1} \}$, we can evaluate the B-SPLine basis functions at $\xi \in [\xi_1, \xi_{n+p+1}]$ using the Cox-de Boor recursive formula:

First, for degree $p = 0$ (piecewise constant, Box B-SPLine)

$$N_{i,0}(\xi) = \begin{cases} 1, & \text{if } \xi_i \leq \xi < \xi_{i+1} \\ 0, & \text{otherwise} \end{cases}$$

The piecewise constant does not include the right edge ξ_{i+1} in order to ensure partition of unity, as the next basis function begins at that edge. The last function, however, includes both left and right edge, in order to be defined for the whole Knot Span.

$$N_{n+p,0}(\xi) = \begin{cases} 1, & \text{if } \xi_{n+p} \leq \xi \leq \xi_{n+p+1} \\ 0, & \text{otherwise} \end{cases}$$

Afterwards, for degree $p = 1, 2, \dots$:

$$N_{i,p}(\xi) = \frac{\xi - \xi_i}{\xi_{i+p} - \xi_i} \cdot N_{i,p-1}(\xi) + \frac{\xi_{i+p+1} - \xi}{\xi_{i+p+1} - \xi_{i+1}} \cdot N_{i+1,p-1}(\xi)$$

with the assumption of $\frac{0}{0} \doteq 0$.

We keep the same symbols with Isogeometric Analysis: Toward Integration of CAD and FEA (J. Austin Cottrell, Thomas J. R. Hughes, Yuri Bazilevs - Wiley, 2009), which is quite popular, because we want the reader to browse through this thesis conveniently. In the software implementation of this method, however, we discourage the use of symbolizations and instead represent the variables with full names.

2.3.2 Knot Value Vector as Boundary of Basis Functions Support

Knots define the boundaries of the model's basis functions. They represent “switches” which turn “on” or “off” a certain piece of a B-Spline basis function. In order to acquire the Knots and the basis functions, a Knot Vector must be defined.

A Knot Vector Ξ is usually defined in bibliography as a set of coordinates ξ_i , with $\xi_i \leq \xi_{i+1}$. It can contain the same number multiple times and generates the basis in a unique way.

In order to improve efficiency and communication between members of GiGA Team, we define as

- “Knot Value Vector”: the whole set of non-decreasing coordinates (“Knot Values”).
- “Knot Vector”: the set of unique coordinates (“Knots”).

For example, a Knot Value Vector could be $\{0 \ 1 \ 1 \ 1 \ 2 \ 2 \ 3 \ 3\}$ where 0, 1, 1, 1, 2, 2, 3, 3 are the separate Knot Values. The corresponding Knot Vector is $\{0 \ 1 \ 2 \ 3\}$ where 0, 1, 2, 3 are the separate Knots.

Let p be the polynomial degree of the basis function. If the first and the last Knots are repeated $p+1$ times, the Knot Value Vector is considered “Open”, because it has C^{-1} Continuity on the edges, creating an open curve that is interpolatory at these points. If Knot Values are equally spaced, the Knot Value Vector is considered “Uniform”. In CAD community, non-uniform, open Knot Value Vectors are widely used. An example of such a Knot Value Vector with $p = 2$ is:

$$\{0 \ 0 \ 0 \ 0.5 \ 1 \ 1.5 \ 2 \ 2.5 \ 3 \ 3 \ 3\}$$

A Knot Value Vector may contain integers or decimals. In fact, the actual numerical content of Knot Values is of no importance. What matters is the relative distance between them. This means a Knot Value Vector can be multiplied by any number, or have a number added to every Knot Value and the resulting basis would still be the same.

In GiGA Team, we generally prefer to use Knot Value Vectors that start from 0 and span by 1, as it is more convenient for the human mind to use an integer system.

2.3.3 Control Points as the Center of the Support

Control Points exist in all three spaces. Their parametric coordinates are defined as the center of the support in the Index Space. Recall that for the i^{th} basis function of order p the support is $[\xi_i, \xi_{i+p+1})$. The support contains $p+1$ Knot Value Spans, therefore $p+2$ Knot Values (including the right boundary value ξ_{i+p+1}).

For even degrees, the center of the support in the Index Space lies between two sequential Knot Values, $i + \frac{p}{2}$ and $i + \frac{p}{2} + 1$. As a result, the coordinate of the Control Point is defined as the average of these Knot Values:

$$\xi_{\text{CP}} = 0.5 \cdot \left(\xi_{i+\frac{p}{2}} + \xi_{i+\frac{p}{2}+1} \right)$$

which means that a Control Point of even degree can either be on a Knot, or in the middle of a Knot Span.

For odd degrees, the center of the support is the Knot Value $i + \frac{p+1}{2}$. Therefore, for odd degrees, Control Points are always coincident with Knots.

2.3.4 Full Tensor Product as a characteristic of B-SPLine Basis Functions

B-SPLine basis functions are of full-tensor product nature. Consequently, it is easy to combine B-SPLines across different directions, in order to evaluate a multi-directional B-SPLine Shape function.

2D B-SPLine Shape functions can be evaluated as tensor product of basis functions $N_{i,p}(\xi)$ and $M_{j,q}(\eta)$:

$$R_{i,j}^{p,q}(\xi, \eta) = N_{i,p}(\xi) \cdot M_{j,q}(\eta)$$

3D B-SPLine Shape functions are a tensor product of basis functions on three directions, $N_{i,p}(\xi)$, $M_{j,q}(\eta)$ and $L_{k,r}(\zeta)$:

$$R_{i,j,k}^{p,q,r}(\xi, \eta, \zeta) = N_{i,p}(\xi) \cdot M_{j,q}(\eta) \cdot L_{k,r}(\zeta)$$

It is understood that all properties of B-SPLine basis functions in one direction are inherited by the multi-directional Shape functions. As a result, thorough adaptation to one-directional B-SPLine basis function properties and techniques is very important for understanding multi-directional complex geometries.

2.3.5 B-SPLine Basis Function Properties

According to “The NURBS Book”, B-SPLine basis functions possess the following important properties:

1. Local support:

$$N_{i,p}(\xi) = 0 \quad \forall \xi \notin [\xi_i, \xi_{i+p+1})$$

2. In any given Knot Span, at most $p + 1$ functions of order p are non-zero.

3. Nonnegativity:

$$N_{i,p}(\xi) \geq 0 \quad \forall \xi, i, p$$

4. Partition of unity:

$$\sum_{i=1}^n N_{i,p}(\xi) = 1 \quad \forall \xi, p$$

5. C^{p-m} Continuity across Knots with multiplicity m .

6. $N_{i,p}(\xi)$ has exactly one maximum value, except for $p=0$.

7. A non-periodic Knot Value Vector that produces n functions of order p has $n + p + 1$ Knot Values.

8. Every B-SPLine basis function shares support with $2p$ B-SPLines.

2.1.1.1 Local support

Local support means that basis functions are non-zero only in certain Knot Spans in Parameter Space. This can be expressed by

$$N_{i,p}(\xi) = 0 \quad \forall \xi \notin [\xi_i, \xi_{i+p+1})$$

Local support is a result of the recursive character of B-SPLines. For the creation of a B-SPLine function of degree p , two consecutive B-SPLine functions of order $p - 1$ are used. For the creation of those consecutive basis functions, three consecutive functions of order $p - 2$ are needed. Inductively, $p + 1$ consecutive box basis functions are required.

Each box function has a support of one Knot Value Span. As a result, the support of the final basis function is defined by the union of the supports of the box functions, hence $p + 1$ consecutive Knot Value Spans.

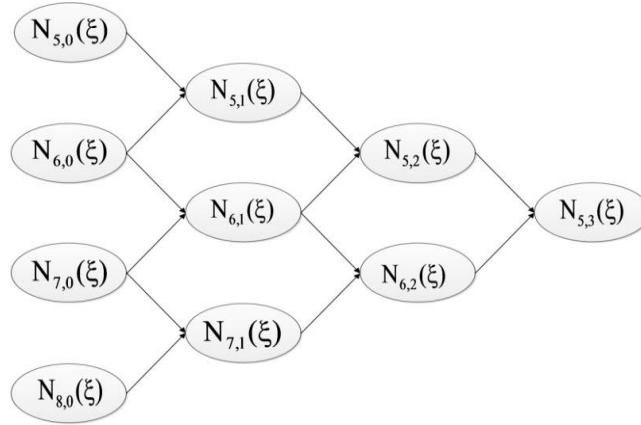


Figure 2.5
Lower-order basis functions required for the creation of $N_{5,3}(\xi)$.

In Figure 2.6, the recursive character of B-SPLines is represented. The box functions, drawn in red, are required in order to build the linear basis functions, drawn in green. Linear functions are combined for the evaluation of quadratic ($p = 2$) basis functions. Bear in mind that some linear and box functions are zero across the entire domain, but still contribute to the evaluation of the next-order B-SPLines.

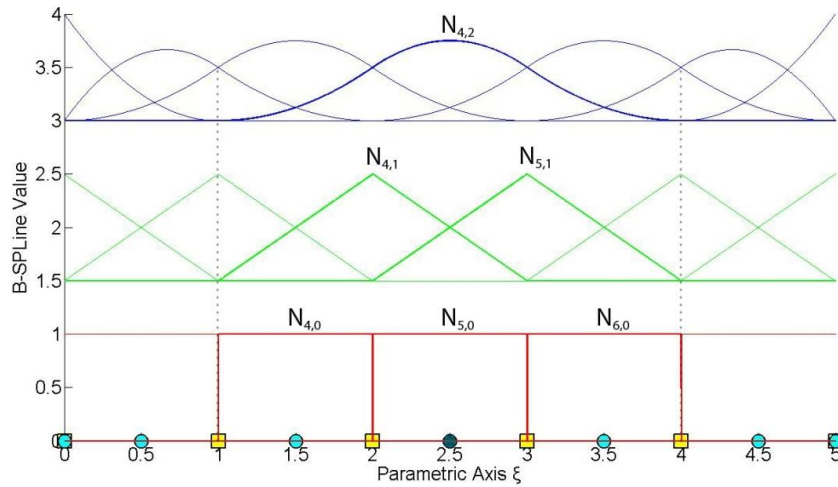


Figure 2.6
B-SPLine recursive character.
Basis functions required for the evaluation of a quadratic B-SPLine function.

For example, $N_{4,2}(\xi)$ in Figure 2.6 is created from $N_{4,1}(\xi)$ and $N_{5,1}(\xi)$. They, in turn, are evaluated from $N_{4,0}(\xi)$, $N_{5,0}(\xi)$ and $N_{5,0}(\xi)$, $N_{6,0}(\xi)$ respectively. The corresponding box functions are non-zero in the Knot Spans $[1,2)$, $[2,3)$ and $[2,3)$, $[3,4)$, thus creating the support $[1,4)$ of $N_{4,2}(\xi)$.

In a similar fashion, a support can be defined with respect to Knot Values contributing to the creation of a B-Spline basis function. These are the $p+2$ Knot Values that are contained in the Knot Value Span support of the function. Both Knot Value Span Support and Knot Value Support are necessary for the understanding of Isogeometric Methods.

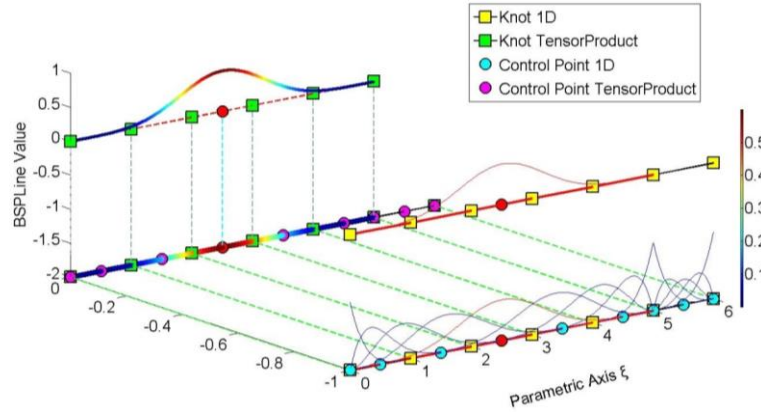


Figure 2.7

B-Spline Basis functions for Knot Value Vector .

$$\Xi = \{0 \ 0 \ 0 \ 0 \ 0 \ 1 \ 2 \ 3 \ 4 \ 5 \ 5 \ 5 \ 5 \ 6 \ 6 \ 6 \ 6 \ 6\}$$

1D Shape Function $N_{5,4}(\xi)$

In Figure 2.7, the degree is $p = 4$, so each basis function has a support of $p + 1 = 4 + 1 = 5$ Knot Value Spans. The selected function $N_{5,4}(\xi)$, drawn in red, is non-zero only in the Knot Value Spans $[0,1)$, $[1,2)$, $[2,3)$, $[3,4)$ and $[4,5)$. The $p + 2 = 6$ Knot Values that define this function are $\{0,1,2,3,4,5\}$ shown in green. There are no trivial spans in this B-Spline function, so it is considered a fully developed basis function.

Bear in mind that Knot Values can be repeated, thus forming trivial spans.

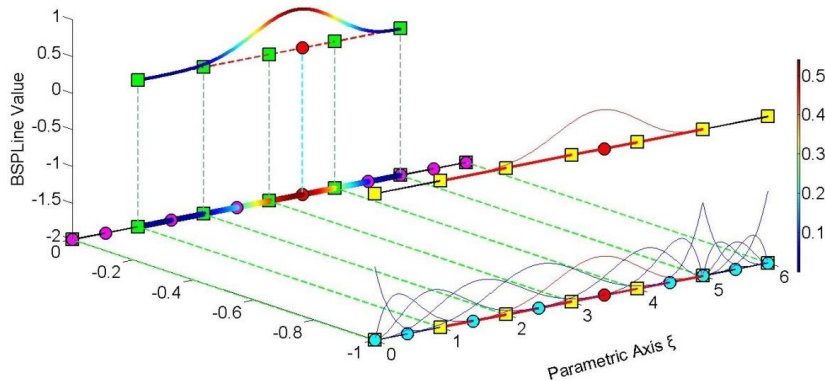


Figure 2.8

B-Spline Basis functions for Knot Value Vector .

$$\Xi = \{0 \ 0 \ 0 \ 0 \ 0 \ 1 \ 2 \ 3 \ 4 \ 5 \ 5 \ 5 \ 5 \ 6 \ 6 \ 6 \ 6 \ 6\}$$

1D Shape function $N_{6,4}(\xi)$

In Figure 2,8 $N_{6,4}(\xi)$ is highlighted. This function is non-zero in the Knot Value Spans $[1,2)$, $[2,3)$, $[3,4)$, $[4,5)$ and $[5,5)$. The corresponding Knot Values shown in green are $\{1,2,3,4,5,5\}$. The support is five Knot Value Spans, but this leads to only four Knot Spans, as a trivial span is contained.

Observe the next basis functions in this example; as more trivial spans are contained, the Knot Span support of each function is reduced. Still, the Knot Value Span support and the corresponding Knot Value support follow the rules already mentioned.

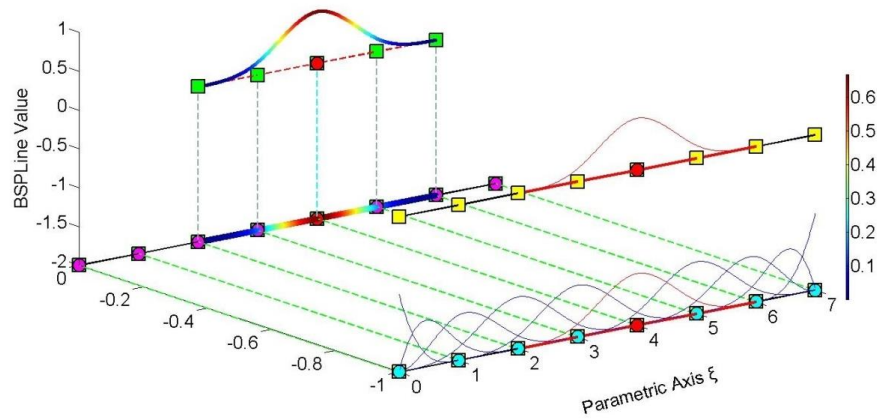


Figure 2.9
 B-Spline Basis functions for Knot Value Vector.
 $\Xi = \{0 \ 0 \ 0 \ 0 \ 1 \ 2 \ 3 \ 4 \ 5 \ 6 \ 7 \ 7 \ 7 \ 7\}$
 1D Shape Function $N_{6,3}(\xi)$

In the above figure, the polynomial degree of the basis functions is $p = 3$. Knot Value Span support is $p + 1 = 4$ Knot Value Spans, which requires Knot Value support of $p + 2 = 5$ Knot Values.

$N_{6,3}(\xi)$ is non-zero in the Knot Value Spans $[2,3)$, $[3,4)$, $[4,5)$ and $[5,6)$. No trivial spans are involved, so this is another fully developed B-Spline. The Knot Value Support consists of the Knot Values $\{2,3,4,5,6\}$.

B-Spline tensor product properties enable the immediate expansion of 1D properties to 2D and 3D B-Spline Shape functions.

$N_{3,2}(\xi)$ in Figure 2.10 has a support of 3 Knot Value Spans per ξ , $[0,1)$, $[1,2)$ and $[2,3)$. It is created by Knot Values $\{0,1,2,3\}$.

$M_{4,2}(\eta)$ has a support of 3 Knot Value Spans per η , $[1,2)$, $[2,3)$ and $[3,4)$. It is created by Knot Values $\{1,2,3,4\}$.

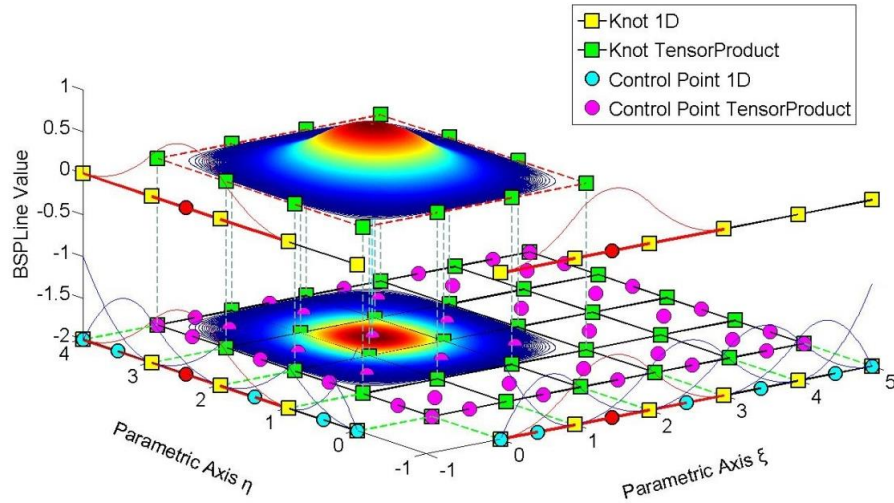


Figure 2.10

Shape Function $R_{i,j}^{p,q} = R_{3,4}^{2,2}(\xi, \eta)$ as a tensor product of $N_{3,2}(\xi)$ and $M_{4,2}(\eta)$

Knot Value Vector $\Xi = \{0 \ 0 \ 0 \ 1 \ 2 \ 3 \ 4 \ 5 \ 5 \ 5\}$

Knot Value Vector $H = \{0 \ 0 \ 0 \ 1 \ 2 \ 3 \ 4 \ 4 \ 4\}$

The 2D Shape function $R_{3,4}^{2,2}(\xi, \eta)$ is the full tensor product of $N_{3,2}(\xi)$ and $M_{4,2}(\eta)$. The support of the Shape function is a rectangle created from the supports of the respective basis functions. It has a total area of $3 \cdot 3 = 9$ Knot Value Rectangles.

Observe that the value of the bidirectional B-Spline is represented both in the third axis of the graph and by projection of the contour in the 2D plane. This is useful for representation of 3D basis functions.

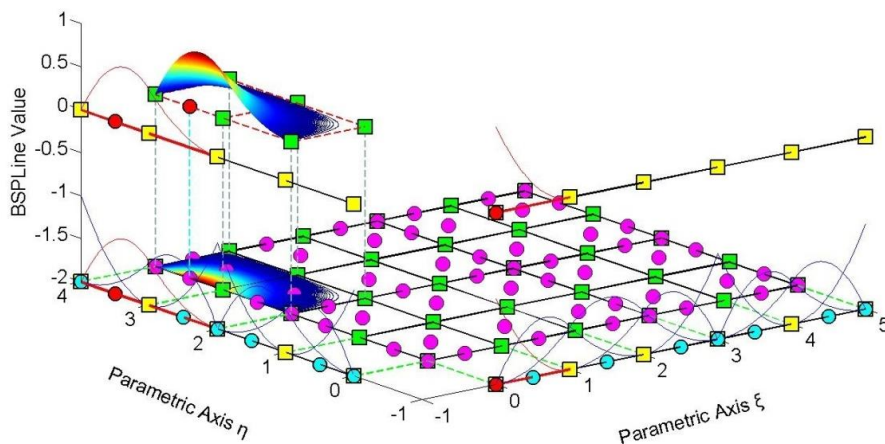


Figure 2.11

Shape Function $R_{i,j}^{p,q} = R_{1,6}^{2,2}(\xi, \eta)$ as a tensor product of $N_{1,2}(\xi)$ and $M_{6,2}(\eta)$

Knot Value Vector: $\Xi = \{0 \ 0 \ 0 \ 1 \ 2 \ 3 \ 3 \ 4 \ 5 \ 5 \ 5\}$

Knot Value Vector $H = \{0 \ 0 \ 0 \ 1 \ 2 \ 2 \ 3 \ 4 \ 4 \ 4\}$

Both 1D basis functions have reduced Continuity in Figure 2.11.

$N_{1,2}(\xi)$ has a Knot Value Span Support of $[0,0)$, $[0,0)$ and $[0,1)$, leading to a Support of a single Knot Span, $[0,1)$. The corresponding Knot Value Support is $\{0,0,0,1\}$.

$M_{6,2}(\eta)$ has a Knot Value Support of $\{2,3,4,4\}$ which leads to a Knot Value Span Support of $[2,3)$, $[3,4)$, $[4,4)$. One trivial and two non-trivial Spans are contained.

Support for the Shape Function $R_{1,6}^{2,2}(\xi, \eta)$ is defined as the tensor product of the supports of the basis functions, namely $1 \cdot 2 = 2$ Knot Rectangles.

3D B-SPLine Shape functions can be represented as in the Figure 2.12.

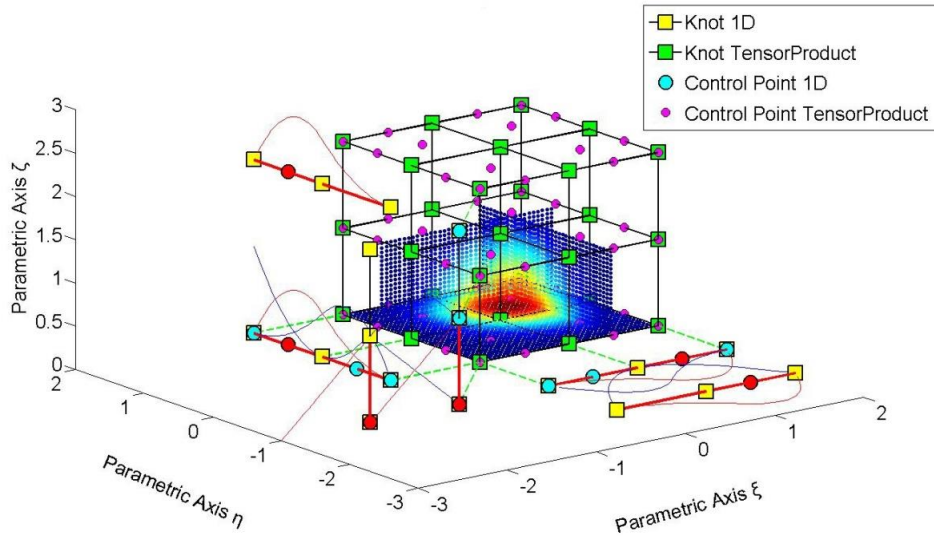


Figure 2.12

Shape Function $R_{i,j,k}^{p,q,r} = R_{3,3,1}^{2,2,1}(\xi, \eta, \zeta)$ as tensor product of $N_{3,2}(\xi)$, $M_{3,2}(\eta)$, $L_{1,1}(\zeta)$.

$$\text{Knot Value Vector } \Xi = \{0 \ 0 \ 0 \ 1 \ 2 \ 2 \ 2\}$$

$$\text{Knot Value Vector } H = \{0 \ 0 \ 0 \ 1 \ 2 \ 2 \ 2\}$$

$$\text{Knot Value Vector } Z = \{0 \ 0 \ 1 \ 2 \ 2\}$$

The three axes represent the three parametric directions ξ, η, ζ . B-Spline basis functions for ξ are drawn in the $\xi - \eta$ plane, functions for η in the $\eta - \zeta$ plane and functions for ζ in the $\zeta - \xi$ plane.

$N_{3,2}(\xi)$ and $M_{3,2}(\eta)$ both have a support of 3 Knot Value Spans, $[0,1)$, $[1,2)$ and $[2,2)$ in their respective directions. Knot Value Support for those functions is $\{0,1,2,2\}$. Knot Span Support is restrained at 2 Knot Spans for each function.

$L_{1,1}(\zeta)$ has a Knot Value Span Support of $[0,0)$ and $[0,1)$, leading to the support of 1 Knot Span. Knot Value Support is defined as $\{0,0,1\}$.

Their tensor product value has been calculated as a function of two parametric directions at the Control Point coordinate of the remaining direction. The resulting contour is projected on a plane that is parallel to the two directions and intersects with the tensor product Control Point. This process is repeated for all three possible combinations, thus creating contours at $\xi - \eta$, $\eta - \zeta$ and $\zeta - \xi$ planes.

For example, Control Point $(3,3,1)$ has coordinates $(\xi, \eta, \zeta) = (1.5, 1.5, 0)$.

$R_{3,3,1}^{2,2,1}(\xi, \eta, 0)$ has been calculated and projected in $\zeta = 0$ plane. The support of the projection shows the support of the 3D Shape function per ξ, η , namely $2 \cdot 2 = 4$ Knot Rectangles.

$R_{3,3,1}^{2,2,1}(\xi, 1.5, \zeta)$ is represented in the plane $\eta = 1.5$. Support of the 3D Shape function per ξ, ζ is $2 \cdot 1 = 2$ Knot Rectangles.

$R_{3,3,1}^{2,2,1}(1.5, \eta, \zeta)$ is projected in $\xi = 1.5$ plane. The support of the 3D Shape function per η, ζ is $2 \cdot 1 = 2$ Knot Rectangles.

The support of the 3D Shape function across the entire domain is the tensor product of the 1D supports. In this particular case, it is $2 \cdot 2 \cdot 1 = 4$ Knot Cuboids. The support is represented by the tensor product of the projections in Figure 2.12.

2.1.1.2 Maximum number of non-zero functions per Knot Span

A box function that is non-zero in one Knot Span contributes to the evaluation of two consecutive B-Spline basis functions of order $p = 1$. These two functions lead to the creation of three consecutive basis functions of order $p = 2$. Inductively, a box function contributes to the creation of $p + 1$ B-Spline basis functions of order p .

It applies from Cox de Boor recursive formula that only one box function is non-zero across a selected Knot Span. As a result, only the corresponding $p + 1$ B-Spline basis functions of order p can be non-zero in that specific Knot Span.

Therefore, at a non-trivial Knot Value Span $[\xi_i, \xi_{i+1})$ only the basis functions $N_{i-p,p}(\xi)$, $N_{i-p+1,p}(\xi)$, ..., $N_{i,p}(\xi)$ are non-zero. This is used efficiently in Stiffness Matrix Formulation, in order to reduce computational cost.

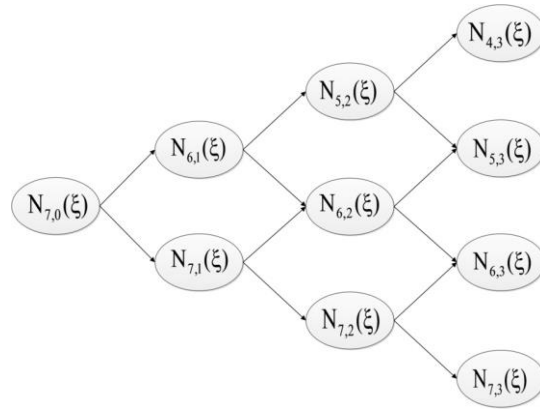


Figure 2.13
Contribution of one box function to the creation of higher-order B-Spline basis functions.

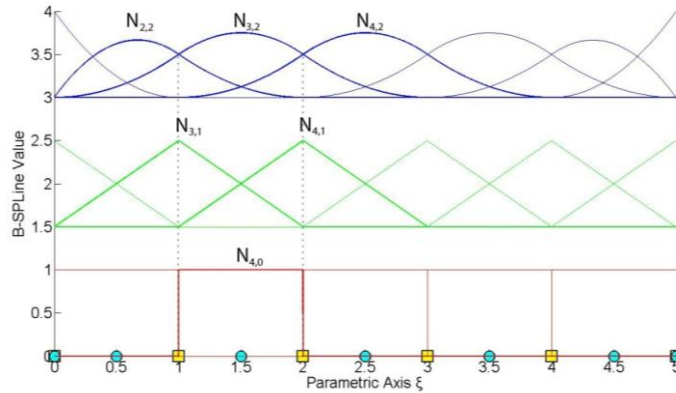


Figure 2.14
Contribution of one box function to non-zero higher-order B-Spline basis functions across Knot Span $[1, 2)$.

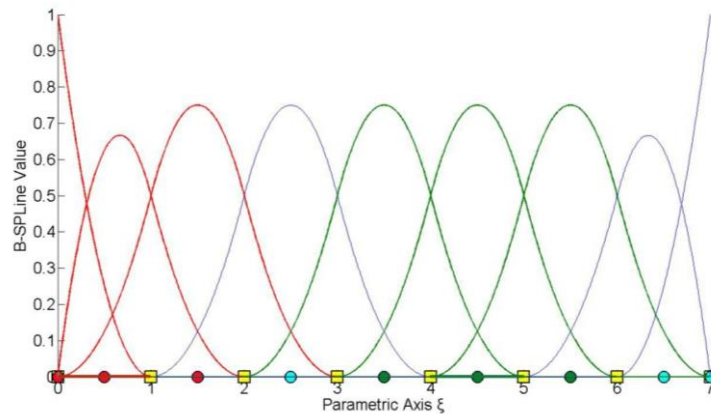


Figure 2.15
B-Spline Basis functions for Knot Value Vector $\Xi = \{0, 0, 0, 1, 2, 3, 4, 5, 6, 7, 7, 7\}$.
Basis functions that are non-zero in Knot Span $[0, 1)$ are drawn in red.
Basis functions that are non-zero in Knot Span $[4, 5)$ are drawn in green.

In Figure 2.15, two separate Knot Spans are examined. For every Knot Span, $p + 1 = 3$ basis functions are non-zero.

For the first Knot Span, $[0, 1) = [\xi_3, \xi_4)$, basis functions $N_{1,p}(\xi)$, $N_{2,p}(\xi)$, $N_{3,p}(\xi)$ are non-zero.

For the second Knot Span, $[4, 5) = [\xi_7, \xi_8)$, basis functions $N_{5,p}(\xi)$, $N_{6,p}(\xi)$, $N_{7,p}(\xi)$ are non-zero.

As a result, in 2D, at a given Knot Rectangle, only the tensor products of the respective non-zero basis functions are non-zero, namely $(p + 1) \cdot (q + 1)$ Shape functions.

Inductively, in 3D, at a given Knot Cuboid, the tensor products of the corresponding non-zero basis functions create $(p + 1) \cdot (q + 1) \cdot (r + 1)$ non-zero Shape functions.

2.1.1.3 Non-negativity

It has been established that:

$$N_{i,p}(\xi) \geq 0 \quad \forall \xi, i, p.$$

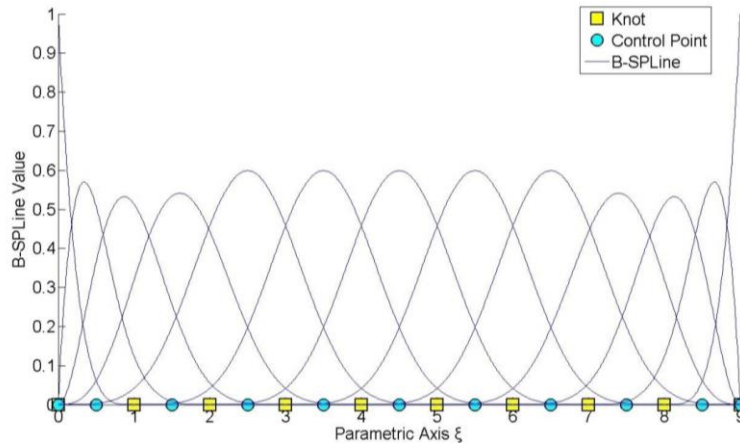


Figure 2.16

B-Spline Basis functions for Knot Value Vector

$$\Xi = \{0 \ 0 \ 0 \ 0 \ 0 \ 1 \ 2 \ 3 \ 4 \ 5 \ 6 \ 7 \ 8 \ 9 \ 9 \ 9 \ 9 \ 9\}$$

The degree in Figure 2.16 is $p = 4$. As we see in the picture above, all the basis functions are positive for every ξ, i . This property is very important for Isogeometric Analysis and it does not apply in the classical Shape functions of Finite Element Analysis. Naturally, it is easier for the human mind to work with only positive values, so this attribute simplifies and encourages the understanding of B-SPLines. Non-negativity applies for 2D and 3D Shape functions as well.

2.1.1.4 Partition of unity

Partition of unity is expressed by

$$\sum_{i=1}^n N_{i,p}(\xi) = 1 \quad \forall \xi, p.$$

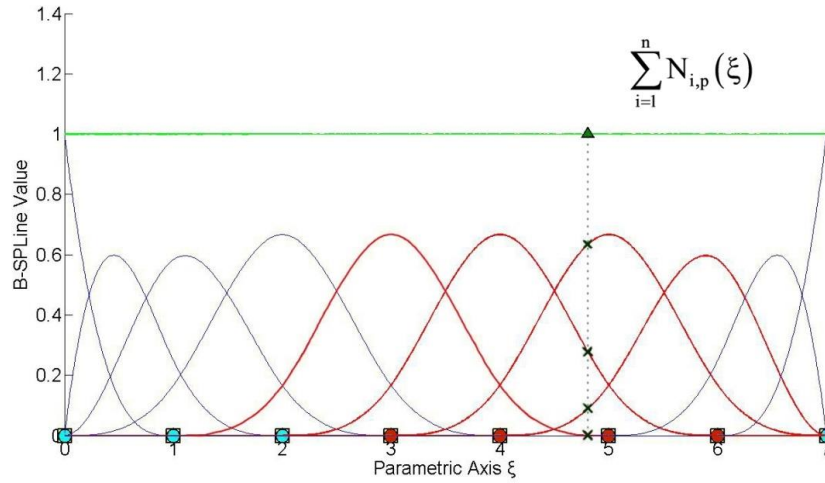


Figure 2.17

B-SPLine Basis functions for Knot Value Vector

$$\Xi = \{0 \ 0 \ 0 \ 0 \ 1 \ 2 \ 3 \ 4 \ 5 \ 6 \ 7 \ 7 \ 7 \ 7\}$$

Sum of B-SPLine function value at every ξ . Partition of Unity.

The degree for the B-SPLine basis functions in Figure 2.17 is $p = 3$. The green horizontal line represents the sum of B-SPLine values at the corresponding ξ , which, of course, is equal to 1 for every ξ .

For example, B-SPLine values have been evaluated for $\xi = 4.81$, with the following results for the four non-zero basis functions:

$$N_{5,3}(4.81) = 0.0011$$

$$N_{6,3}(4.81) = 0.2763$$

$$N_{7,3}(4.81) = 0.6340$$

$$N_{8,3}(4.81) = 0.0886$$

The above yields

$$\sum_{i=1}^{10} N_{i,3}(4.81) = 1$$

as expected.

Partition of unity applies for multi-dimensional Shape functions as well.

In 2D, partition of unity is expressed as

$$\sum_{i=1}^n \sum_{j=1}^m R_{i,j}^{p,q} = \sum_{i=1}^n \sum_{j=1}^m N_{i,p}(\xi) \cdot M_{j,q}(\eta) = 1$$

which is a result of tensor product nature:

$$\sum_{i=1}^n \sum_{j=1}^m R_{i,j}^{p,q} = \sum_{i=1}^n \sum_{j=1}^m N_{i,p}(\xi) \cdot M_{j,q}(\eta) = \left(\sum_{i=1}^n N_{i,p}(\xi) \right) \cdot \left(\sum_{j=1}^m M_{j,q}(\eta) \right) = 1$$

In full analogy, 3D Shape functions also possess partition of unity:

$$\sum_{i=1}^n \sum_{j=1}^m \sum_{k=1}^l R_{i,j,k}^{p,q,r} = \sum_{i=1}^n \sum_{j=1}^m \sum_{k=1}^l N_{i,p}(\xi) \cdot M_{j,q}(\eta) \cdot L_{k,r}(\zeta) = 1$$

Partition of unity is also a property of great importance for the Shape functions that are used in Finite Element Analysis.

2.1.1.5 C^{p-m} Continuity

At a Knot with multiplicity m , $N_{i,p}(\xi)$ produces $p - m$ continuous derivatives or, in other words, it has C^{p-m} Continuity. Continuity less than C^0 is not acceptable for internal Knots, which means they can be repeated up to p times. Bear in mind that as Continuity decreases, B-Spline basis functions tend to be more “steep”.

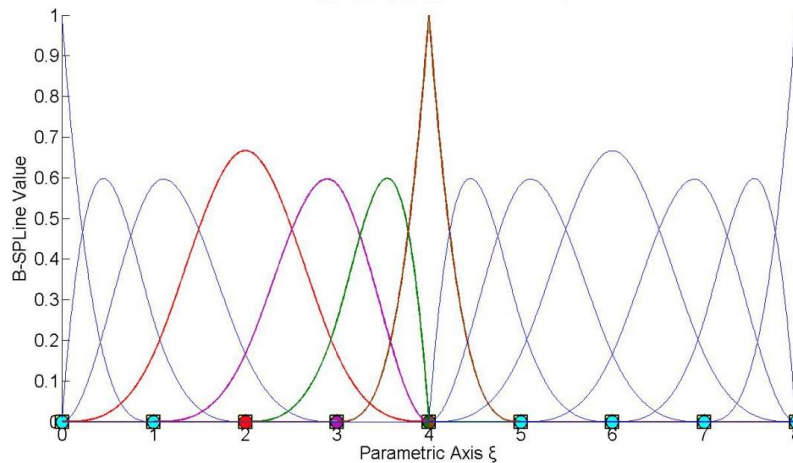


Figure 2.18

B-Spline Basis functions for Knot Value Vector

$$\Xi = \{0 \ 0 \ 0 \ 0 \ 1 \ 2 \ 3 \ 4 \ 4 \ 4 \ 5 \ 6 \ 7 \ 8 \ 8 \ 8 \ 8\}$$

The polynomial order in Figure 2.18 is $p = 3$. Continuity for a basis function is affected only by the corresponding Knot Values. Knot $\xi = 4$ has multiplicity $m = 3$ with respect to the Knot Vector. Its multiplicity with respect to the basis functions depends on each function's Knot Value Support.

$N_{4,3}(\xi)$, a fully developed basis function, drawn in red, has a Knot Value Support of $\{0, 1, 2, 3, 4\}$. The Knot $\xi = 4$ has multiplicity $m = 1$ with respect to the basis function $N_{4,3}(\xi)$, so this function is $C^{p-m} = C^{3-1} = C^2$ Continuous in the entire domain.

The purple basis function, $N_{5,3}(\xi)$ has a Knot Value Support of $\{1, 2, 3, 4, 4\}$. The Knot in question has multiplicity $m = 2$ with respect to the basis function, which makes $N_{5,3}(\xi)$ $C^{p-m} = C^{3-2} = C^1$ Continuous across $\xi = 4$.

Knot Value Support for $N_{6,3}(\xi)$ and $N_{7,3}(\xi)$ is $\{2, 3, 4, 4, 4\}$ and $\{3, 4, 4, 4, 5\}$ respectively. The multiplicity of the Knot is $m = 3$ for both basis functions. Therefore, these functions have $C^{p-m} = C^{3-3} = C^0$ Continuity across $\xi = 4$.

Observe that when a B-Spline basis function $N_{j,p}(\xi)$ has a Knot ξ_m with multiplicity p in the center of the Knot Value Support, it applies that $N_{j,p}(\xi_m) = 1$.

In 2D and 3D cases, Continuity per direction is obtained straight from the Continuity of the corresponding one-directional B-Spline basis functions.

In Figure 2.19.a, $R_{3,4}^{2,2}(\xi, \eta)$ is tensor product of $N_{3,2}(\xi)$ and $M_{4,2}(\eta)$. $N_{3,2}(\xi)$ has $C^{p-m} = C^{2-1} = C^1$ Continuity across $\xi = 3$ and $M_{4,2}(\eta)$ has $C^{p-m} = C^{2-2} = C^0$ Continuity across $\eta = 2$. Therefore, $R_{3,4}^{2,2}(\xi, \eta)$ has C^1 Continuity with respect to ξ and C^0 Continuity with respect to η across $(\xi, \eta) = (3, 2)$.

In Figure 2.19.b, $R_{5,4}^{2,2}(\xi, \eta)$ is tensor product of $N_{5,2}(\xi)$ and $M_{4,2}(\eta)$. Both B-Spline basis functions have C^0 Continuity across $\xi = 3$, $\eta = 2$ respectively. As a result, $R_{5,4}^{2,2}(\xi, \eta)$ has C^0 Continuity across $(\xi, \eta) = (3, 2)$. This particular case of C^0 Continuity for both directions will be utilized in future applications.

Note that C^0 Continuity per both directions leads to $R_{5,4}^{2,2}(3, 2) = N_{5,2}(3) \cdot M_{4,2}(2) = 1$. Non-negativity and Partition of unity properties require that $R_{i,j}^{2,2}(3, 2) = 0$, $\forall (i, j) \neq (5, 4)$.

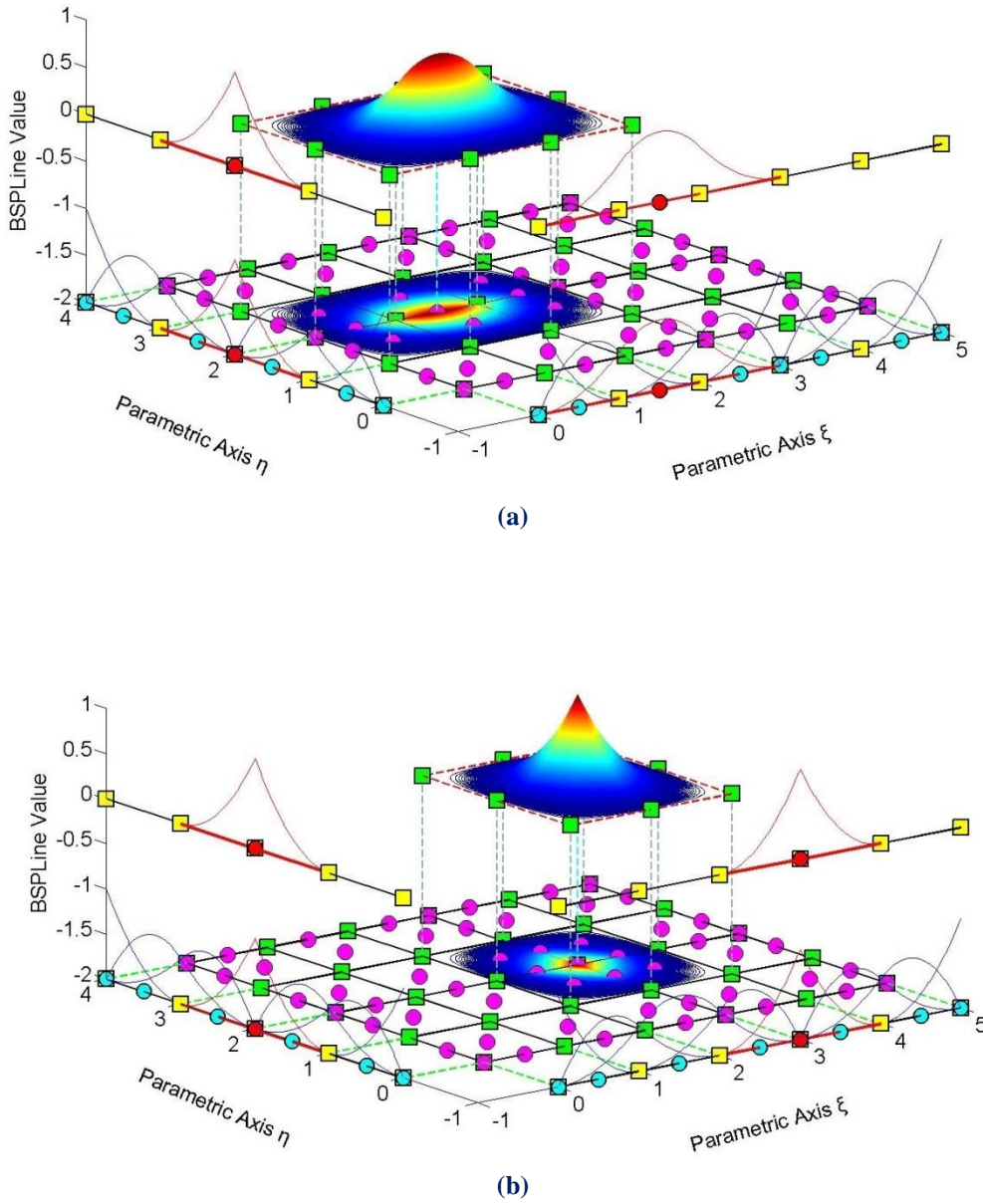


Figure 2.19

B-Spline Basis functions for directions ξ, η

$$\text{Knot Vector } \Xi = \{0 \ 0 \ 0 \ 1 \ 2 \ 3 \ 3 \ 4 \ 5 \ 5 \ 5\}$$

$$\text{Knot Vector } H = \{0 \ 0 \ 0 \ 1 \ 2 \ 2 \ 3 \ 4 \ 4 \ 4\}$$

(a): Shape Function $R_{i,j}^{p,q} = R_{3,4}^{2,2}(\xi, \eta)$ as tensor product of $N_{3,2}(\xi)$ and $M_{4,2}(\eta)$

(b): Shape Function $R_{i,j}^{p,q} = R_{5,4}^{2,2}(\xi, \eta)$ as tensor product of $N_{5,2}(\xi)$ and $M_{4,2}(\eta)$

Figure 2.20 represents $R_{4,3,3}^{2,2,2}(\xi, \eta, \zeta)$, a Shape function formed as a tensor product of three C^0 Continuous functions across $(2,1,1)$. The corresponding basis functions are $N_{4,2}(\xi)$, $M_{3,2}(\eta)$ and $L_{3,2}(\zeta)$. Naturally, at the point of C^0 Continuity for all three directions, it applies that $R_{4,3,3}^{2,2,2}(2,1,1) = N_{4,2}(2) \cdot M_{3,2}(1) \cdot L_{3,2}(1) = 1$.

Observe that all functions of reduced Continuity tend to be more “steep”. This happens because they contain multiple Knot Values of the same Knot, and therefore develop across trivial spans. This “steepness” is the first indication that a basis function has reduced Continuity.

Moreover, internal C^0 Continuity produced exactly the same B-Spline basis functions as C^{-1} Continuity on the edge of the Knot Vector. This means that at every Knot with multiplicity $m = p$, only one function remains non-zero. Due to partition of unity, that function’s value at that Knot is equal to 1.

In multi-dimensional functions, C^0 Continuity across a Knot requires the basis functions per all directions to be C^0 Continuous at that point. In this case, the value of the multi-dimensional Shape function across this Knot is equal to 1.

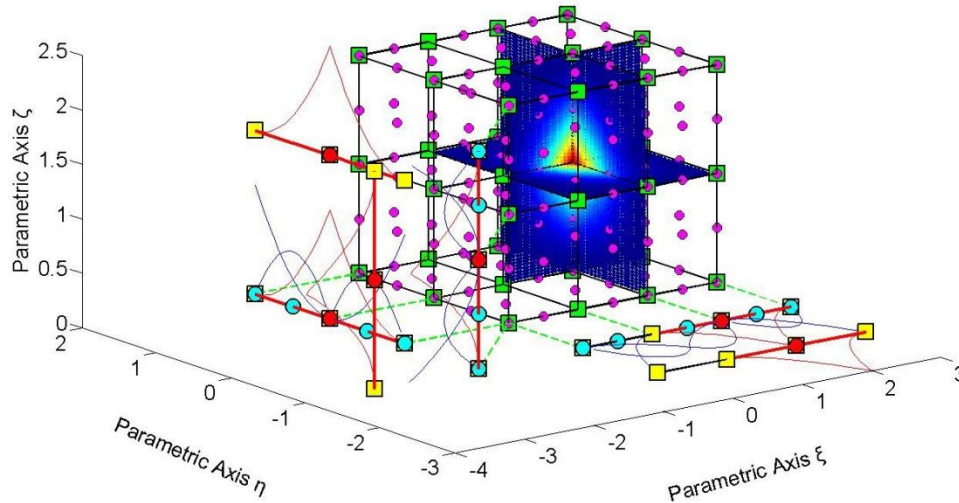


Figure 2.20

$$\text{Shape Function } R_{i,j,k}^{p,q,r}(\xi, \eta, \zeta) = R_{4,3,3}^{2,2,2}(\xi, \eta, \zeta)$$

$$\text{Knot Value Vector } \Xi = \{0 \ 0 \ 0 \ 1 \ 2 \ 2 \ 3 \ 3 \ 3\}$$

$$\text{Knot Value Vector } H = \{0 \ 0 \ 0 \ 1 \ 1 \ 2 \ 2 \ 2\}$$

$$\text{Knot Value Vector } Z = \{0 \ 0 \ 0 \ 1 \ 1 \ 2 \ 2 \ 2\}$$

2.1.1.6 Linear Independence

Given a finite number of distinct vectors $\{u_1 \ u_2 \ \dots \ u_n\}$ and scalars $\{a_1 \ a_2 \ \dots \ a_n\}$, the subset S of a vector space V is called linearly independent if the equation $a_1u_1 + a_2u_2 + \dots + a_nu_n = 0$ leads to the unique solution $a_1 = a_2 = \dots = a_n = 0$. Thus the subset is linearly independent if a linear combination of the vectors is the zero vector, only for $a_1 = a_2 = \dots = a_n = 0$. The linear independence in Isogeometric Analysis applies for the basis functions $\{N_{1,p}(\xi) \ N_{2,p}(\xi) \ \dots \ N_{n,p}(\xi)\}$. The equation

$$a_1 \cdot N_{1,p}(\xi) + a_2 \cdot N_{2,p}(\xi) + \dots + a_n \cdot N_{n,p}(\xi) = 0$$

leads to $a_1 = a_2 = \dots = a_n = 0$. We can reach the conclusion that no B-Spline basis function can be expressed as a linear combination of the other B-Spline basis functions.

These linearly independent vectors form a basis for the vector space V . Some interesting attributes of such vectors include:

- The basis of the vector space V can be formed by different sets of linearly independent vectors. Any set can be used, provided that the vectors are linearly independent and all the properties above apply for every vector. Thus, in Isogeometric Analysis, we can choose different sets of B-Spline basis functions in order to represent the vector space.
- The number of vectors of any basis chosen is equal to the dimension of V , often represented as $\dim(V)$. In Isogeometric Analysis $\dim(V)$ is equal to the number of Control Points and, consequently, the number of basis functions used.
- Let there be a mass of vectors $\{u_1 \ u_2 \ \dots \ u_n\}$ which form the basis of a vector space with $\dim(V) = n$ and the numbers $\{a_1 \ a_2 \ \dots \ a_n\}$, called the coordinates of u . In Isogeometric Analysis, the basis of the vector space is the set of B-Spline basis functions $\{N_{1,p}(\xi) \ N_{2,p}(\xi) \ \dots \ N_{n,p}(\xi)\}$ and the numbers are the coordinates $\{X_1 \ X_2 \ \dots \ X_n\}$ of the Control Points of the curve. A random vector u of the vector space V can be represented by the equation:

$$u = a_1u_1 + a_2u_2 + \dots + a_nu_n$$

which in Isogeometric Analysis applies as

$$C(\xi) = X_1 \cdot N_{1,p}(\xi) + X_2 \cdot N_{2,p}(\xi) + \dots + X_n \cdot N_{n,p}(\xi)$$

Any vector in V can be described as a linear combination of the basis. The numbers $\{a_1 \ a_2 \ \dots \ a_n\}$ are the coordinates of u and they are unique for this specific u and this specific basis.

Vector space V in \mathbb{R} is a mass of vectors with the properties below:

1. Commutativity of addition:

$$u + v = v + u, \quad \forall u, v \in V$$

In Isogeometric Analysis this property applies as

$$C_1(\xi) + C_2(\xi) = C_2(\xi) + C_1(\xi)$$

2. Associativity of addition:

$$u + (v + w) = (u + v) + w, \quad \forall u, v, w \in V$$

Respectively in Isogeometric Analysis,

$$C_1(\xi) + (C_2(\xi) + C_3(\xi)) = (C_1(\xi) + C_2(\xi)) + C_3(\xi)$$

3. Identity element of addition: There is an element $0 \in V$, the zero vector, so that

$$u + 0 = u, \quad \forall u \in V$$

In Isogeometric Analysis the equation applies as

$$C(\xi) + 0 = C(\xi)$$

4. Inverse elements of addition: There is an element $-u \in V$ such that

$$u + (-u) = 0, \quad \forall u \in V$$

The $-u$ is called the additive inverse of u . The equivalent in Isogeometric Analysis is

$$C(\xi) + (-C(\xi)) = 0$$

5. Identity element of scalar multiplication: For the real number 1, it applies:

$$1 \cdot u = u, \quad \forall u \in V$$

Respectively, in Isogeometric Analysis

$$1 \cdot C(\xi) = C(\xi)$$

6. Distributivity of scalar multiplication with respect to vector addition: $\forall a \in \mathbb{R}$ and $\forall u, v \in V$ applies the relation

$$a \cdot (u + v) = a \cdot u + a \cdot v$$

In Isogeometric Analysis this equation applies as

$$a \cdot (C_1(\xi) + C_2(\xi)) = a \cdot C_1(\xi) + a \cdot C_2(\xi)$$

7. Distributivity of scalar multiplication with respect to field addition: $\forall a, b \in \mathbb{R}$ and $\forall u \in V$ applies the relation

$$(a + b) \cdot u = a \cdot u + b \cdot u$$

which is implemented in Isogeometric Analysis as

$$(a + b) \cdot C(\xi) = a \cdot C(\xi) + b \cdot C(\xi)$$

8. Compatibility of scalar multiplication with field multiplication: $\forall a, b \in \mathbb{R}$ and $\forall u \in V$ applies the equation

$$a \cdot (b \cdot u) = (a \cdot b) \cdot u$$

Its equivalent in Isogeometric Analysis is

$$a \cdot (b \cdot C(\xi)) = (a \cdot b) \cdot C(\xi)$$

B-Spline basis functions are indeed the basis for a vector space with $\dim(V) = n$, where n is the number of Control Points. Control Points are the coordinates that transform the basis functions at any point in the given Physical Space. Conclusively,

$$\{N_{1,p}(\xi) \quad N_{2,p}(\xi) \quad \dots \quad N_{n,p}(\xi)\}$$

is the basis of the Vector space, while

$$\{X_1 \quad X_2 \quad \dots \quad X_n\}$$

are the coordinates for a vector $C(\xi)$. The familiar linear combination applies:

$$C(\xi) = X_1 \cdot N_{1,p}(\xi) + X_2 \cdot N_{2,p}(\xi) + \dots + X_n \cdot N_{n,p}(\xi)$$

Due to linear independence and vector space properties, it is understood that for a specific set of basis functions, only one set of Control Points can yield the appropriate geometry. If one wants to change the basis functions, the Control Points have to be shifted accordingly.

2.1.1.7 Fixed Number of Knot Values

A non-periodic Knot Value Vector that produces n functions of order p has $n + p + 1$ Knot Values.

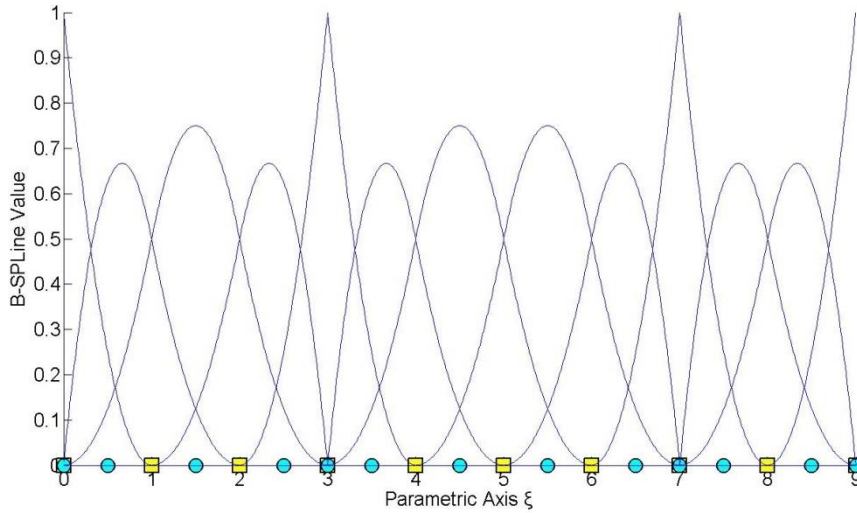


Figure 2.21
B-Spline Basis functions for Knot Value Vector
 $\Xi = \{0 \ 0 \ 0 \ 1 \ 2 \ 3 \ 3 \ 4 \ 5 \ 6 \ 7 \ 7 \ 8 \ 9 \ 9 \ 9\}$

In this example the degree is $p = 2$ and we have thirteen basis functions produced, so $n = 13$.

We observe that the Knot Value Number is $k = n + p + 1 = 13 + 2 + 1 = 16$. This occurs because for the creation of n basis functions of degree p , needed to construct the curve, $n + p$ basis functions of order $p = 0$ are used, hence $n + p + 1$ Knot Values are needed.

In another approach, each Control Point has a Knot Value Support of $p + 2$ Knot Values. For n Control Points, $n \cdot (p + 2)$ Knot Values are needed. There are $(p + 1)$ Knot Values repeated in $(n - 1)$ Control Point interconnections. The total number of Knot Values is:

$$n \cdot (p + 2) - (n - 1) \cdot (p + 1) = n \cdot p + 2n - n \cdot p - n + p + 1 = n + p + 1$$

Therefore, $n + p + 1$ Knot Values are required.

2.1.1.8 Shared Support

Each B-Spline shares support with at most $2p$ B-Splines. More specifically, each basis function shares support with at most p basis functions on each side. This results in higher interconnection, compared to equivalent Finite Element Method Shape functions. Basis function overlapping leads to interconnectivity between Control Points as well.

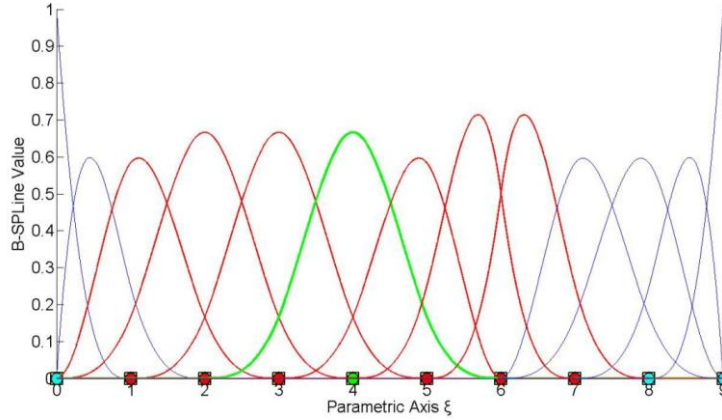


Figure 2.22

Shared support for $N_{6,3}(\xi)$.

$$\Xi = \{0 \ 0 \ 0 \ 0 \ 1 \ 2 \ 3 \ 4 \ 5 \ 6 \ 6 \ 7 \ 8 \ 9 \ 9 \ 9 \ 9\}$$

$N_{6,3}(\xi)$ interacts with $p = 3$ basis functions on each side, $N_{3,2}(\xi)$, $N_{4,2}(\xi)$ and $N_{5,2}(\xi)$ on the left, $N_{7,2}(\xi)$, $N_{8,2}(\xi)$, $N_{9,2}(\xi)$ on the right. As a result, the respective positions in the Stiffness Matrix will be non-zero.

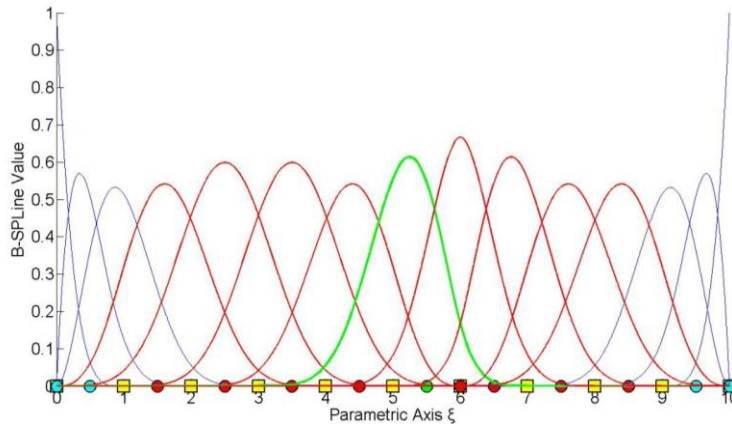


Figure 2.23

Shared support for $N_{8,4}(\xi)$.

$$\Xi = \{0 \ 0 \ 0 \ 0 \ 0 \ 1 \ 2 \ 3 \ 4 \ 5 \ 6 \ 6 \ 7 \ 8 \ 9 \ 10 \ 10 \ 10 \ 10 \ 10\}$$

$N_{8,4}(\xi)$ shares support with $2p = 8$ basis functions, 4 on each side. Greater-order basis functions tend to create more dense Stiffness Matrices and therefore demand more computational power.

2.3.6 B-SPLine Basis Function Derivatives

Basis function derivatives are widely used in Isogeometric Analysis. Deformation and Stiffness Matrices are built upon the derivatives of Shape functions. As a result, the distribution of stresses and strains across the model is based on those derivatives. The derivatives of B-SPLines, as obtained from the recursive formula, are represented as a linear combination of previous polynomial order basis functions:

$$\frac{d}{d\xi} N_{i,p}(\xi) = \frac{p}{\xi_{i+p} - \xi_i} \cdot N_{i,p-1}(\xi) - \frac{p}{\xi_{i+p+1} - \xi_{i+1}} \cdot N_{i+1,p-1}(\xi)$$

This leads to a generalized equation for the k^{th} derivative:

$$\begin{aligned} \frac{d^k}{d\xi^k} N_{i,p}(\xi) &= \frac{p!}{(p-k)!} \cdot \sum_{j=0}^k a_{k,j} \cdot N_{i+j,p-k}(\xi) \\ a_{0,0} &= 1 \\ a_{k,0} &= \frac{a_{k-1,0}}{\xi_{i+p-k+1} - \xi_i} \\ a_{k,j} &= \frac{a_{k-1,j} - a_{k-1,j-1}}{\xi_{i+p+j-k+1} - \xi_{i+j}}, \quad j=1, \dots, k-1, \\ a_{k,k} &= \frac{-a_{k-1,k-1}}{\xi_{i+p+1} - \xi_{i+k}} \end{aligned}$$

The partial derivatives of two-directional B-SPLine Shape functions can be easily obtained by application of the quotient rule:

$$\begin{aligned} \frac{\partial}{\partial \xi} R_{i,j}^{p,q}(\xi, \eta) &= \left(\frac{d}{d\xi} N_{i,p}(\xi) \right) \cdot M_{j,q}(\eta) \\ \frac{\partial}{\partial \eta} R_{i,j}^{p,q}(\xi, \eta) &= N_{i,p}(\xi) \cdot \left(\frac{d}{d\eta} M_{j,q}(\eta) \right) \end{aligned}$$

3D Shape function derivatives per direction can be obtained in the same manner

$$\begin{aligned} \frac{\partial}{\partial \xi} R_{i,j,k}^{p,q,r}(\xi, \eta, \zeta) &= \left(\frac{d}{d\xi} N_{i,p}(\xi) \right) \cdot M_{j,q}(\eta) \cdot L_{k,r}(\zeta) \\ \frac{\partial}{\partial \eta} R_{i,j,k}^{p,q,r}(\xi, \eta, \zeta) &= N_{i,p}(\xi) \cdot \left(\frac{d}{d\eta} M_{j,q}(\eta) \right) \cdot L_{k,r}(\zeta) \\ \frac{\partial}{\partial \zeta} R_{i,j,k}^{p,q,r}(\xi, \eta, \zeta) &= N_{i,p}(\xi) \cdot M_{j,q}(\eta) \cdot \left(\frac{d}{d\zeta} L_{k,r}(\zeta) \right) \end{aligned}$$

2.3.7 B-SPLine Curves, Surfaces and Solids

Given a Knot Value Vector Ξ and a polynomial order p , we can evaluate the B-SPLine functions at every ξ . In order to create the B-SPLine curve, we also need a vector of coordinates for each basis function, the Control Points $\mathbf{X}_i = \{X_i \ Y_i \ Z_i\}$. The curve is evaluated for every ξ as a linear combination of basis functions:

$$C(\xi) = \sum_{i=1}^n \{N_{i,p}(\xi) \cdot \mathbf{X}_i\}$$

After evaluating the Shape functions, the B-SPLine surface is defined in analogy to the B-SPLine curve:

$$S(\xi, \eta) = \sum_{i=1}^n \sum_{j=1}^m \{N_{i,p}(\xi) \cdot M_{j,q}(\eta) \cdot \mathbf{X}_{i,j}\} = \sum_{i=1}^n \sum_{j=1}^m \{R_{i,j}^{p,q} \cdot \mathbf{X}_{i,j}\}$$

Using the tensor product properties, we can also evaluate the solid function:

$$S(\xi, \eta, \zeta) = \sum_{i=1}^n \sum_{j=1}^m \sum_{k=1}^l \{N_{i,p}(\xi) \cdot M_{j,q}(\eta) \cdot L_{k,r}(\zeta) \cdot \mathbf{X}_{i,j,k}\} = \sum_{i=1}^n \sum_{j=1}^m \sum_{k=1}^l \{R_{i,j,k}^{p,q,r}(\xi, \eta, \zeta) \cdot \mathbf{X}_{i,j,k}\}$$

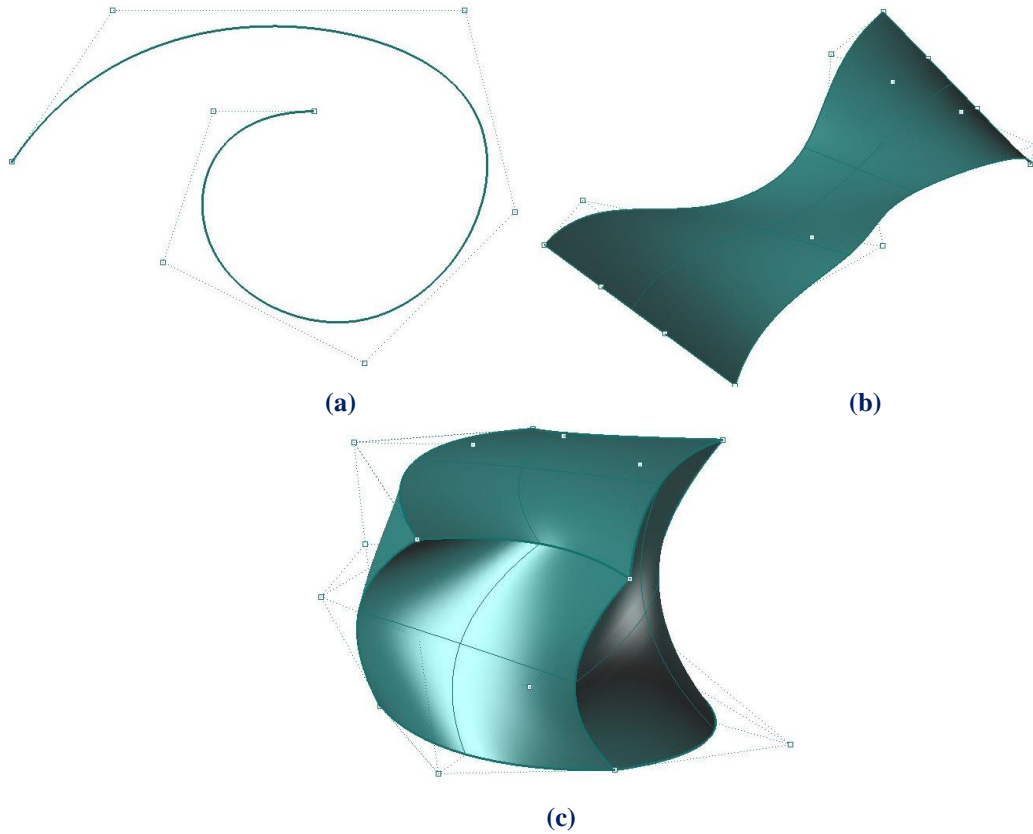


Figure 2.24

B-SPLine Entities. (a) Curve, (b) Surface and (c) Solid.

2.3.8 B-SPLine Curve Properties

B-SPLine curve entities have the following properties, as obtained from Piegl, Tiller:

1. B-SPLine curves are a generalization of Bezier curves.
2. $C(\xi)$ is a piecewise polynomial curve.
3. Each basis function corresponds to a certain Control Point.
4. The first and last Control Point as well as internal Control Points corresponding to C^0 Continuous basis functions are interpolatory to the curve.
5. B-SPLine curves possess strong convex hull property.
6. Moving a Control Point X_i only changes part of the curve.
7. The Control Polygon represents a piecewise linear approximation to the curve.
8. It is possible to use multiple Control Points with the same coordinates.
9. Any transformation applied to the curve can be applied directly at the Control Points. This property is known as “affine invariance” or “affine covariance”.
10. In every Knot Span, at most $p+1$ Control Points contribute to the definition of the curve, corresponding to the $p+1$ non-zero basis functions.
11. Since $C(\xi)$ is a linear combination of $N_{i,p}(\xi)$, curve Continuity and differentiability are obtained straight from the basis functions.
12. No line has more intersections with the curve, than with the Control Polygon.

2.1.1.9 Generalization of Bezier curves

B-SPLine curves are a generalization of Bezier curves. Given an open Knot Vector and $n = p+1$ Control Points, a Bezier curve is produced.

Bezier curves were utilized in CAD methods before B-SPLines. Figure 2.25 presents a Bezier curve with $p=3$, an open Knot Value Vector $\{0 \ 0 \ 0 \ 0 \ 1 \ 1 \ 1 \ 1\}$ and $n = p+1=4$ Control Points. Bezier curves are B-SPLine curves defined in only one Knot Span. As a result, every basis function is non-zero across the entire parameter space and Control Points affect the shape of the entire curve. Bezier surfaces are a special case of one-rectangle B-SPLine surfaces and Bezier solids a special case of one-cuboid B-SPLine solids as well.

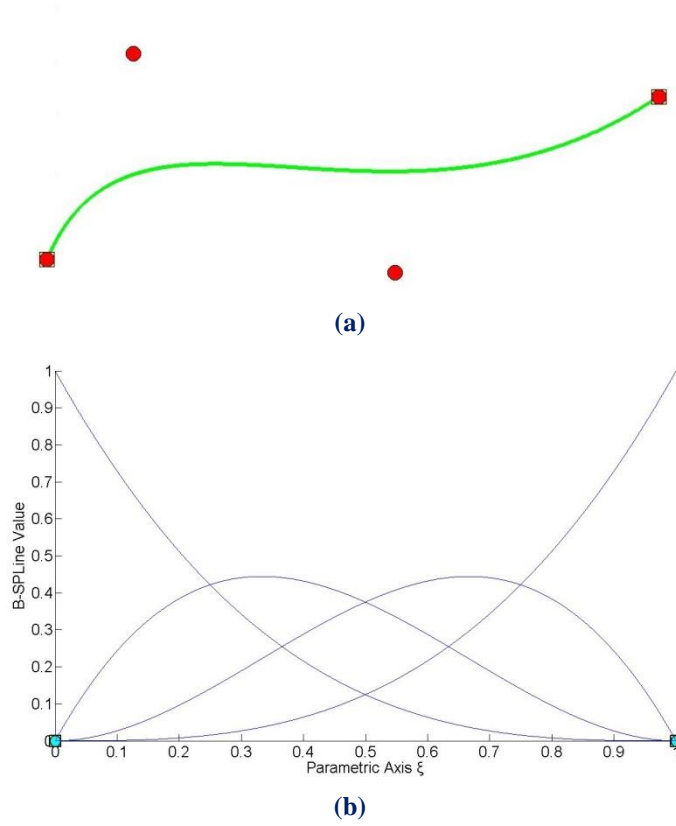


Figure 2.25
B-Spline as generalization of Bezier curves. (a) Physical Space and (b) basis functions

2.1.1.10 Piecewise polynomial curve

$C(\xi)$ is formed from piecewise polynomials $N_{i,p}(\xi)$, and therefore is a piecewise polynomial curve.

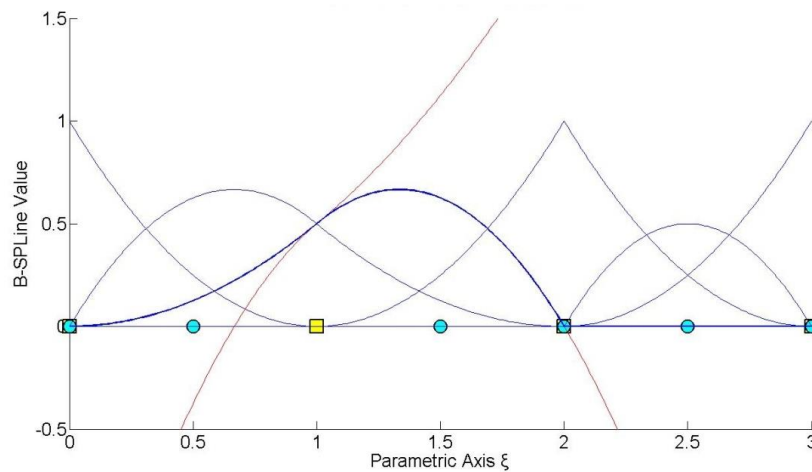


Figure 2.26
Piecewise polynomials that form a B-Spline basis function. Knots represent the boundaries of the pieces.

A B-Spline curve is obtained through the curve function:

$$C(\xi) = \sum_{i=1}^n N_{i,p}(\xi) \cdot X_i$$

which is a linear combination of piecewise polynomial basis functions. This applies in multi-directional entities as well. Tensor product Shape functions are piecewise polynomials with respect to the corresponding directions, thus B-Spline Surfaces and Solids are also piecewise polynomials. The term B-Spline, after all, stands for Basis - Smooth Polynomial Line.

2.1.1.11 Control Point – Basis Function Correspondence

Each basis function corresponds to a certain Control Point. There are n basis functions and n Control Points in a B-Spline curve.

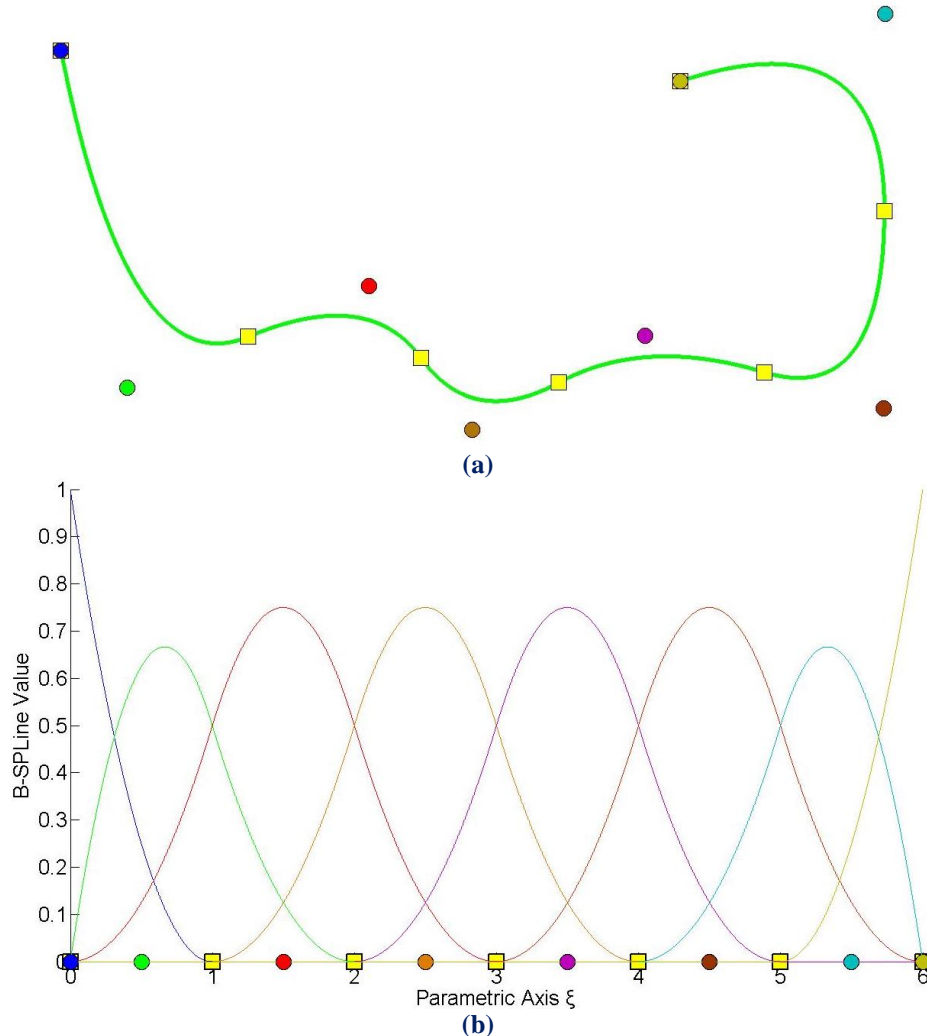


Figure 2.27
 (a) Physical Space and (b) basis functions with the corresponding Control Points.

In Figure 2.27, Control Points are represented both in Parameter and Physical Space. Each Point controls a specific basis function. This property also applies for multiple directions. Every Control Point of the surface or the solid is tensor product of a Control Point in directions ξ , η and ζ . By extension, the corresponding B-Spline is tensor product of the basis functions. In the most general case, there are $n \cdot m \cdot l$ Control Points and basis functions.

2.1.1.12 Interpolation to the Curve

The first and last Control Points are interpolatory to the curve. Any internal Control Point corresponding to C^0 Continuous basis function is also interpolatory to the curve.

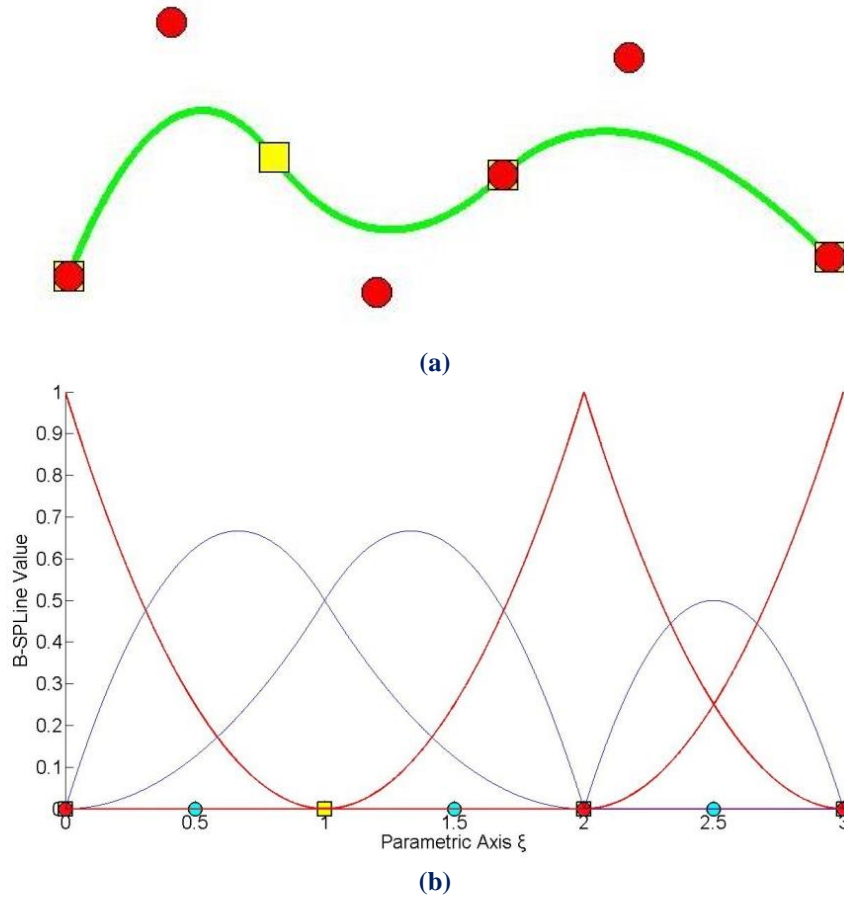


Figure 2.28
Control Point interpolation. (a) B-Spline curve and (b) the reciprocal basis functions

In Figure 2.28, the first and the last Control Point, which have C^{-1} Continuity, are interpolatory to the curve. This can be explained with the help of the equation of the curve:

$$C(\xi) = \sum_{i=1}^n \{N_{i,2}(\xi) \cdot X_i\}$$

For $\xi = 0$, it applies that:

$$C(0) = \sum_{i=1}^n N_{i,2}(0) \cdot X_i$$

where,

$$N_{1,2}(0) = 1$$

$$N_{i,2}(0) = 0, \quad i = 2, \dots, 6$$

so,

$$C(0) = N_{1,2}(0) \cdot X_1 = X_1$$

And for $\xi = 3$:

$$C(3) = \sum_{i=1}^n N_{i,2}(3) \cdot X_i$$

$$N_{6,2}(3) = 1$$

$$N_{i,2}(3) = 0, \quad i = 1, \dots, 5$$

so,

$$C(3) = N_{6,2}(3) \cdot X_6 = X_6$$

Likewise, the internal Control Point, with C^0 Continuity across $\xi = 2$ is interpolatory to the curve because:

$$C(2) = \sum_{i=1}^n \{N_{i,2}(2) \cdot X_i\}$$

$N_{4,2}(2) = 1$, as this is the only non-zero basis function across $\xi = 2$

$$N_{i,2}(2) = 0, \quad i \neq 4$$

so,

$$C(2) = N_{4,2}(2) \cdot X_4 = X_4$$

Observe that both the form of the curve and the form of the basis functions indicate that this geometry could be represented by two different sets of Knot Vectors and Control Points, with absolutely no deflections from the current representation. This will be examined thoroughly later.

Interpolation also applies for Surfaces and Solids, when appropriately reduced Continuity is used for all directions at a Knot. C^{-1} Continuity is required for external Knots and C^0 for internal.

In Figure 2.29, $N_{5,2}(\xi)$ at axis ξ and $M_{6,2}(\eta)$ at axis η have C^0 Continuity. Therefore the Control Point corresponding to $R_{5,6}^{2,2}(\xi, \eta)$ is interpolatory to the surface. The external Control Points with C^{-1} Continuity at both directions are also interpolatory to the surface.

In Figure 2.30, $N_{4,2}(\xi)$ at parametric axis ξ and $M_{4,2}(\eta)$ at parametric axis η have C^0 Continuity, thus Control Points corresponding to the Shape functions $R_{4,4,1}^{2,2,1}(\xi, \eta, \zeta)$ and $R_{4,4,2}^{2,2,1}(\xi, \eta, \zeta)$, are interpolatory to the solid. As we can see, the external Control Points are also interpolatory to the solid, because Continuity is reduced to C^{-1} .

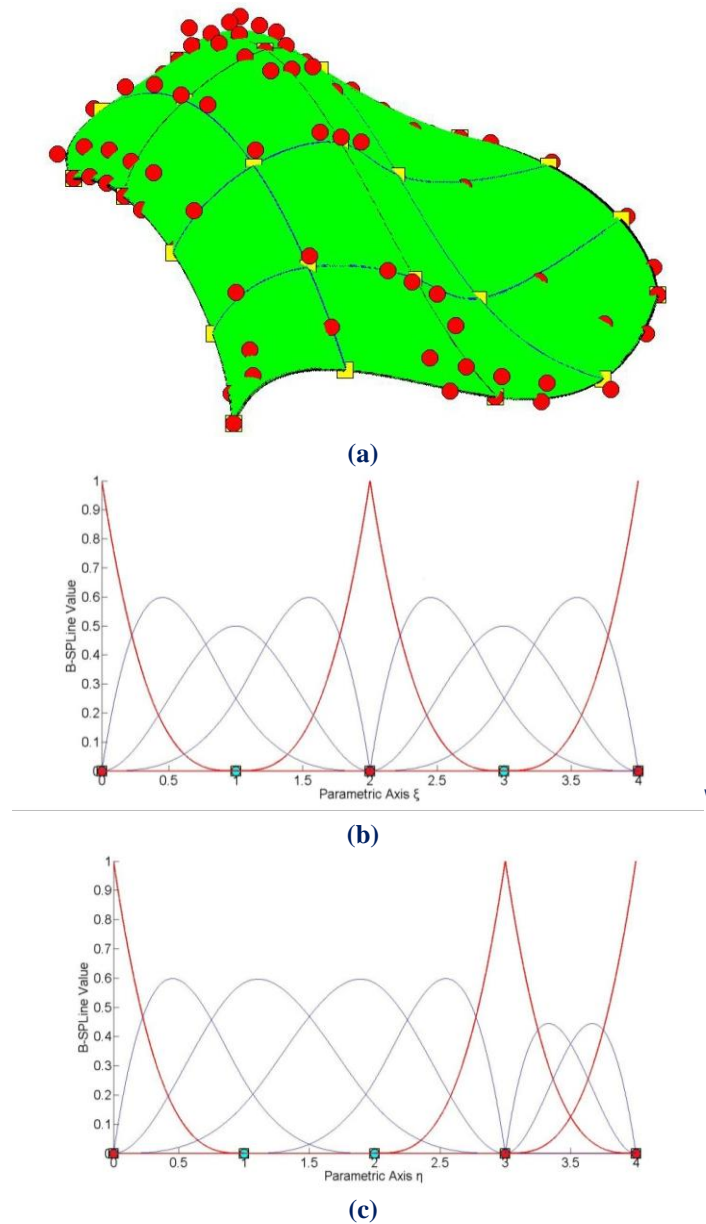
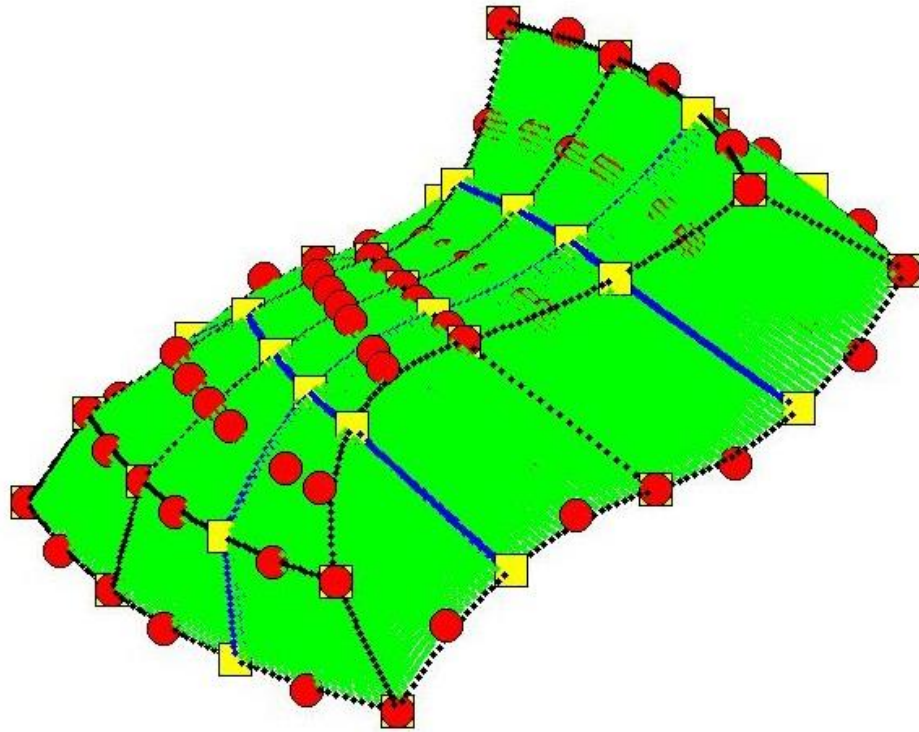
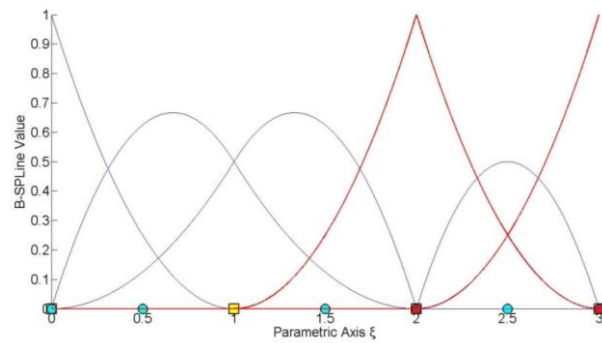


Figure 2.29

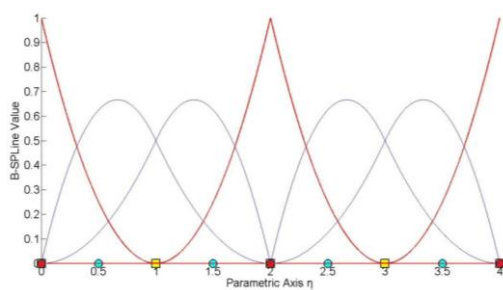
(a) B-SPLine Surface and (b), (c) the corresponding basis functions in axes ξ, η .



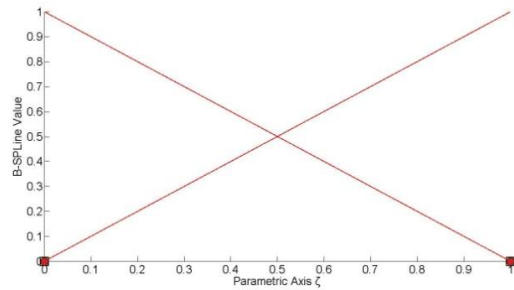
(a)



(b)



(c)



(d)

Figure 2.30
 (a) Solid in the Physical Space
 with (b), (c), (d) the associated basis functions in axes ξ, η, ζ .

2.1.1.13 Convex Hull

B-SPLine curves possess strong convex hull property. The convex hull of the curve is defined as the sum of the convex hulls of $p+1$ consecutive Control Points. The curve is always contained in the convex hull.

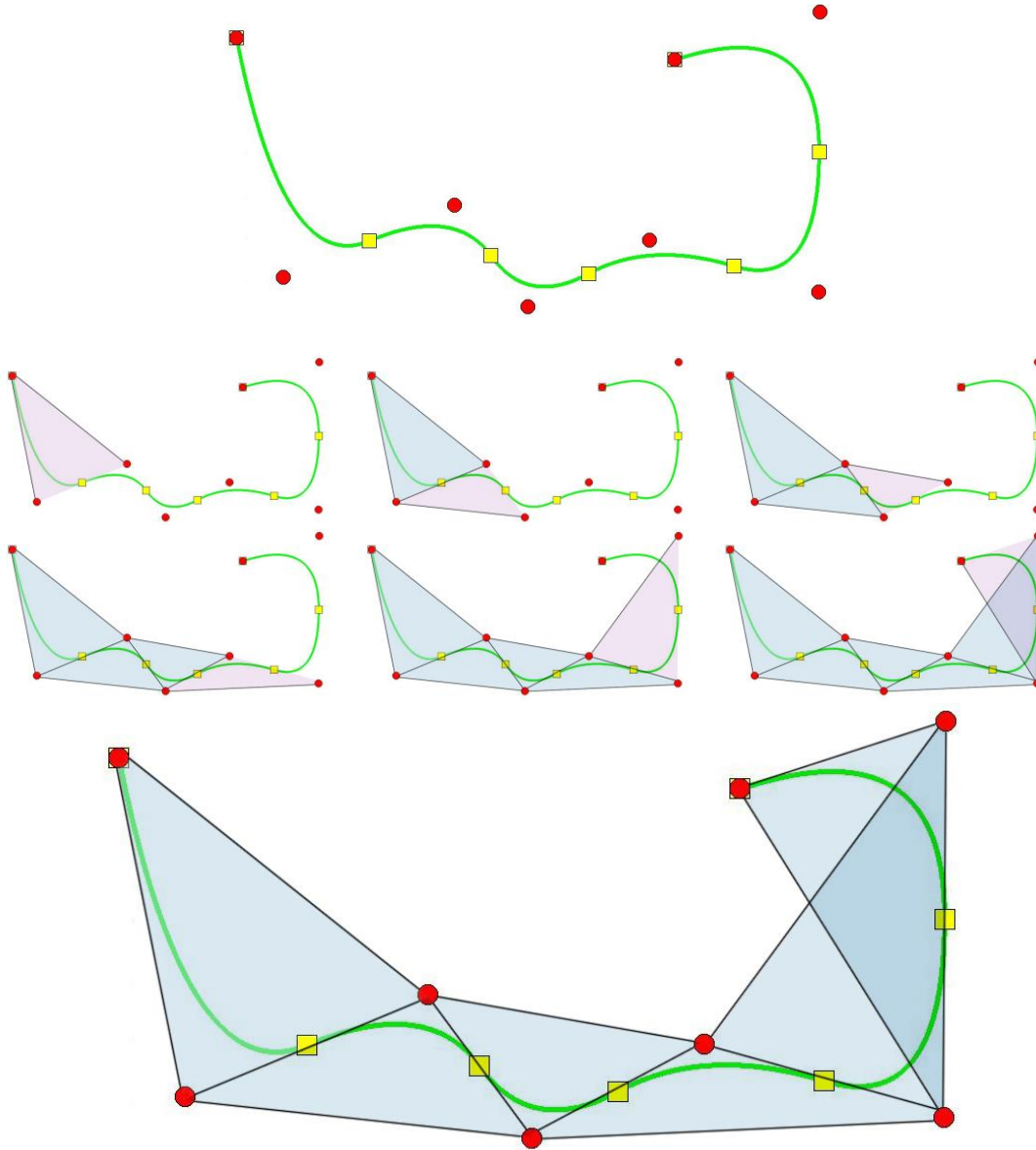


Figure 2.31
Step-by-step convex hull creation for a B-SPLine curve.

The curve in Figure 2.31 has a degree of $p = 2$. The convex hull is formed by connecting each Control Point with the $p = 2$ successive ones. As we can easily see in the figure, the union of the convex hulls contains the curve. The convex hull is a way to assume the general form of a B-SPLine curve.

2.1.1.14 Control Point Local support

Moving a Control Point X_i only changes part of the curve, more specifically the part corresponding to the $[\xi_i, \xi_{i+p+1})$ Knot Value Spans. This is a result of the local support of the corresponding B-Spline function.

Moving along the curve, basis function $N_{i,p}(\xi)$ is switched “on” at the Knot Value ξ_i and then again switched “off” at the Knot Value ξ_{i+p+1} , where the function $N_{i+p+1,p}(\xi)$ is switched “on”.

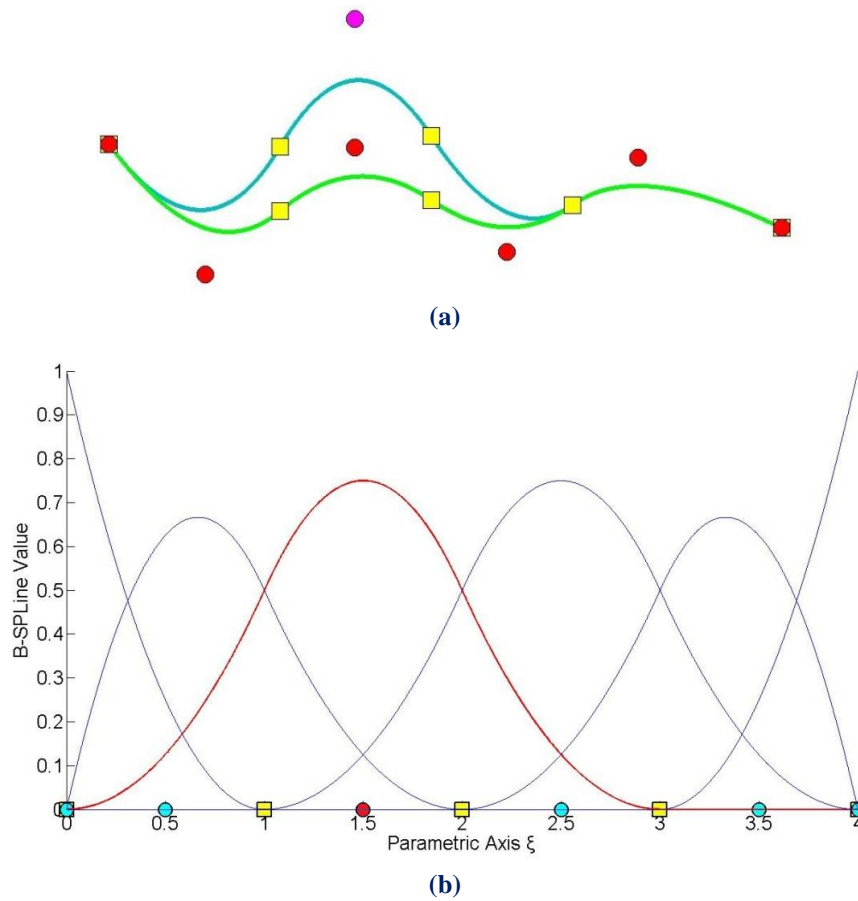


Figure 2.32
Control Point Local support (a) in Physical and (b) in Parameter Space.

Every Control Point is associated with a basis function. Support of the Control Point is defined by the support of the corresponding basis function. Therefore, Control Points affect only part of the curve. In Figure 2.32, a curve with $p = 2$ and Knot Value Vector $\{0 \ 0 \ 0 \ 1 \ 2 \ 3 \ 4 \ 4 \ 4\}$, is presented. The Control Point for $i = 3$ is moved and this affects partially the entity.

In this example, $N_{3,2}(\xi)$ spans from $\xi = 0$ to $\xi = 3$. The Knots act as boundaries of the support. For $\xi = 3$, $N_{3,2}(\xi)$ is switched “off” and $N_{6,2}(\xi)$ is switched “on”.

Local support of Control Points is also expanded by tensor product properties. The local support of a Multi-directional Control Point is the tensor product of the respective supports.

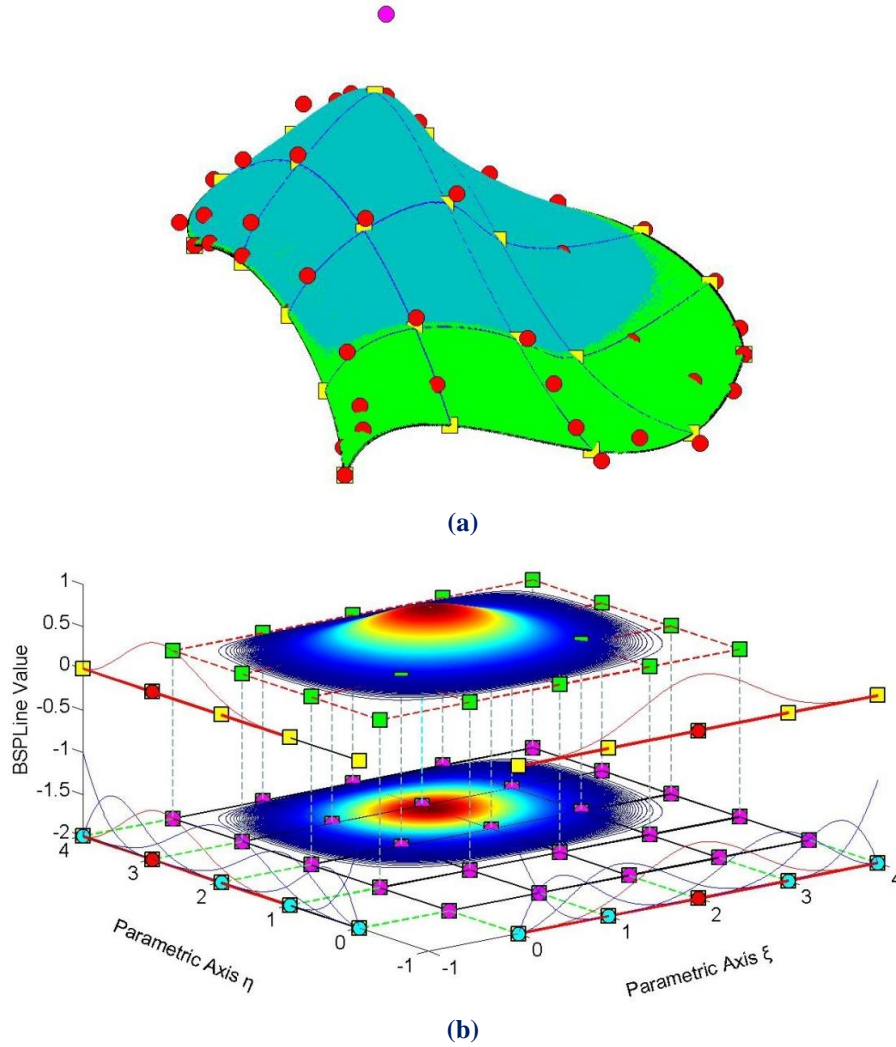


Figure 2.33
Local support of a 2D Control Point.
Surface (a) in Physical and (b) in Parameter Space.

Figure 2.33 represents the local support in the parametric axis ξ, η of $N_{4,2}(\xi)$ and $M_{3,2}(\eta)$ B-Spline curves respectively. In parametric axis ξ the local support expands throughout the axis, whereas in parametric axis η the basis function is switched “on” at the second Knot Span. In Figure 2.33.a, the tensor product of the respective supports for ξ, η is represented in cyan. It spans across $4 \times 3 = 12$ Knot Rectangles in total.

The same properties apply for B-Spline solids as well.

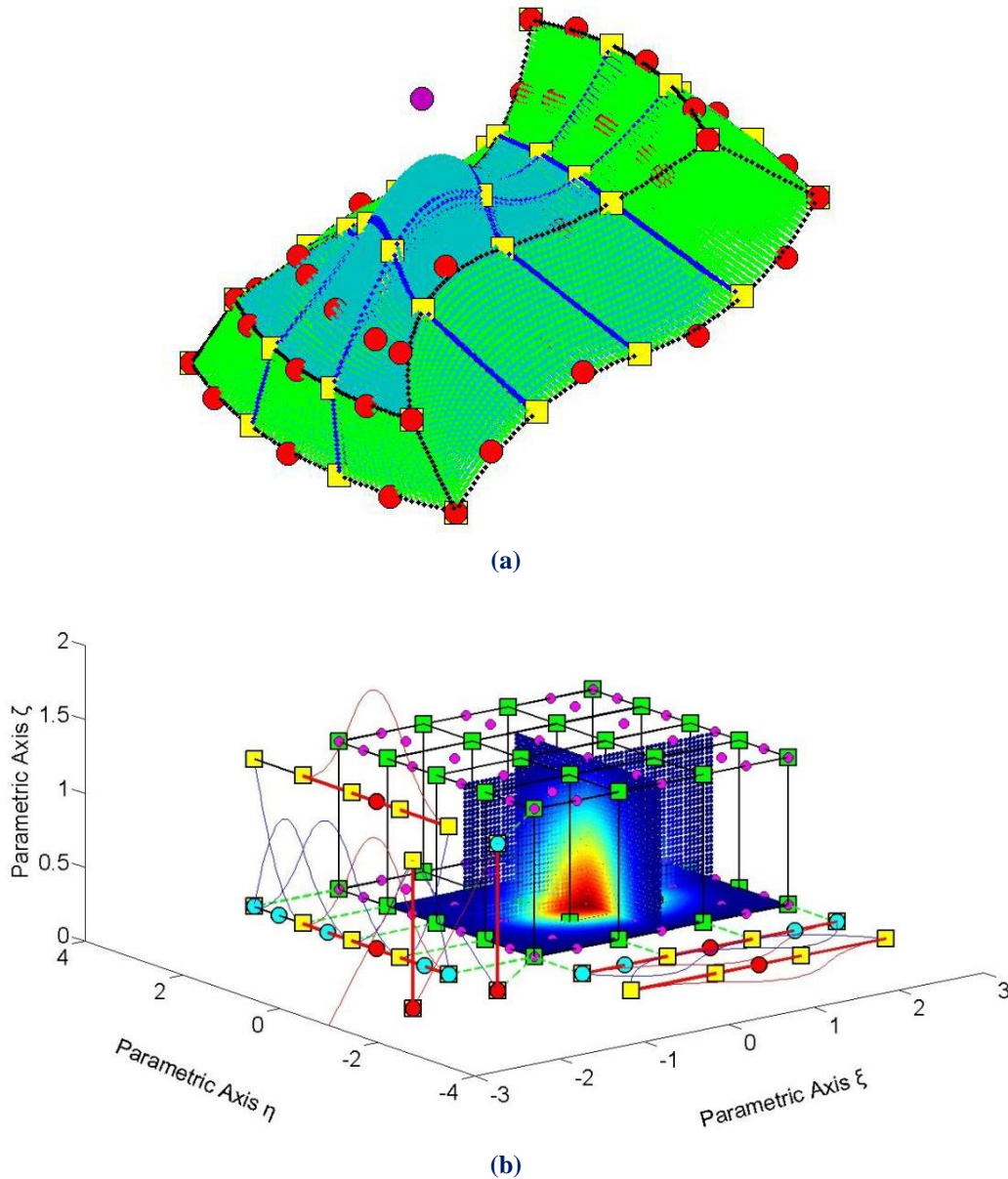


Figure 2.34
 Local support of a 3D Control Point.
 Solid (a) in Physical and (b) in Parameter Space.

Figure 2.34.b presents the local support of $N_{3,2}(\xi)$, $M_{4,2}(\eta)$ and $L_{1,1}(\zeta)$. In parametric axes ξ , ζ , the local support expands at all Knot Spans, whereas in the parametric axis η the local support spans between Knots 1 and 4. In Figure 2.34.a, the local support is displayed in cyan and it does not reach all the Knot Spans in parametric axis η . A total of $3 \cdot 3 \cdot 1 = 9$ Knot Cuboids represent the Support of the Control Point.

2.1.1.15 Control Polygon approximation

The Control Polygon represents a piecewise linear approximation to the curve. Due to convex hull properties, Refinement by knot insertion or order elevation brings the Control Polygon closer to the curve.

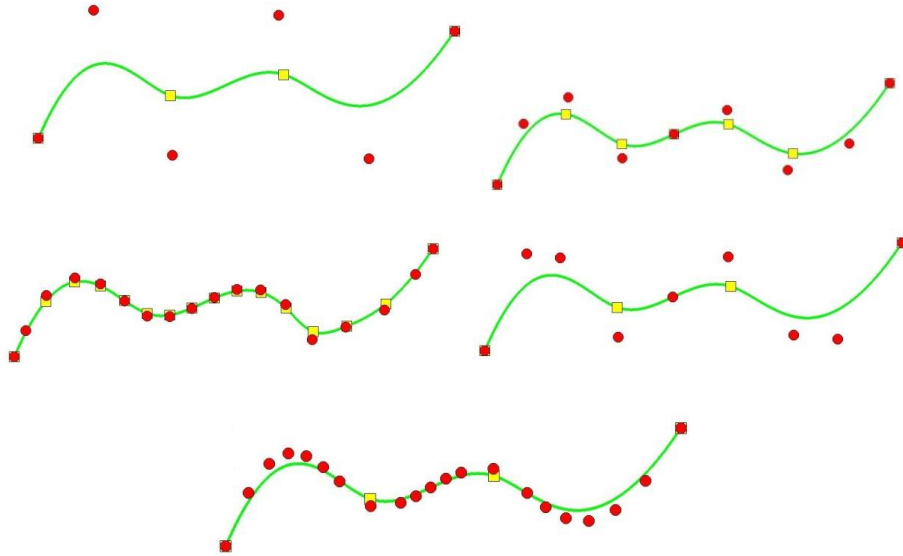


Figure 2.35
Control Polygon approximation through Refinement.

In Figure 2.35 a curve of degree $p=3$ is designed. The Control Polygon already represents a linear approximation to the curve. When consecutive h- or p- Refinements are applied, the Control Polygon is brought even closer to the curve. Refined Control Polygons provide a general idea of the form of the curve. This property also applies for multiple directions.

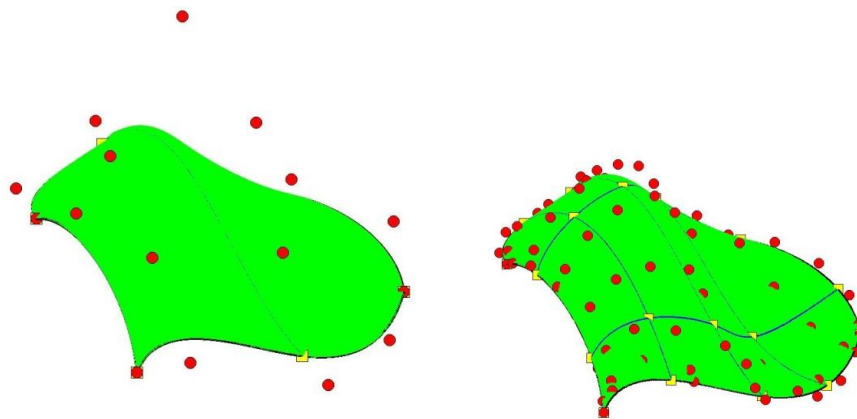


Figure 2.36
Control Net approximation through Surface h-Refinement.

For example, in Figure 2.36, the Refinements, that were made, brought the Control Net closer to the surface.

2.1.1.16 Multiple Control Points

It is possible to use multiple Control Points with the same coordinates. This can prove to be very useful.

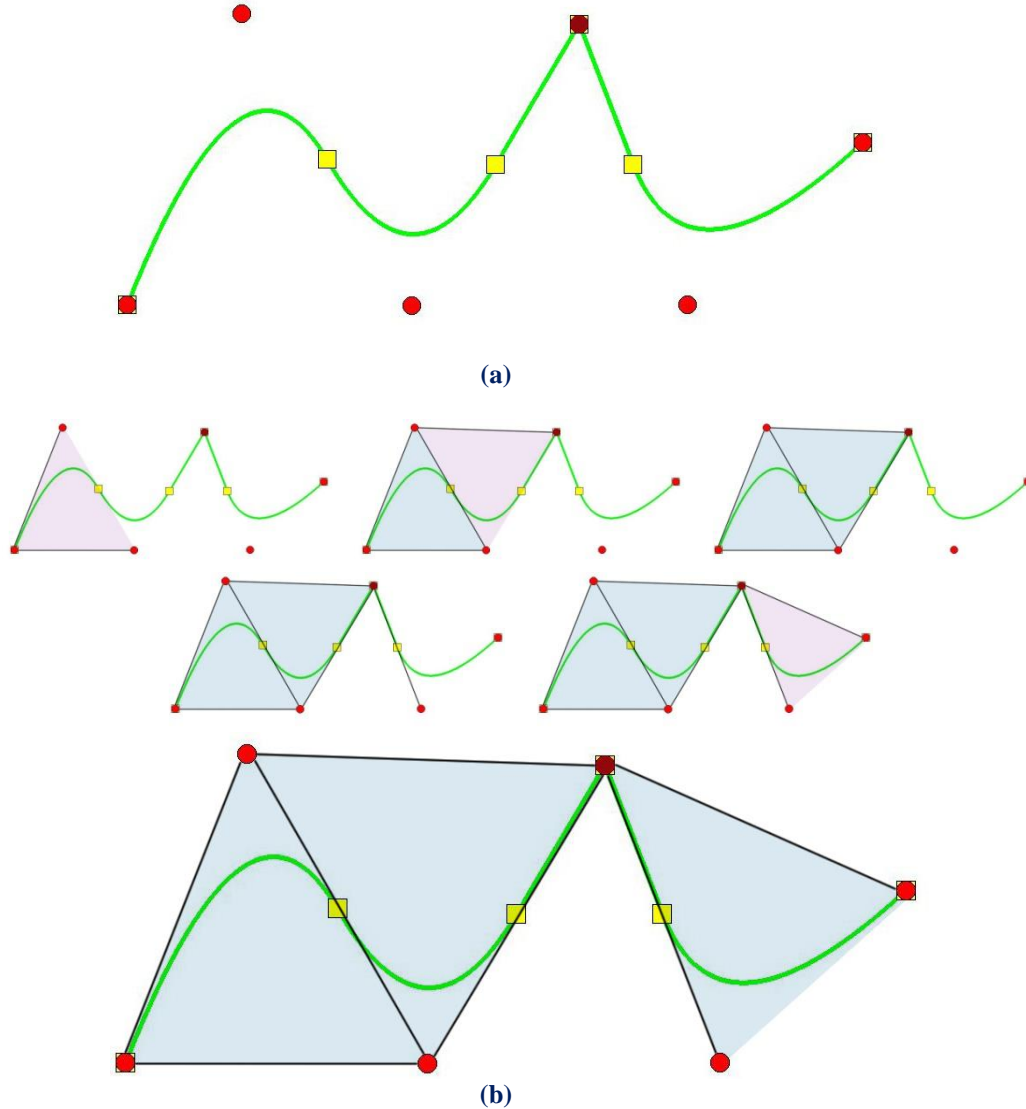


Figure 2.37
(a) Physical Space and **(b)** Convex Hull creation for a curve with two coincident Control Points (drawn in deep red).

In Figure 2.37.a, a quadratic curve with a double Control Point is designed. The curve is interpolatory at these Points and a sharp edge is formed. This is explained in Figure 2.37.b, where the convex hull of the curve is designed. The curve is always contained in the convex hull, therefore a sharp edge has to be formed exactly at the double Point coordinates. Inductively, this applies when p coincident Control Points are used in a curve of polynomial degree p .

2.4 Non-Uniform Rational B-SPLines

B-SPLine geometries may have many promising attributes, but they also have several weaknesses in geometrical representation. Some basic geometrical forms cannot be presented as B-SPLine entities, such as circles or conic sections in general. In order to solve this problem, the CAD industry introduced Non-Uniform Rational B-Splines (NURBS). The basic idea is simple. A NURBS entity is produced from the actual section of a cone with a plane.

2.4.1 Basic Idea

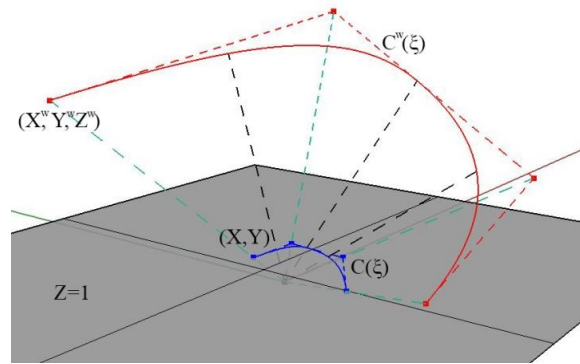


Figure 2.38
B-SPLine curve and projective transformation to NURBS Curve.

As shown in Figure 2.38, the projective B-SPLine curve $C^w(\xi)$ is created from the projective 3D Control Points $X^w = \{X^w \ Y^w \ Z^w\}$.

Projection of the curve and Control Points on the plane $z = 1$ produces the NURBS curve $C(\xi)$ and the 2D Control Points:

$$X = \{X \ Y\}$$

where,

$$\{X_i \ Y_i\} = \left\{ \begin{array}{cc} X_i^w & Y_i^w \\ Z_i^w & Z_i^w \end{array} \right\}$$

The Weights of the NURBS curve are defined as:

$$w = \{Z^w\}$$

In generalization, n -dimensional Rational B-SPLines are projections of $(n+1)$ -dimensional non-rational B-SPLines.

2.4.2 NURBS Shape Functions

In order to evaluate NURBS Shape functions, the Weighting function is defined:

$$W(\xi) = \sum_{i=1}^n \{N_{i,p}(\xi) \cdot w_i\}$$

In most engineering applications, Weights have positive values. Unless otherwise stated, they will be considered positive for the scope of this thesis. $W(\xi)$ is in fact the Z-coordinate of the projective B-SPLine curve. Projective transformation is applied by dividing the other two coordinates of the B-SPLine curve with the Z-coordinate. NURBS Shape functions are calculated from

$$R_i^p(\xi) = \frac{N_{i,p}(\xi) \cdot w_i}{W(\xi)} = \frac{N_{i,p}(\xi) \cdot w_i}{\sum_{i'=1}^n \{N_{i',p}(\xi) \cdot w_{i'}\}}$$

$R_i^p(\xi)$ are piecewise rational functions. The expression “the order of NURBS” refers to the order of the projective B-SPLine curve.

NURBS Shape Functions in multiple directions can be obtained as tensor products of one-directional basis functions:

Shape functions for two directions:

$$R_{i,j}^{p,q}(\xi, \eta) = \frac{N_{i,p}(\xi) \cdot M_{j,q}(\eta) \cdot w_{ij}}{\sum_{i'=1}^n \sum_{j'=1}^m \{N_{i',p}(\xi) \cdot M_{j',q}(\eta) \cdot w_{i'j'}\}}$$

$$W(\xi, \eta) = \sum_{i'=1}^n \sum_{j'=1}^m \{N_{i',p}(\xi) \cdot M_{j',q}(\eta) \cdot w_{i'j'}\}$$

Similarly, we expand the equations in order to obtain tensor product 3D Shape functions:

$$R_{i,j,k}^{p,q,r}(\xi, \eta, \zeta) = \frac{N_{i,p}(\xi) \cdot M_{j,q}(\eta) \cdot L_{k,r}(\zeta) \cdot w_{ijk}}{\sum_{i'=1}^n \sum_{j'=1}^m \sum_{k'=1}^l \{N_{i',p}(\xi) \cdot M_{j',q}(\eta) \cdot L_{k',r}(\zeta) \cdot w_{i'j'k'}\}}$$

The Weighting function is now defined as:

$$W(\xi, \eta, \zeta) = \sum_{i'=1}^n \sum_{j'=1}^m \sum_{k'=1}^l \{N_{i',p}(\xi) \cdot M_{j',q}(\eta) \cdot L_{k',r}(\zeta) \cdot w_{i'j'k'}\}$$

Observe that for $w_{ijk} = 1, \forall i, j, k$, it applies that NURBS Shape functions downgrade to B-SPLine basis functions. Actually, NURBS entities are a generalization of B-SPLine entities. All the B-SPLine properties examined in this thesis apply for NURBS as well.

2.4.3 NURBS Shape Function Derivatives

Simple application of the quotient rule yields the derivatives of NURBS Shape functions for one and multiple directions.

$$\frac{d}{d\xi} R_i^p(\xi) = w_i \cdot \frac{\left(\frac{d}{d\xi} N_{i,p}(\xi) \right) \cdot W(\xi) - \left(\frac{d}{d\xi} W(\xi) \right) \cdot N_{i,p}(\xi)}{(W(\xi))^2}$$

where

$$\frac{d}{d\xi} W(\xi) = \sum_{i=1}^n \left(\frac{d}{d\xi} N_{i,p}(\xi) \right) \cdot w_i$$

For bidirectional Shape functions:

$$\frac{\partial}{\partial \xi} R_{i,j}^{p,q}(\xi, \eta) = w_{ij} \cdot \frac{\left(\frac{d}{d\xi} N_{i,p}(\xi) \right) \cdot M_{j,q}(\eta) \cdot W(\xi, \eta) - \left(\frac{\partial}{\partial \xi} W(\xi, \eta) \right) \cdot N_{i,p}(\xi) \cdot M_{j,q}(\eta)}{(W(\xi, \eta))^2}$$

$$\frac{\partial}{\partial \eta} R_{i,j}^{p,q}(\xi, \eta) = w_{ij} \cdot \frac{N_{i,p}(\xi) \cdot \left(\frac{d}{d\eta} M_{j,q}(\eta) \right) \cdot W(\xi, \eta) - \left(\frac{\partial}{\partial \eta} W(\xi, \eta) \right) \cdot N_{i,p}(\xi) \cdot M_{j,q}(\eta)}{(W(\xi, \eta))^2}$$

Derivatives of 3D Shape functions per direction are evaluated as shown

$$\begin{aligned} & \frac{\partial}{\partial \xi} R_{i,j,k}^{p,q,r}(\xi, \eta, \zeta) = \\ & = w_{ijk} \cdot \frac{\left(\frac{d}{d\xi} N_{i,p}(\xi) \right) \cdot M_{j,q}(\eta) \cdot L_{k,r}(\zeta) \cdot W(\xi, \eta, \zeta) - \left(\frac{\partial}{\partial \xi} W(\xi, \eta, \zeta) \right) \cdot N_{i,p}(\xi) \cdot M_{j,q}(\eta) \cdot L_{k,r}(\zeta)}{(W(\xi, \eta, \zeta))^2} \end{aligned}$$

$$\begin{aligned} & \frac{\partial}{\partial \eta} R_{i,j,k}^{p,q,r}(\xi, \eta, \zeta) = \\ & = w_{ijk} \cdot \frac{N_{i,p}(\xi) \cdot \left(\frac{d}{d\eta} M_{j,q}(\eta) \right) \cdot L_{k,r}(\zeta) \cdot W(\xi, \eta, \zeta) - \left(\frac{\partial}{\partial \eta} W(\xi, \eta, \zeta) \right) \cdot N_{i,p}(\xi) \cdot M_{j,q}(\eta) \cdot L_{k,r}(\zeta)}{(W(\xi, \eta, \zeta))^2} \end{aligned}$$

$$\begin{aligned} & \frac{\partial}{\partial \zeta} R_{i,j,k}^{p,q,r}(\xi, \eta, \zeta) = \\ & = w_{ijk} \cdot \frac{N_{i,p}(\xi) \cdot M_{j,q}(\eta) \cdot \left(\frac{d}{d\zeta} L_{k,r}(\zeta) \right) \cdot W(\xi, \eta, \zeta) - \left(\frac{\partial}{\partial \zeta} W(\xi, \eta, \zeta) \right) \cdot N_{i,p}(\xi) \cdot M_{j,q}(\eta) \cdot L_{k,r}(\zeta)}{(W(\xi, \eta, \zeta))^2} \end{aligned}$$

2.4.4 NURBS Entities

NURBS entities are created as a linear combination of NURBS Shape functions, exactly the same way as B-Spline entities. The following is the equation for the creation of NURBS Curves:

$$C(\xi) = \sum_{i=1}^n \{R_i^p(\xi) \cdot X_i\}$$

Surfaces:

$$S(\xi, \eta) = \sum_{i=1}^n \sum_{j=1}^m \{R_{i,j}^{p,q}(\xi, \eta) \cdot X_{i,j}\}$$

and Solids:

$$S(\xi, \eta, \zeta) = \sum_{i=1}^n \sum_{j=1}^m \sum_{k=1}^l \{R_{i,j,k}^{p,q,r}(\xi, \eta, \zeta) \cdot X_{i,j,k}\}$$

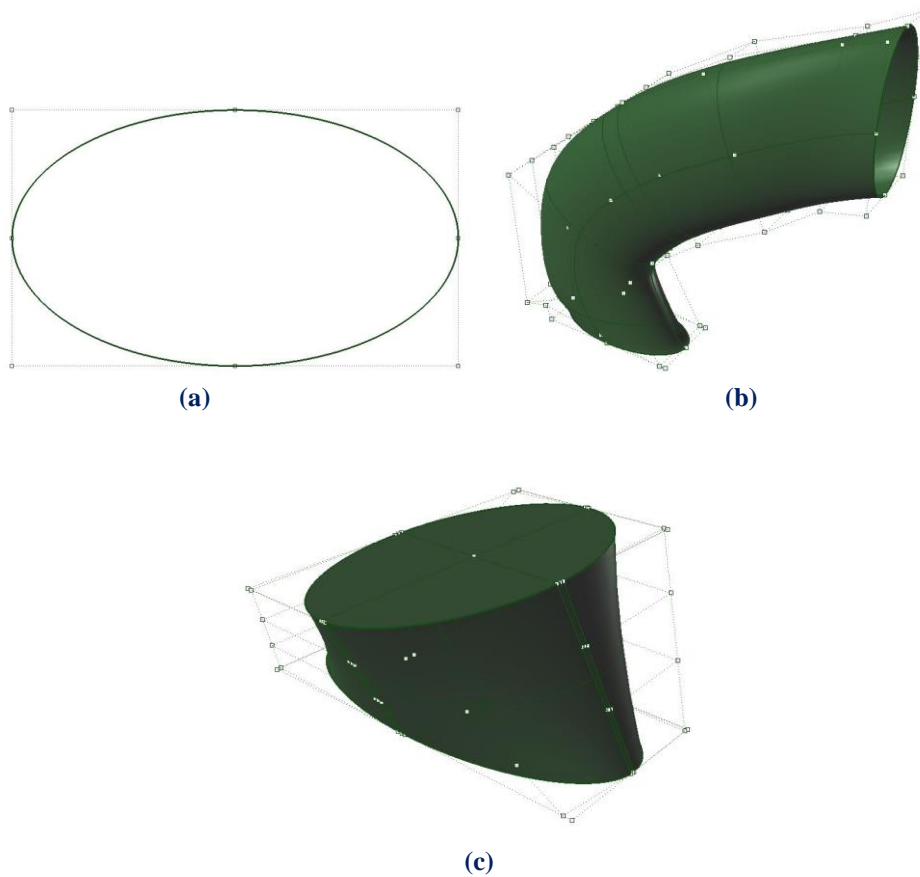


Figure 2.39
NURBS elliptical Entities.
(a) Curve, (b) Surface and (c) Solid.

2.4.5 NURBS Examples

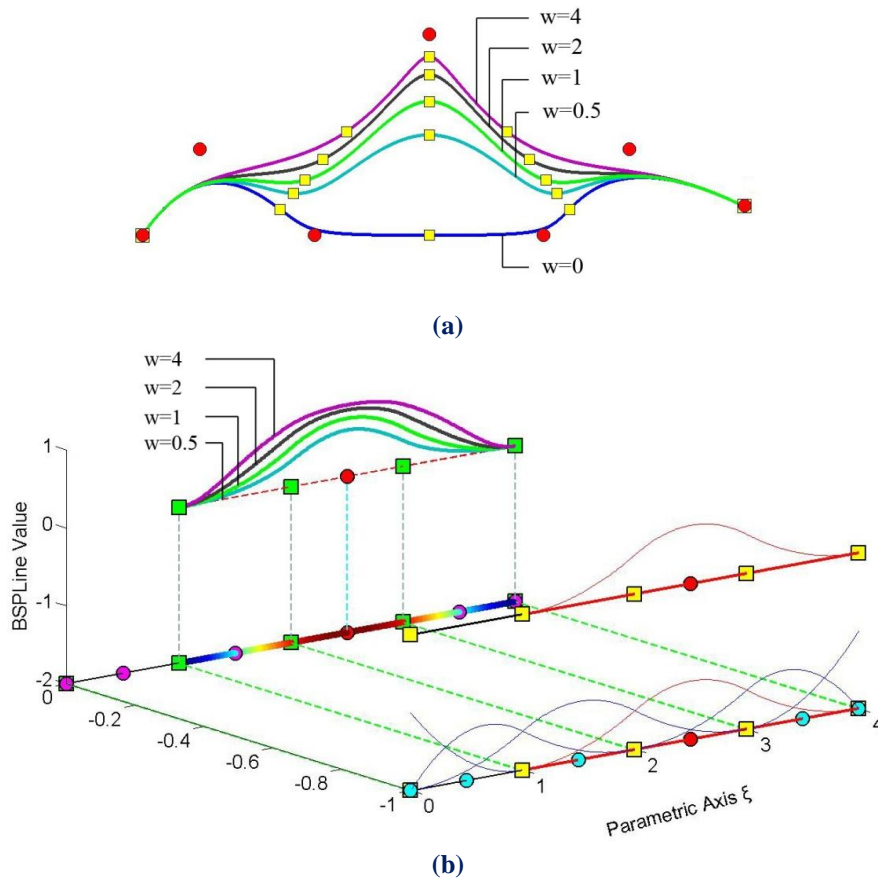


Figure 2.40
 (a) NURBS curves and (b) Shape Functions for different Weight values.

In Figure 2.40, five NURBS Curves with the same set of Control Point Coordinates are represented. The corresponding Weights are $w_i = 1$, for $i \neq 3$. The third Control Point has a different Weight for each curve. Observe that, as the Weight value increases, the Shape function and, as a result, the corresponding Control Point tends to dominate the $p + 1$ Knot Spans of the support. Thus, the Knots are gravitated closer to the corresponding Control Point.

According to *Isogeometric Analysis: Toward Integration of CAD and FEA* (J. Austin Cottrell, Thomas J. R. Hughes, Yuri Bazilevs - Wiley, 2009), in order to accurately represent an arc of $\theta < 180$ degrees, three Control Points are required. Weights for the first and last Points are $w_1 = w_3 = 1$, whereas the middle one has a weight of $w_2 = \cos\left(\frac{\theta}{2}\right)$.

In Figure 2.41, the same circle is represented by NURBS Shape functions of different order. This is a closed curve, so the first and last Control Points coincide. Weights are shown for each Control Point. A NURBS circle is usually represented by four consecutive Patches, bound together by a common Knot Value Vector.

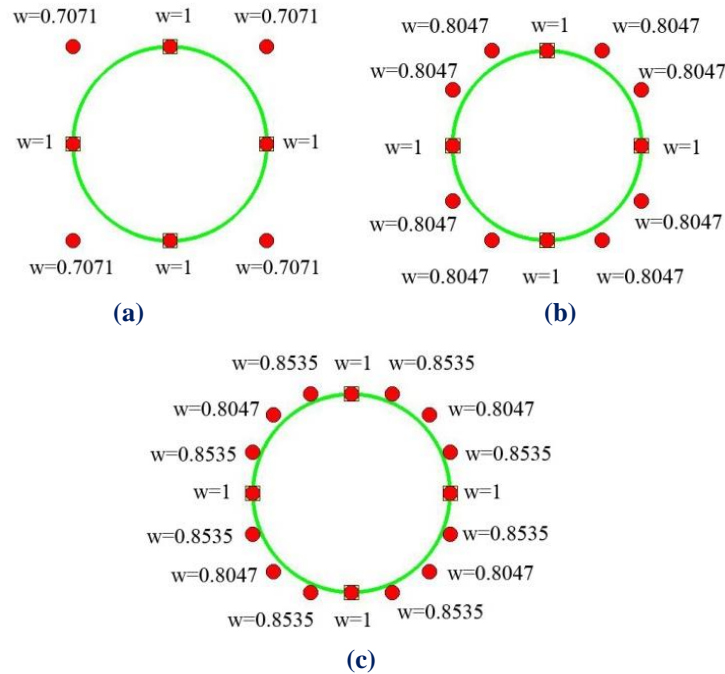


Figure 2.41

NURBS Circle of different polynomial degree. Weight values for each Control Point.

(a) Quadratic basis functions. Knot Value Vector

$$\Xi = \{0 \ 0 \ 0 \ 1 \ 1 \ 2 \ 2 \ 3 \ 3 \ 4 \ 4 \ 4\}$$

(b) Cubic basis functions. Knot Value Vector

$$\Xi = \{0 \ 0 \ 0 \ 0 \ 1 \ 1 \ 1 \ 2 \ 2 \ 2 \ 3 \ 3 \ 3 \ 4 \ 4 \ 4 \ 4\}$$

(c) Quadric basis functions. Knot Value Vector

$$\Xi = \{0 \ 0 \ 0 \ 0 \ 0 \ 1 \ 1 \ 1 \ 1 \ 2 \ 2 \ 2 \ 2 \ 3 \ 3 \ 3 \ 3 \ 4 \ 4 \ 4 \ 4\}$$

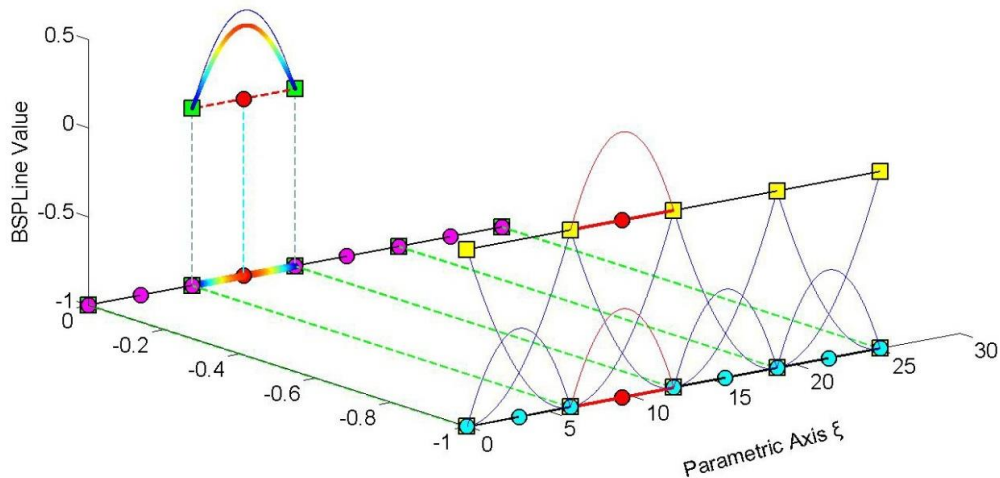


Figure 2.42

Basis functions for circle represented in Figure 2.41.

Contour distribution for Shape Function $R_5^2(\xi)$, with corresponding Weight $\frac{\sqrt{2}}{2} = 0.7071$.

Comparison with basis function $N_{5,2}(\xi)$ shown in blue.

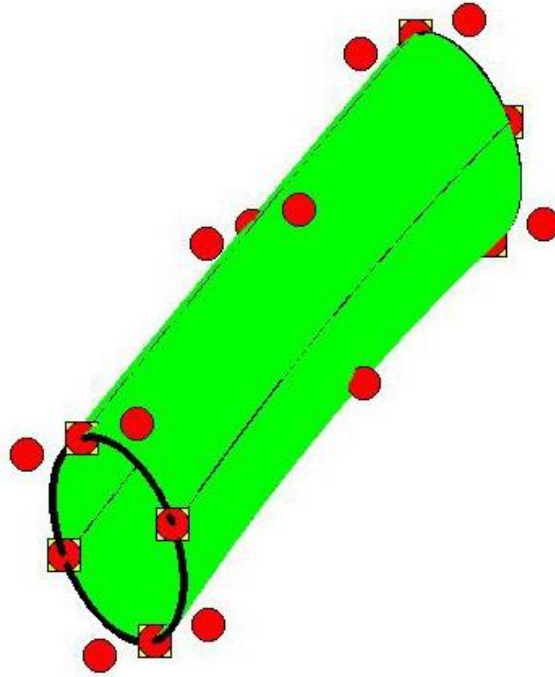


Figure 2.43
NURBS Surface created from consecutive circle cross-sections.

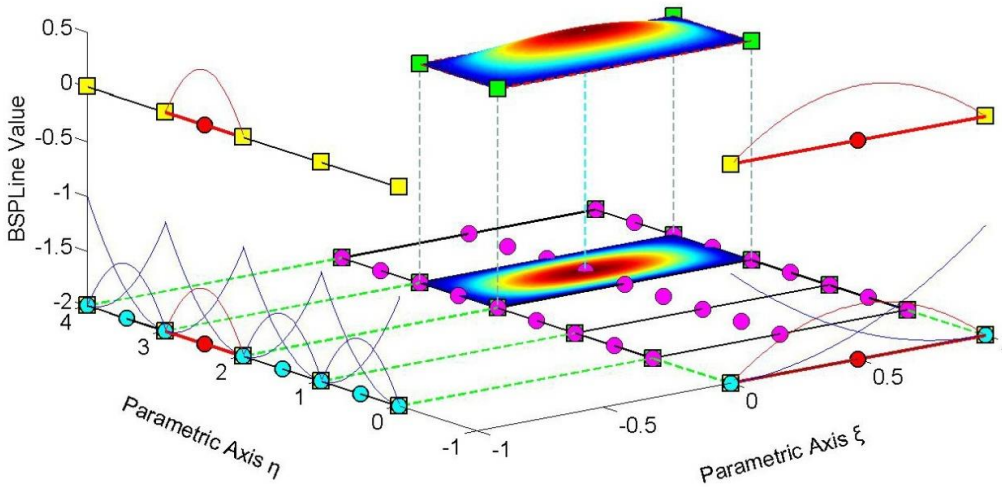


Figure 2.44
Shape Function $R_{2,6}^{2,2}(\xi, \eta)$ for the surface of Figure 2.43.

The corresponding Weight is $\frac{\sqrt{2}}{2} = 0.7071$.

The representation and main attributes are exactly the same as those of B-Spline Shape Functions.

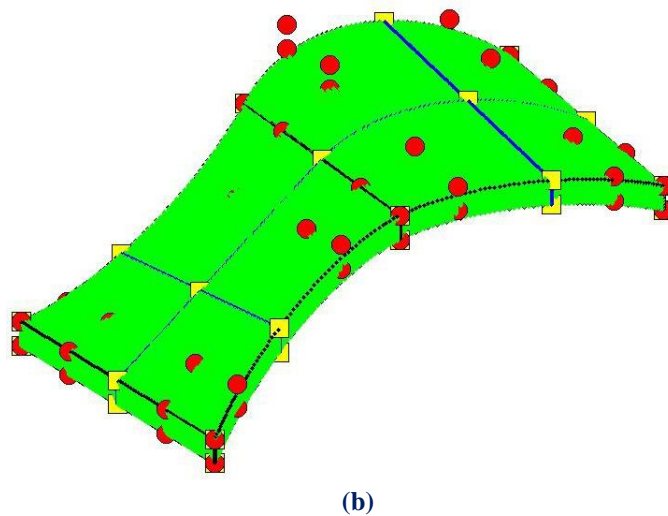
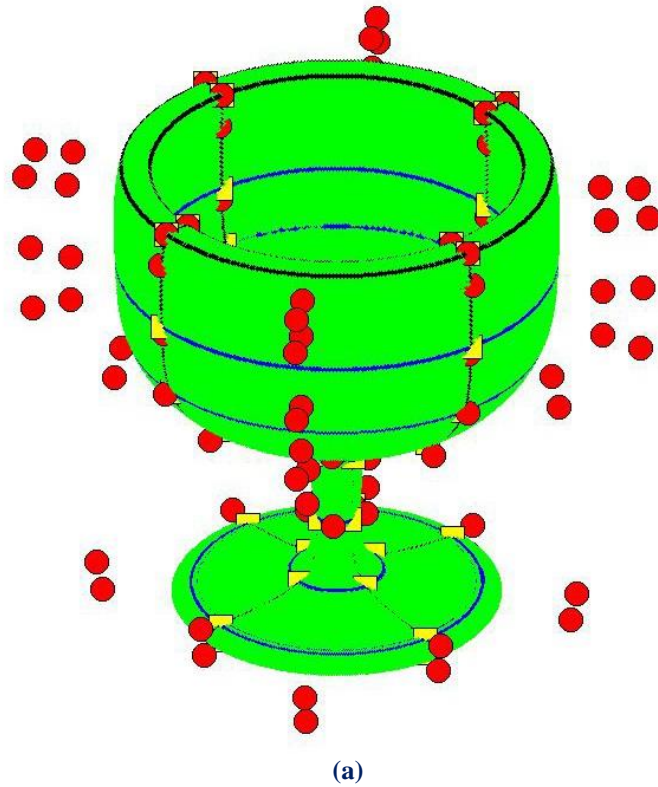


Figure 2.45
NURBS Solids.
(a) Wine Glass and (b) Abstract NURBS Solid

The glass of wine displayed in Figure 2.45.a is a 3D NURBS solid. The potential of Isogeometric Analysis is clearly represented in this model. Observe the exact representation of conic sections and smooth surfaces, in combination with immediate mesh generation. The mesh, that is depicted in the picture, can be instantly used for analysis. An abstract form of another NURBS solid is represented in Figure 2.45.b.

2.5 Patches

NURBS entities are created by transforming a simple Parametric shape (line, rectangle, cube) to a model in Physical Space (curve, surface, solid). They are used for the exact and efficient representation of complex geometrical structures. Sometimes, the mapping of a single Parametric shape is not the optimum solution. A designer might need two or three parametric cubes in order to efficiently represent solids with major changes in geometrical attributes. As displayed in Figure 2.46, each of these cubes, mapped to a portion of the solid in Physical Space, is a NURBS Patch. As expected, each Patch has continuity C^{p-m} on interior Knots and C^{-1} on the edge.

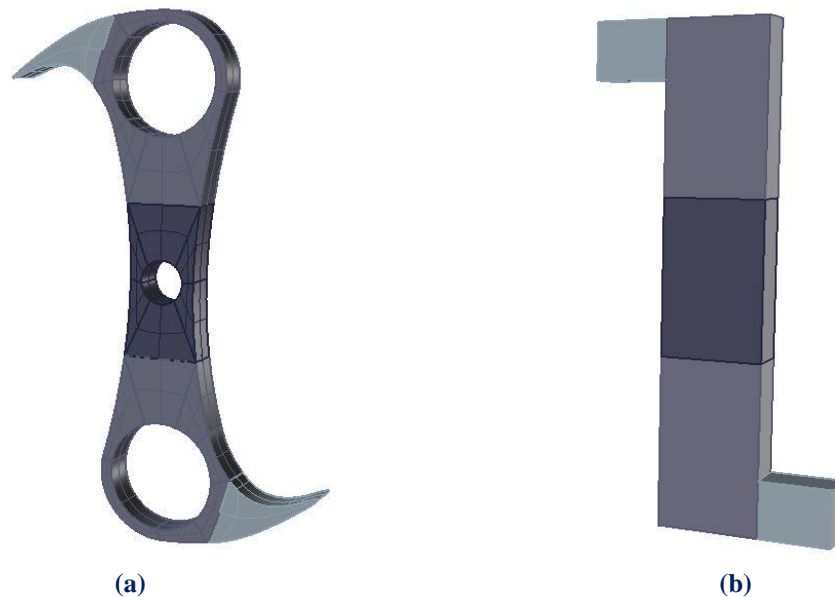


Figure 2.46
 (a) Geometrical Representation of the famous Falkirk Wheel “abutment”.
 Five separate patches are used.

(b) Each Patch portrays a cube in Parameter Space mapped as a complex shape in Physical Space.

Interconnection between Patches can be roughly achieved by choosing coincident Control Points on the edges. Still, Patch connection rarely is leak-proof. This is one of the major disadvantages of NURBS, downsized and eliminated in the next version of SPLines (T-SPLines etc.).

Sometimes, Patches exist for other reasons. For example, a major change in material properties, as displayed in Figure 2.47, requires a Patch boundary. Interpolation through a certain Control Point calls for Patch boundary to be established there. Even application of C^0 Continuity, for analysis purposes, is enabled by introduction of a Patch. If the same polynomial order is used, the mapping can be unified. In these special occasions, the separate Parameter Spaces of the Patches can be united in one Parameter Space, using one set of basis functions and one Knot Value Vector. The distinction between Patches can be applied by enforcing C^0 Continuity across the boundary. In the examples used in this book, the latter option is preferred, when possible.

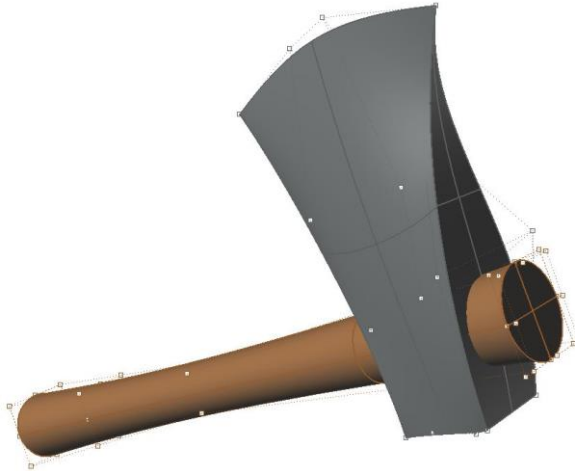


Figure 2.47

NURBS Patches enforced in order to distinct timber from steel. Each material requires separate Patch Stiffness Matrix evaluation, before Global Stiffness Matrix creation.

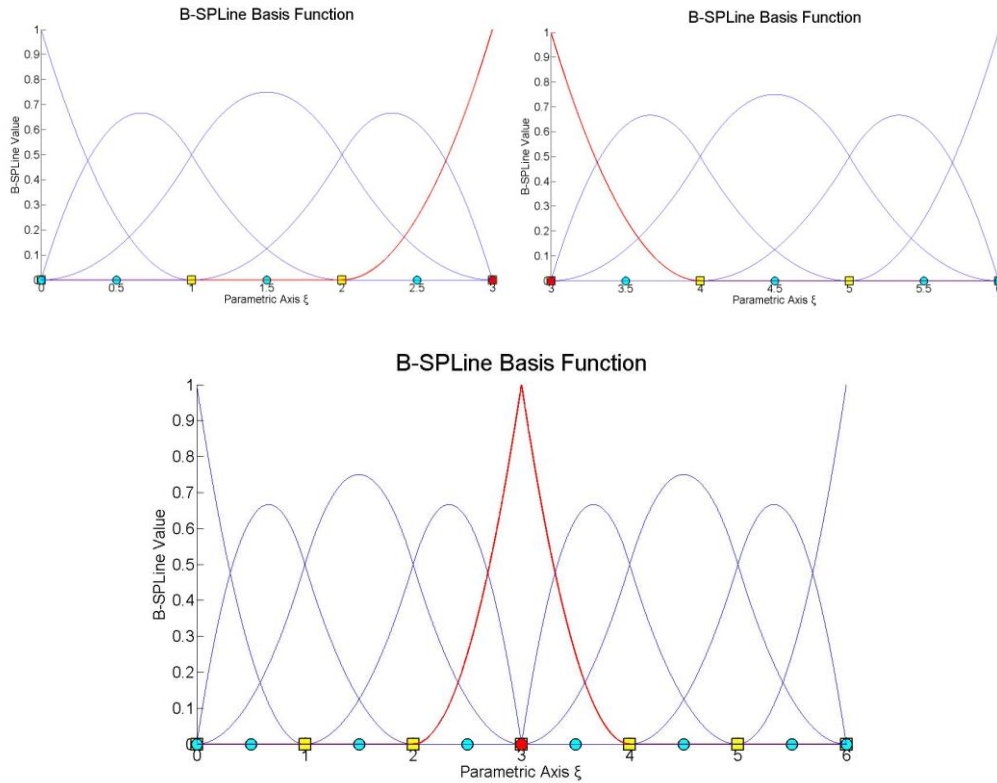


Figure 2.48

Separate Knot Vectors united into one. The Control Points at the boundary are merged. C^0 Continuity is applied.

In the geometrical models presented in this thesis, Knot boundaries are drawn in blue and Patch boundaries in black. This separates C^{-1} and C^0 Continuity from C^1 and greater Continuity. The importance of Continuity in Analysis is examined in the following Chapters.

3. Fluid Analysis

3.1 CFD-Computational Fluid Dynamics

3.1.1 Introduction to CFD

CFD is a branch of fluid dynamics. It uses numerical methods and computers, in order to solve complicate fluid problems. CFD is the simulation of fluids engineering systems using modeling and numerical methods. It is a simulation of an experiment on the computer and the solution is reached with the help of mathematical models. It actually explains how a fluid (liquid or gas) will move around a solid object.

In order to explain how a fluid will behave, partial differential equations are used. With this way, conservation laws about energy, mass and momentum are represented. CFD actually replaces these partial differential equations with algebraic equations that a computer can solve.

3.1.2 Comparison with EFD

It is usually preferred in place of Experimental Fluid Dynamics (EFD), as it is more cost effective and has a high fidelity database. CFD investigates all desired quantities at the same time, while EFD gives results for one quantity at a time. Also, in many cases and phenomena, simulation is easier done than a real experiment.

Such cases are:

- Meteorological phenomena (e.g. wind, storms)
- Environmental effects(air pollution,
- Equipment in large scale (e.g. ships, planes)
- Heating, ventilation and air conditioning of buildings
- Hazards (e.g. explosions, nuclear pollutions)
- Medical processes (e.g. breathing, blood flow)

The error in CFD has its sources from:

- the modeling procedure
- implementation
- iteration and
- discretization

unlike EFD where the error comes from measurements errors.

3.1.3 CFD Analysis Process

A basic procedure is followed in every problem:

1. Geometry
The geometry (physical bounds) of the problem is defined.
2. Problem statement
Information about the flow and the fluid.
3. Mathematical model
The mathematical model is chosen, according to the problem.
4. Mesh generation
The mesh is created by the division of the fluid volume into discrete cells. The mesh can be uniform or non-uniform.
5. Modelling
The physical modelling is defined with the help of the needed equations.
6. Boundary Conditions
Boundary conditions are set. The fluid behavior and the boundaries' properties must be defined.
7. Space and time discretization
Discretization with coupled ODE/DAE and algebraic systems
8. Simulation/Solution
The simulation begins and the equations are solved iteratively.
9. Implementation
Software implementation with simultaneous debugging
10. Postprocessing
A postprocessor is used for the analysis and visualization of the resulting solution.
11. Verification
Model validation / adjustment

Modelling includes all five first stages. It is the setup of a problem while using all the known data (geometry, boundary conditions and equations).

3.1.4 Applications of CFD

CFD is usually used in:

- aerospace
- automotive
- marine engineering
- bioengineering

In these cases, CFD is usually used on the stage of the product's design. Examples of these applications are given in the next figures:

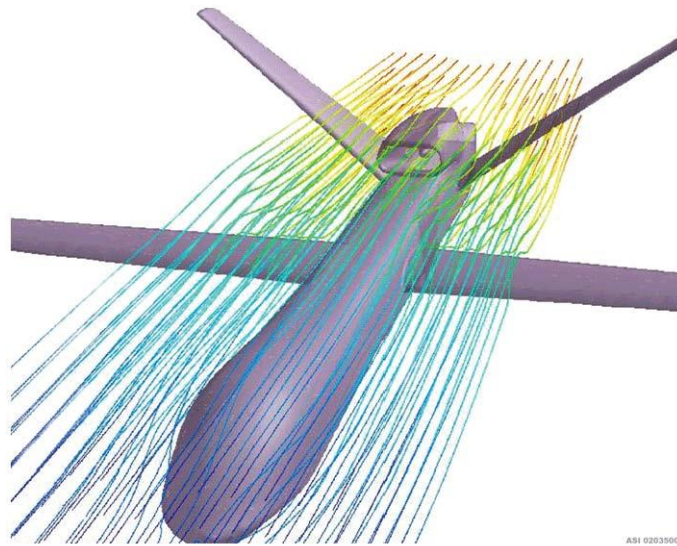


Figure 3.1
Simulation of air flow
(http://www.alentecinc.com/cfd_modeling.htm)

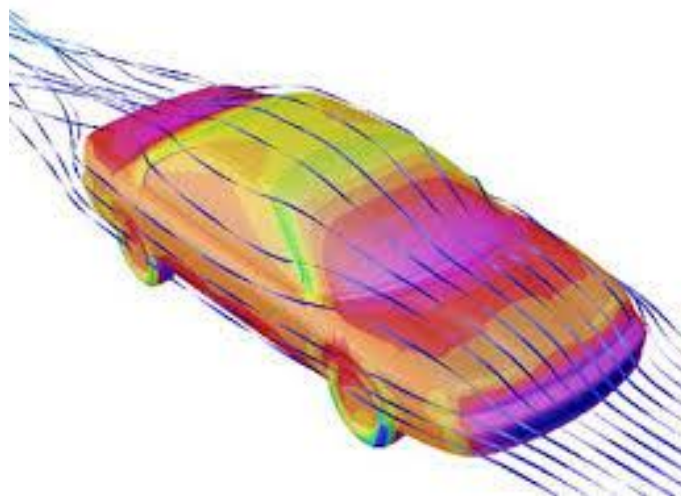


Figure 3.2
Aerodynamic shape design
(http://www.alentecinc.com/cfd_modeling.htm)

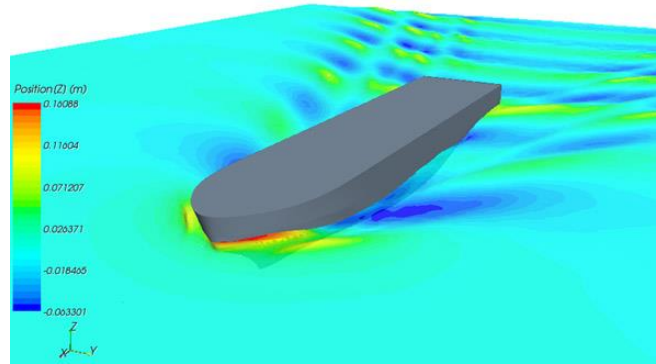


Figure 3.3

Use of CFD in ship design projects
(<http://www.marin.nl/web/Facilities-Tools/CFD.htm>)



Figure 3.4

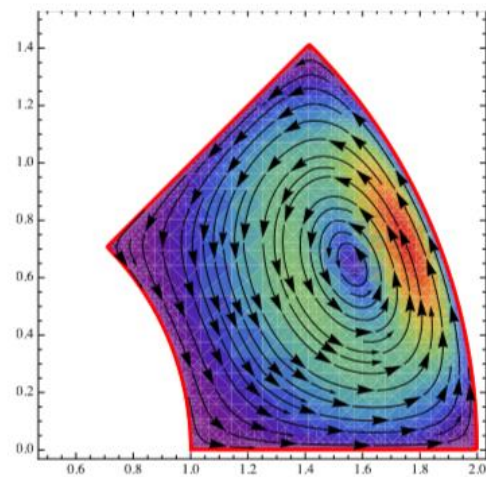
3D printing of the simulation of wall shear stress in artery
(Vincent Lab at the Imperial College London)

Finite element analysis is usually used for the analysis of this kind of problems, but in our case Isogeometric Analysis is used. Also, it is important to be reported, that an integration of CAD/ CAE is needed for the solution of the problem. This is ideal, as Geomiso is a software that combines both CAD and CAE functions.

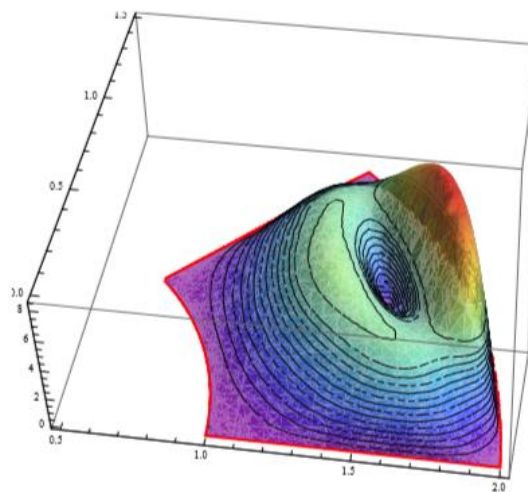
The results of CFD analysis are not always reliable, as the input data are usually based on assumptions or they are not very precise. Also, the chosen mathematical model might be inadequate for the investigated case. Last but not least, there is an error of accuracy due to the available computing power. So, CFD should be used with some reservation and only in cases where the source of error is known and expected.

3.2 Navier Stokes Equations

Navier Stokes equations are a group of equations that describe the motion of fluids. They are widely used in CFD problems. They are the result of application of the second law of Newton on fluid motion. In order to apply this law, an assumption is made, that the fluid substance is described by viscous flow. They explain the connection between velocity, pressure, temperature and density of a moving fluid substance. They also show the effect of the viscosity of the fluid.



(a) Velocity streamlines



(b) Modulus of velocity

Figure 3.5

Domain geometry and velocity component of the exact solution
(Isogeometric Analysis: new stable elements for the Stokes equation)

Note that the blood is not described by viscous flow.

The pair of the following equations shows the solution to the Stokes problem.

$$\begin{cases} -\mu\nabla^2 u + \nabla p = f & \text{in } \Omega \\ \nabla \cdot u = 0 & \text{in } \Omega \end{cases}$$

- u : exact velocity
- p : exact pressure
- f : load
- μ : constant viscosity

An approximation of the exact solution is reached when the next two equations are solved. h is an index that shows the element mesh.

$$a(u_h, v) + b(v, p_h) = \int_{\Omega} f \cdot v \quad \forall v \in V_h$$

$$b(q, u_h) = 0 \quad \forall q \in Q_h$$

- a and b are bilinear forms that show the relation between the approximate and the exact solution. Further explanation of these relations is given in the following two equations respectively
- u_h : approximate velocity
- p_h : approximate pressure
- V_h : domain of velocity
- Q_h : domain of pressure

$$a(u, v) = \int_{\Omega} \mu \nabla u : \nabla v$$

$$b(v, q) = -\int_{\Omega} d \operatorname{div} v$$

Ω is physical domain.

$\hat{\Omega}$ is parametric domain.

U_h, p_h are the finite dimensional velocity and pressure at the elements of mesh. They are approximate solutions to the problem. Based on these solutions, the values of velocity and pressure on every point are calculated (through shape functions).

It must be noted that certain appropriate shape functions must be chosen, in order to have an optimized approximation of U_h to v and minimize the error.

Div stands for divergence. In cartesian coordinates it is computed as below:

$$\text{div } F = \nabla \cdot F = \frac{\partial U}{\partial x} + \frac{\partial V}{\partial y} + \frac{\partial W}{\partial z}$$

Gradient is the generalization of the derivative of a function in one dimension to a function in several dimensions. In cartesian coordinates it is computed as below:

$$\nabla f = \frac{\partial f}{\partial x} \mathbf{i} + \frac{\partial f}{\partial y} \mathbf{j} + \frac{\partial f}{\partial z} \mathbf{k}$$

$$\vec{\nabla} p + \mu \vec{\nabla}^2 \vec{v} = \vec{f}$$

The load \vec{f} is known and it is in the form of a vector. Below, \vec{f} is further expanded. Pressure p is unknown and in scalar form, as it changes from point to point. The result of $\vec{\nabla} p$ though is in vector form. Viscosity μ is also in scalar form, for the same reasons as pressure, but its value is known. Finally, velocity \vec{v} is in vector form and its value is unknown. The result of $\vec{\nabla}^2 \vec{v}$ is also in vector form and it is explained in the next page.

External Load Vector

$$\vec{f} = f_x \vec{i} + f_y \vec{j} = (f_x, f_y) = [f_x(x, y), f_y(x, y)]$$

Pressure Space

$$p = p(x, y) \quad (3.9)$$

$$\vec{\nabla} p = \frac{\partial p}{\partial x} \vec{i} + \frac{\partial p}{\partial y} \vec{j}$$

Velocity Space

$$v = v_x \vec{i} + v_y \vec{j} = (v_x, v_y) = [v_x(x, y), v_y(x, y)]$$

$$\text{div } \vec{v} = \vec{\nabla} \cdot \vec{v} = \left(\frac{\partial}{\partial x}, \frac{\partial}{\partial y} \right) \cdot (v_x, v_y) = \frac{\partial v_x}{\partial x} + \frac{\partial v_y}{\partial y}$$

The result is in scalar form

$$\vec{\nabla}^2 \vec{v} = \vec{\nabla} \cdot (\vec{\nabla} \vec{v}) = \left(\frac{\partial}{\partial x}, \frac{\partial}{\partial y} \right) \left(\frac{\partial v_x}{\partial x} + \frac{\partial v_y}{\partial y} \right) = \left(\frac{\partial^2 v_x}{\partial x^2} + \frac{\partial^2 v_y}{\partial x \partial y}, \frac{\partial^2 v_x}{\partial x \partial y} + \frac{\partial^2 v_y}{\partial y^2} \right)$$

The result is in vector form. A more analytic explanation of the equation is shown below in equation 3.13.

$$\vec{\nabla} p + \mu \vec{\nabla}^2 \vec{v} = \vec{f}$$

$$\left(\frac{\partial p}{\partial x} \vec{i} + \frac{\partial p}{\partial y} \vec{j} \right) + \mu \left[\left(\frac{\partial^2 v_x}{\partial x^2} + \frac{\partial^2 v_y}{\partial x \partial y} \right) \vec{i} + \left(\frac{\partial^2 v_x}{\partial x \partial y} + \frac{\partial^2 v_y}{\partial y^2} \right) \vec{j} \right] = f_x \vec{i} + f_y \vec{j}$$

$$\frac{\partial p}{\partial x} + \mu \frac{\partial^2 v_x}{\partial x^2} + \mu \frac{\partial^2 v_y}{\partial x \partial y} = f_x$$

$$\frac{\partial p}{\partial y} + \mu \frac{\partial^2 v_x}{\partial x \partial y} + \mu \frac{\partial^2 v_y}{\partial y^2} = f_y$$

As the fluid is incompressible, this assumption is made:

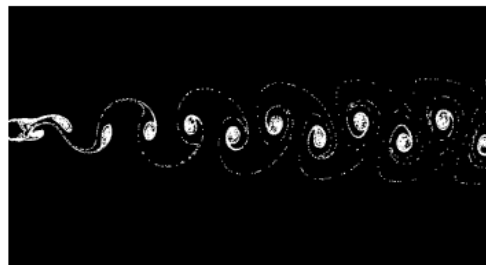
$$\vec{\nabla} \cdot \vec{v} = \left(\frac{\partial}{\partial x}, \frac{\partial}{\partial y} \right) \cdot (v_x, v_y) = \frac{\partial v_x}{\partial x} + \frac{\partial v_y}{\partial y}$$

$$\vec{\nabla} \cdot \vec{v} = 0 \Rightarrow \frac{\partial v_x}{\partial x} + \frac{\partial v_y}{\partial y} = 0 \Rightarrow \frac{\partial v_x}{\partial x} = -\frac{\partial v_y}{\partial y}$$

An ideal fluid is incompressible that is, it has no shear stress, only normal stress.



real experiment



CFD simulation

Figure 3.6

Depiction of a real experiment and a virtual simulation of a flow
(<http://www.mathematik.ni-dortmund.de>)

4. Geomiso Bio

4.1 Introduction

- Geomiso Bio is an innovative diagnostic tool that works as a plugin for Geomiso. It utilizes the graphic environment and the refinement solver of Geomiso, so that the user can draw the model of thoracic and abdominal aorta (the coarse mesh). Next, the required fine mesh will be produced and entered as data in the plugin. Post processing of the results will also utilize the graphic environment of Geomiso. The Geomiso will also provide the external load solver, the boundary condition solver and the transition functions of the values from the control points to the material points.

The geometry will be exported from the MRI apparatus. The initial coarse mesh of the geometry of the thoracic/abdominal aorta will be created by Geomiso. Then, through the automated solver, the required fine mesh will be produced. This fine mesh will be used, in order to create the BioMesh.

BioMesh contains the following fields:

1. Geometry
2. Pressure
3. Velocity
4. Stiffness Matrix
5. External Load
6. Boundary Condition
7. Solver
8. Fluid Parameter

The required results (the output of Geomiso Bio) are the velocity and pressure at control points. From the values of the pressure at control points and the corresponding shape functions, the distribution of pressure at all material points of the model is resulting. The same procedure is followed for the velocity.

This distribution will be depicted with contours. The contours will diagnose the problematic areas with high values of pressure. Parametric investigation will be conducted for the systole and the diastole of the heart. The illustration points are used for the purpose of research.

The parameterization of geometry is given at the corresponding sheet, while the data of pressure are given at the sheet “Bio”.

The Geomiso Bio solver works with fluid analysis. The difference between fluid and linear analysis of elements is that the velocity and the pressure are the unknowns. Furthermore, the isoparametric concept in this case is relaxed, because we need to define different shape functions for pressure and velocity.

The input for the solver is always a coarse mesh of the physical space, as CAD works with the minimum required control points. Then, solver applies refinement to the coarse mesh in order to produce a finer one. Refinement refers to pressure space, means that the mesh of the pressure space is the fine mesh of the corresponding coarse mesh of the geometry.

Index space is just helpful for the nurbs. Index space helps the user to understand how the control points are defined (as the middle of the influence field of a base function). The influence field of a base function equals always $p+1$ knot value spans. Knot spans are the non-trivial knot value spans. This is how the rule $n+p+1 = \text{number of knot values occurred}$. The determinant space is the parametric space.

Geomiso distinguishes the patches by primary and secondary. The primary patches are defined by the variant “Patch_Number”. Every primary patch has its own Knot Value Vector and it is described only by discontinuities C-1. The primary patch may contain secondary patches, which are described by discontinuities C-1, as well as by discontinuities C-0. The secondary patches do not have their own Knot Value Vectors.

Every space is described with different shape functions. The geometry space is described by NURBS shape functions, while the pressure and velocity spaces are described by B-Spline shape functions.

Some details about velocity and pressure space:

12. The pressure is applied perpendicularly on the surface while the velocity is on the same direction with the surface
13. The freedom degrees of velocity on the direction x and y are independent between them
14. Velocity and pressure have common mesh, finite elements and gauss points. They have different continuity, shape functions, control points and knot value spans.

4.2 Element Types

On analysis, three types of finite fluid elements are used: Raviart-Thomas, Taylor-Hood, Nedelec. The element type defines the way from which velocity space is constructed by the corresponding pressure space. We have the same number of knot spans for both cases. The difference is the continuity and the knot value spans. In the three types, the pressure space is the same:

$$\hat{Q}_h^{RT} \equiv \hat{Q}_h^{RT}(p, a) = S_{a,a}^{p,p}(Q_h)$$

$$\hat{Q}_h^N \equiv \hat{Q}_h^N(p, a) = S_{a,a}^{p,p}(Q_h)$$

$$\hat{Q}_h^{TH} \equiv \hat{Q}_h^{TH}(p, a) = S_{a,a}^{p,p}(Q_h)$$

- p: degree
- a: continuity

The Velocity Space though is calculated differently, depending on the type of element. Velocity space consists of a velocity space along the axis x and the velocity space along the axis y.

$$\hat{V}_h^{RT} \equiv \hat{V}_h^{RT}(p, a) = S_{a+1,a}^{p+1,p}(Q_h) \times S_{a,a+1}^{p,p+1}(Q_h)$$

$$\hat{V}_h^N \equiv \hat{V}_h^N(p, a) = S_{a+1,a}^{p+1,p+1}(Q_h) \times S_{a,a+1}^{p+1,p+1}(Q_h)$$

$$\hat{V}_h^{TH} \equiv \hat{V}_h^{TH}(p, a) = S_{a,a}^{p+1,p+1}(Q_h) \times S_{a,a}^{p+1,p+1}(Q_h)$$

- **Taylor Hood**

The Taylor Hood element is the simplest of all three elements. It is a standard stable element used for the Stoke equations. The velocity shape function have less than the maximum continuity in both directions (ξ, η). Also, there is no requirement of Piola Transformation. The boundary conditions are simple, the velocity is zero at all sides.

The drawback of Taylor Hood elements is that they are not point-wise divergence free. Also, due to continuous pressure space use, the element wise mass is not conserved.

- **Nedelec**

The Nedelec element is something in between of Taylor Hood and Raviart Thomas elements. The velocity shape functions have in one of the directions the maximum continuity. Piola Transformation, in this case, is required in order to approximate the velocity field. The boundary conditions are simple, the velocity is zero at all sides.

- **Raviart Thomas**

It is the most promising but also the most troublesome of all three elements. The velocity shape functions have in all directions the maximum continuity. Piola Transformation is also required in order to approximate the velocity field. The problem lies on boundary conditions. Beside the zero velocity at all sides, zero pressure is required on all corners. This leads to a poor approximation on the pressure field and to a restriction of accuracy to first order.

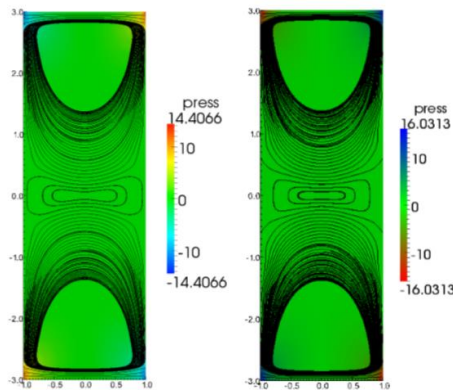


Figure 4.1

Pressure and velocity streamlines in Raviart Thomas elements (left) and Taylor Hood elements (right) in a driven cavity

(Isogeometric Analysis: new stable elements for the Stokes equation)

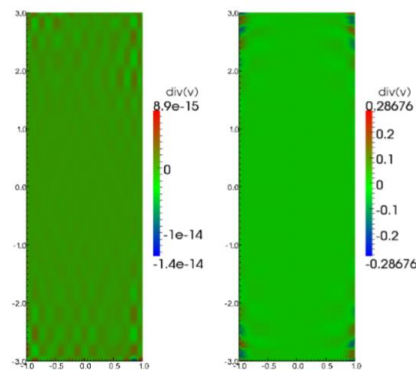


Figure 4.2

Divergence of velocity in Raviart Thomas elements (left) and Taylor Hood elements (right) in a driven cavity

(Isogeometric Analysis: new stable elements for the Stokes equation)

4.3 Piola Transformation

It is a different way of approximation of the velocity field. It is required on Nedelec and Raviart Thomas elements, in order to get stable discretizations. The Piola Transformation is a rotation of the coordinate system. The new shape functions are obtained from this formula:

$$T_i = \frac{[J]}{\det J} \cdot R_i$$

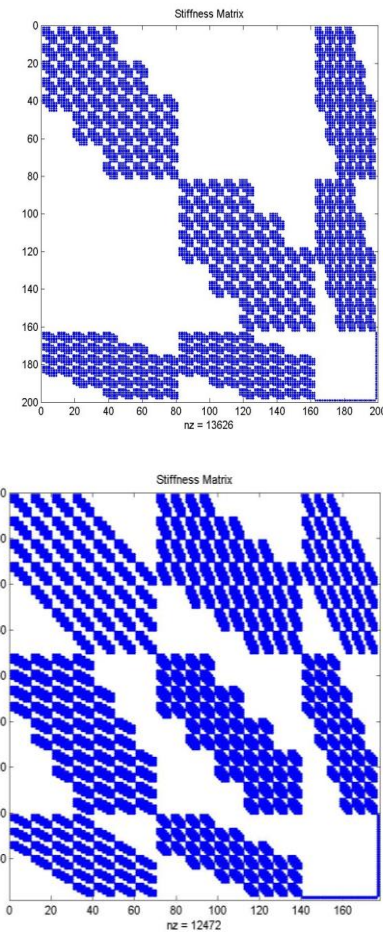


Figure 4.3

The difference between a Taylor-Hood stiffness matrix and a Nedelec stiffness matrix (after the Piola Transformation)

(created by Eleni Michael with Geomiso Bio)

Especially on Raviart Thomas elements, an affine transformation is not appropriate, as this kind of transformation does not preserve orthogonality of vectors and thus the enforcement of continuity is not available. The Piola transformation has this ability and therefore it is preferred.

The procedure of Piola Transformation is presented in the following flowchart:

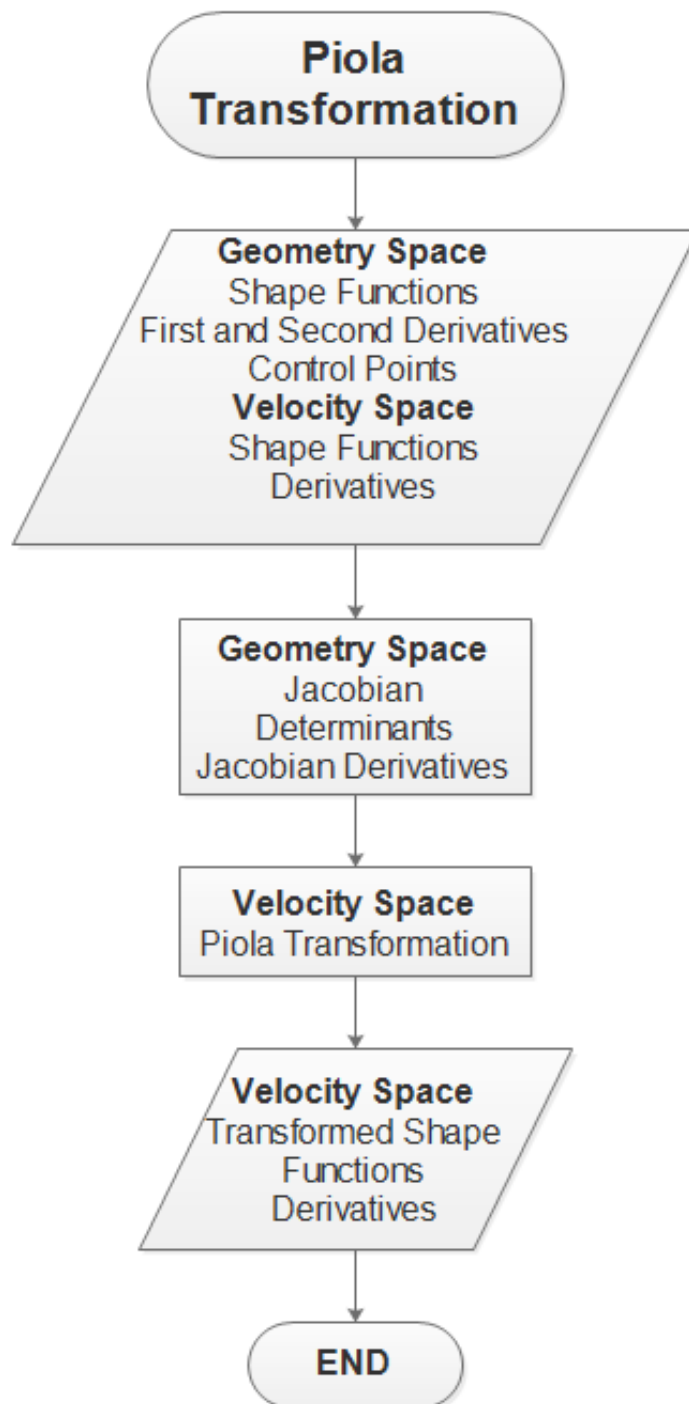


Figure 4.4
Flowchart of Piola Transformation
(Created by Eleni Michael with Edraw Flowchart)

4.4 Stiffness Matrix

The stiffness matrix in fluid analysis consists of:

- the viscosity matrix (it matches the velocity degrees of freedom)
- the pressure matrix (it shows the relation between velocity and pressure degrees of freedom)
- the equation that shows that the average pressure is zero

Special care has to be taken to assure the correct calculation of the Jacobian. The positive direction of axes in parameter and physical space must coincide, or else the determinant of the Jacobian will be negative and the matrix $[J]$ irreversible. Numerical integration on points of singularity, such as two points on parameter space mapped into the same point on physical space, has to be avoided as well as far as NURBS are concerned.

The Jacobian is calculated with the geometry data. The equation that gives the Jacobian is:

$$[J] = [D_N] \cdot [XY]$$

(2×2) $(2 \times NCP)$ $(NCP \times 2)$

$$[J]_{(2 \times 2)} = \begin{bmatrix} R_{1,\xi}(\xi, \eta) & R_{2,\xi}(\xi, \eta) & \dots & \dots & \dots & R_{N,\xi}(\xi, \eta) \\ R_{1,\eta}(\xi, \eta) & R_{2,\eta}(\xi, \eta) & \dots & \dots & \dots & R_{N,\eta}(\xi, \eta) \end{bmatrix} \cdot \begin{bmatrix} X_1 & Y_1 \\ X_2 & Y_2 \\ \cdot & \cdot \\ \cdot & \cdot \\ \cdot & \cdot \\ X_N & Y_N \end{bmatrix}$$

where N is the total number of control points.

The inverse Jacobian matrix is used in stiffness matrix calculation:

$$[J]_{(2 \times 2)}^{-1} = \begin{bmatrix} J_{11}^* & J_{12}^* \\ J_{21}^* & J_{22}^* \end{bmatrix} = \frac{1}{\det[J]} \cdot \begin{bmatrix} J_{22} & -J_{12} \\ -J_{21} & J_{11} \end{bmatrix}$$

The determinant of the Jacobian matrix is also required and is equal to:

$$\det[J] = J_{11} \cdot J_{22} - J_{21} \cdot J_{12}$$

This means that the cartesian coordinates of the geometry control points are used as XY and the derivatives of the shape functions (calculated from the parameterization of geometry) as D_N .

The next step is to calculate the matrices $[B_1]$ and $[B_2]$. The matrix $[B_1]$ transfers the strains of the element from Parameter to Physical Space and the matrix $[B_2]$ transfers the nodal displacements of the elements to the strains at the Parameter Space. Therefore, the matrices $[B_1]$ and $[B_2]$ can be calculated from the equations below:

$$[B_1(\xi, \eta)]_{(3 \times 4)} = \frac{1}{\det[J]} \cdot \begin{bmatrix} J_{22} & -J_{12} & 0 & 0 \\ 0 & 0 & -J_{21} & J_{11} \\ -J_{21} & J_{11} & J_{22} & -J_{12} \end{bmatrix}$$

$$[B_2(\xi, \eta)]_{(4 \times 2N)} = \begin{bmatrix} R_{1,\xi} & 0 & R_{2,\xi} & 0 & \dots & \dots & \dots & R_{N,\xi} & 0 \\ R_{1,\eta} & 0 & R_{2,\eta} & 0 & \dots & \dots & \dots & R_{N,\eta} & 0 \\ 0 & R_{1,\xi} & 0 & R_{2,\xi} & \dots & \dots & \dots & 0 & R_{N,\xi} \\ 0 & R_{1,\eta} & 0 & R_{2,\eta} & \dots & \dots & \dots & 0 & R_{N,\eta} \end{bmatrix}$$

After that, the Deformation Matrix is evaluated.

$$[B(\xi, \eta)]_{(3 \times 2N)} = [B_1(\xi, \eta)]_{(3 \times 4)} \cdot [B_2(\xi, \eta)]_{(4 \times 2N)}$$

Both Deformation Matrix and Jacobian are used for the formulation of each part of the stiffness matrix. After all the individual matrices are computed, the stiffness matrix is assembled. The general integration for the matrices is:

$$[K]_{(2N \times 2N)} = \int_{\xi_0}^{\xi_{n+p+1}} \int_{\eta_0}^{\eta_{m+q+1}} [B(\xi, \eta)]_{(2N \times 3)}^T \cdot [E]_{(3 \times 3)} \cdot [B(\xi, \eta)]_{(3 \times 2N)} \cdot t \cdot \det[J] \, d\eta d\xi$$

- GP_ξ : the total number of Gauss Points per ξ for the specific Patch
- GP_η : the total number of Gauss Points per η for the specific Patch
- ξ_i, η_j : the coordinates of the tensor product Gauss Point i, j
- $w_i^{GP\xi}, w_j^{GP\eta}$: the corresponding weights
- $[K]$: viscosity or pressure matrix
- $[E]$: matrix with viscosity values or values of shape functions and the divergence (div).

With numerical integration the values of the matrix are computed with a very small error. The Viscosity Matrix has a similar way of calculation with solids (the first derivative of shape functions is used). The only difference is the use of viscosity instead of Young's module and Poisson coefficient.

The Pressure matrix is even more different as it utilizes the values of shape functions and the divergence (div).

The form of the stiffness matrix is the following:

- [A] : Stiffness Viscosity Matrix (Velocity - Velocity DoFs)
- [B]: Stiffness Pressure Matrix (Velocity – Pressure DoFs)
- [E]: Equation for Average Pressure=0 (1 line)

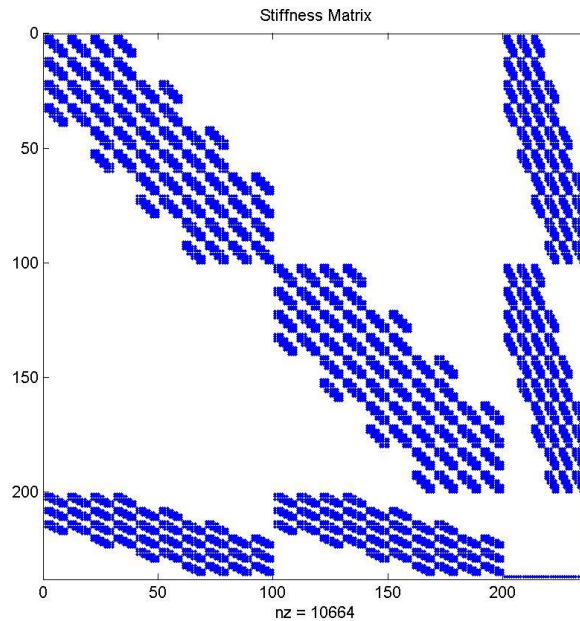
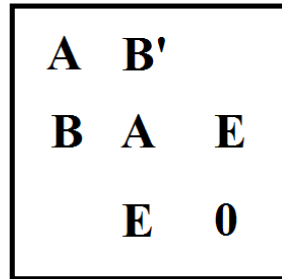


Figure 4.5
 The form of the Stiffness Matrix
 (created by Eleni Michael with Geomiso Bio)

The structure of the code is presented in the following diagram:

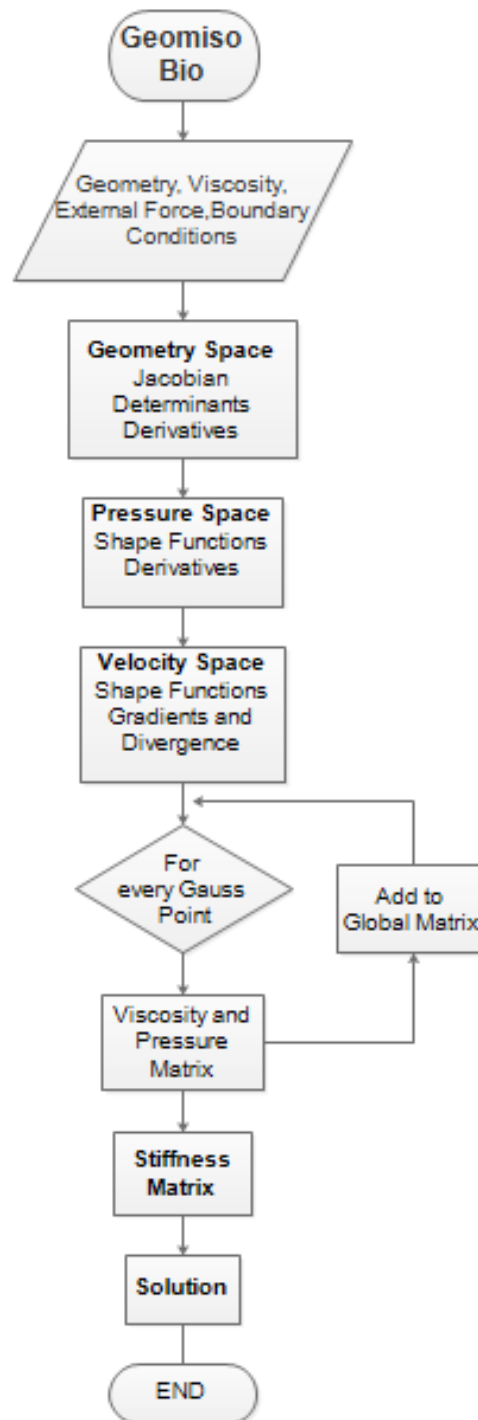


Figure 4.6
Flowchart of Geomiso Bio
(Created by Eleni Michael with Edraw Flowchart)

4.5 Parameterization

4.5.1 Introduction

The CAD researchers wish for the minimum number of control points. On the other hand, CAE researchers seek for maximum number of control points. As the input will be given from a CAD program, the initial mesh will always be coarse. As the analysis proceeds, a refinement on the mesh is required, so that the maximum number of control points (that the CAE program requires) is achieved.

As a first step a simple equivalent geometry of the aorta is investigated.

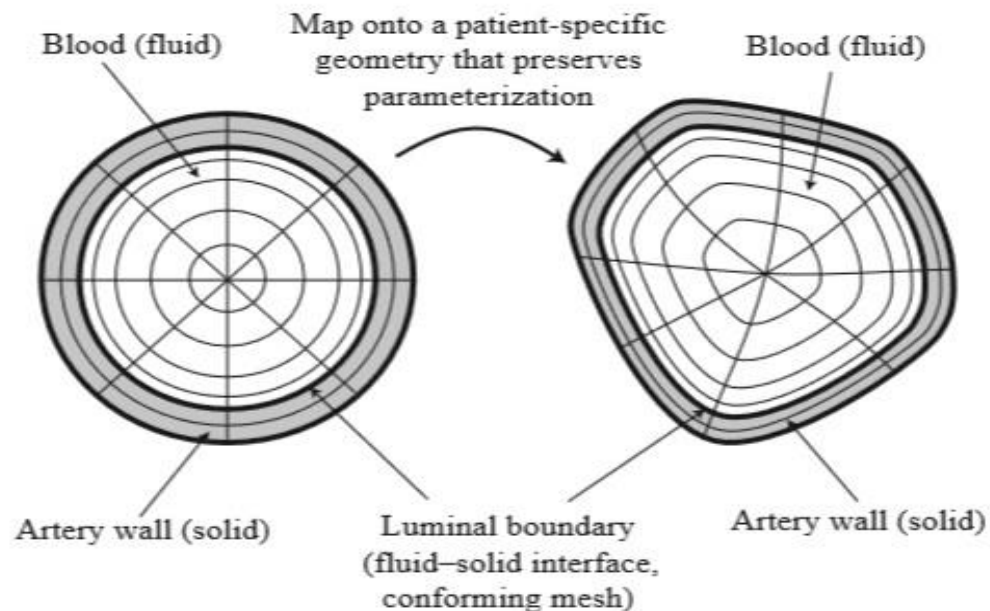


Figure 4.7

Arterial cross-section template based on a NURBS mesh of a circle that is subsequently mapped onto a patient-specific geometry. Fluid and solid regions are identified and separated by an interface (Isogeometric Analysis Toward Integration of CAD and FEA, J. Austin Cottrell, Thomas J. R. Hughes, Yuri Bazilevs, p.261,f.10.7)

- Coarse mesh of a circle

The minimum required control points, in order to create a circle are nine. The minimum case is a triangle.

In the following figures, the procedure of designing the geometry model is shown step by step.

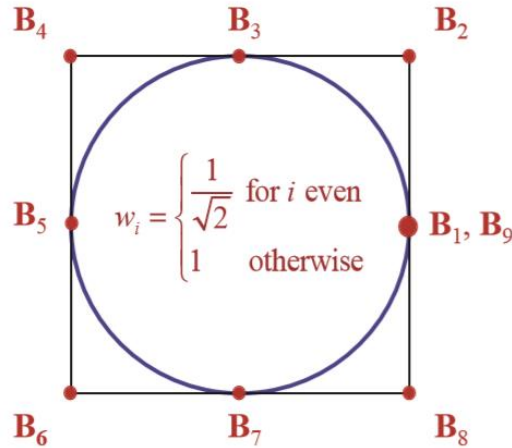


Figure 4.8

The NURBS mesh for a circle comprised of four 90° arcs. All of the control points lie on a square in which the circle is inscribed. Five of the control points (one repeated value) are on the circle itself and have a weight of 1, while the remaining control points are at the corners of the square and have a weight of $1/\sqrt{2}$. (Isogeometric Analysis Toward Integration of CAD and FEA, J. Austin Cottrell, Thomas J. R. Hughes, Yuri Bazilevs, p.59,f.2.35)

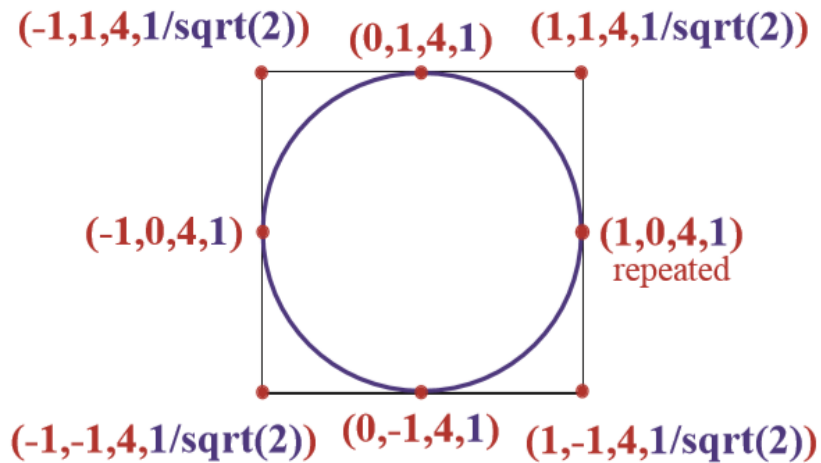


Figure 4.8

Control points for the inner edge at the top of the pipe. Note that the weights (in blue) are frequently stored as the fourth component of the control point that they are associated with, but we do not consider them to be part of the control point itself.

(Isogeometric Analysis Toward Integration of CAD and FEA, J. Austin Cottrell, Thomas J. R. Hughes, Yuri Bazilevs, p.61,f.2.37)

- Coarse mesh of an annulus

In order to describe as simple as possible the geometry of the section of the aorta, an annulus is used.

The minimum required control points for the annulus are 18 (9 for the outer circle and 9 for the inner circle).

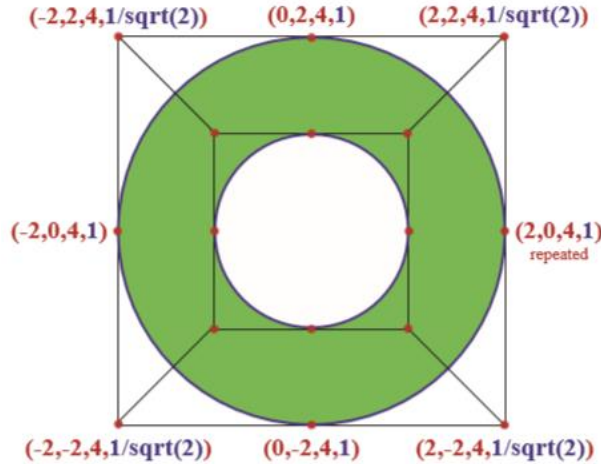


Figure 4.9

The annular surface at the top of the pipe. The control points for the outer edge are shown. (Isogeometric Analysis Toward Integration of CAD and FEA, J. Austin Cottrell, Thomas J. R. Hughes, Yuri Bazilevs, p.61,f.2.38)

	X	Y	Z	W
B1	1	0	0	1
B2	1	1	0	0,707107
B3	0	1	0	1
B4	-1	1	0	0,707107
B5	-1	0	0	1
B6	-1	-1	0	0,707107
B7	0	-1	0	1
B8	1	-1	0	0,707107
B9	1	0	0	1
B10	2	0	0	1
B11	2	2	0	0,707107
B12	0	2	0	1
B13	-2	2	0	0,707107
B14	-2	0	0	1
B15	-2	-2	0	0,707107
B16	0	-2	0	1
B17	2	-2	0	0,707107
B18	2	0	0	1

Figure 4.10

Table with all the coordinates of the control points of the annulus (Table created by Eleni Michael)

- Parametric axis ζ

The simplified geometry of a section of the aorta has already been described on the previous sections. The geometry of the aorta is simulated as a cylinder.

The minimum control points of cylindrical annulus are 36.

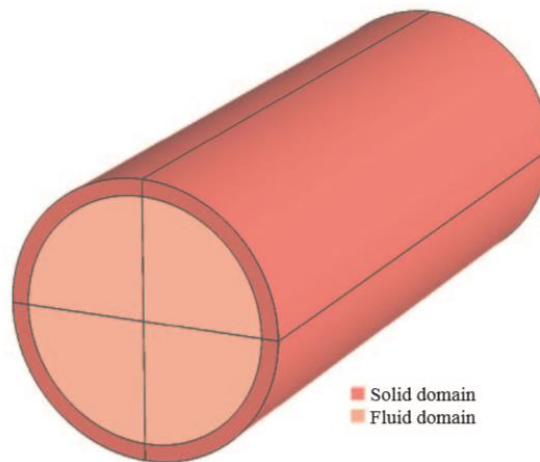


Figure 4.11

The artery template should be refined somewhat before deformation to fit the patient- specific geometry.

Smaller elements in the fluid domain near the fluid–solid boundary allow for better resolution of the resulting boundary layer.

(Isogeometric Analysis Toward Integration of CAD and FEA, J. Austin Cottrell, Thomas J. R. Hughes, Yuri Bazilevs, p.275,f.10.A.2)

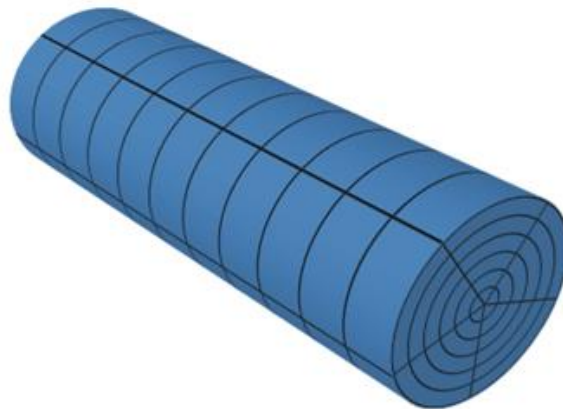


Figure 4.12

The geometrical mapping of this solid cylinder has a degeneracy along its axis. This results in a singularity in the inverse mapping. In practice, however, such meshes have been used successfully.

(Isogeometric Analysis Toward Integration of CAD and FEA, J. Austin Cottrell, Thomas J. R. Hughes, Yuri Bazilevs, p.58,f.2.33)

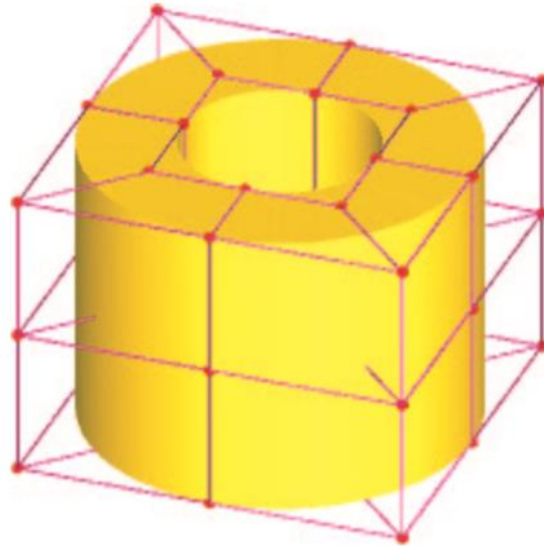


Figure 4.13

The control lattice for the cylindrical portion of the pipe. Note that there are three levels of control points, one corresponding to each of the three quadratic NURBS functions in the ζ -direction of this element. (Isogeometric Analysis Toward Integration of CAD and FEA, J. Austin Cottrell, Thomas J. R. Hughes, Yuri Bazilevs, p.62,f.2.40)

	X	Y	Z	W		X	Y	Z	W
B1	1	0	0	1	B19	1	0	4	1
B2	1	1	0	0,707107	B20	1	1	4	0,707106781
B3	0	1	0	1	B21	0	1	4	1
B4	-1	1	0	0,707107	B22	-1	1	4	0,707106781
B5	-1	0	0	1	B23	-1	0	4	1
B6	-1	-1	0	0,707107	B24	-1	-1	4	0,707106781
B7	0	-1	0	1	B25	0	-1	4	1
B8	1	-1	0	0,707107	B26	1	-1	4	0,707106781
B9	1	0	0	1	B27	1	0	4	1
B10	2	0	0	1	B28	2	0	4	1
B11	2	2	0	0,707107	B29	2	2	4	0,707106781
B12	0	2	0	1	B30	0	2	4	1
B13	-2	2	0	0,707107	B31	-2	2	4	0,707106781
B14	-2	0	0	1	B32	-2	0	4	1
B15	-2	-2	0	0,707107	B33	-2	-2	4	0,707106781
B16	0	-2	0	1	B34	0	-2	4	1
B17	2	-2	0	0,707107	B35	2	-2	4	0,707106781
B18	2	0	0	1	B36	2	0	4	1

Figure 4.15

Table with all the coordinates of the control points of the cylindrical pipe (Table created by Eleni Michael)

Simulation of Human Aorta and Isogeometric Fluid Analysis

The following figures show a case of an abdominal aneurysms and the various models of geometry, as done by J. Austin Cottrell, Thomas J. R. Hughes, Yuri Bazilevs in “Isogeometric Analysis Toward Integration of CAD and FEA”.



(a) Patient-specific imaging data



(b) Skeleton of the NURBS mesh



(c) Isogeometric Analysis Toward Integration of CAD and FEA with color-coded patches. The computational mesh consists of 44,892 quadratic NURBS elements.

Figure 4.16

Flow in a patient-specific abdominal aorta with aneurysm, obtained by using a 64-slice CT angiography. ((Isogeometric Analysis Toward Integration of CAD and FEA, J. Austin Cottrell, Thomas J. R. Hughes, Yuri Bazilevs, p.262,f.10.8)

The number of patches that are needed to describe the aorta is seven:

1. Abdominal aorta
2. Descending aorta
3. Aortic arch
4. Ascending aorta
5. Sinotubular junction
6. Aortic root
7. Annulus

Areas, like the annulus, have a very complex geometry and thus, isogeometric analysis is the best approach for bioengineering problems. In medicine, even the smallest detail matters, as in many cases is a matter of life and death.

4.6 External Load

Having created the stiffness matrix with the procedure described in 4.4, it is now imperative to define loads, which comply with the actual load situation of the examined structure. In finite element analysis (FEA), external loads act on the nodes of the structure, which are at the same time material points. In isogeometric analysis (IGA), external loads are imposed not on material points, but on the control net. It is obvious that this handling is far away from a young engineer's perception, who is used to act loads directly on points belonging to the model geometry. The only case in IGA where a load imposed at a control point and a material point at the same time is at interpolatory control points. We should keep in mind that, regardless the type of the external loads chosen for the analysis, the final forces will be implemented on interpolatory control points, due to the fact that only interpolatory control points can be loaded. In case a $f(\xi, \eta, \zeta)$ load has to be distributed on control points, that are not interpolatory to the curve, it has to be transformed into equivalent concentrated loads by integration :

$$\{\mathbf{F}\}_{(N \times 1)} = \int_{\xi_0}^{\xi_{n+p+1}} \int_{\eta_0}^{\eta_{m+q+1}} \int_{\zeta_0}^{\zeta_{l+r+1}} \left\{ \mathbf{R}(\xi, \eta, \zeta) \right\}_{(N \times 1)} \cdot f(\xi, \eta, \zeta)_{(1 \times 1)} \cdot \det[\mathbf{J}] \, d\zeta d\eta d\xi$$

More specifically, for each case:

1D:

$$\{\mathbf{F}\}_{(N \times 1)} = \int_{\xi_0}^{\xi_{n+p+1}} \left\{ \mathbf{R}(\xi) \right\}_{(N \times 1)} \cdot f(\xi)_{(1 \times 1)} \cdot \det[\mathbf{J}] \, d\xi$$

2D:

$$\{\mathbf{F}\}_{(N \times 1)} = \int_{\xi_0}^{\xi_{n+p+1}} \int_{\eta_0}^{\eta_{m+q+1}} \left\{ \mathbf{R}(\xi, \eta) \right\}_{(N \times 1)} \cdot f(\xi, \eta)_{(1 \times 1)} \cdot \det[\mathbf{J}] \, d\eta d\xi$$

3D:

$$\{\mathbf{F}\}_{(N \times 1)} = \int_{\xi_0}^{\xi_{n+p+1}} \int_{\eta_0}^{\eta_{m+q+1}} \int_{\zeta_0}^{\zeta_{l+r+1}} \left\{ \mathbf{R}(\xi, \eta, \zeta) \right\}_{(N \times 1)} \cdot f(\xi, \eta, \zeta)_{(1 \times 1)} \cdot \det[\mathbf{J}] \, d\zeta d\eta d\xi$$

This way, the load vector $\{\mathbf{F}\}$ is assembled.

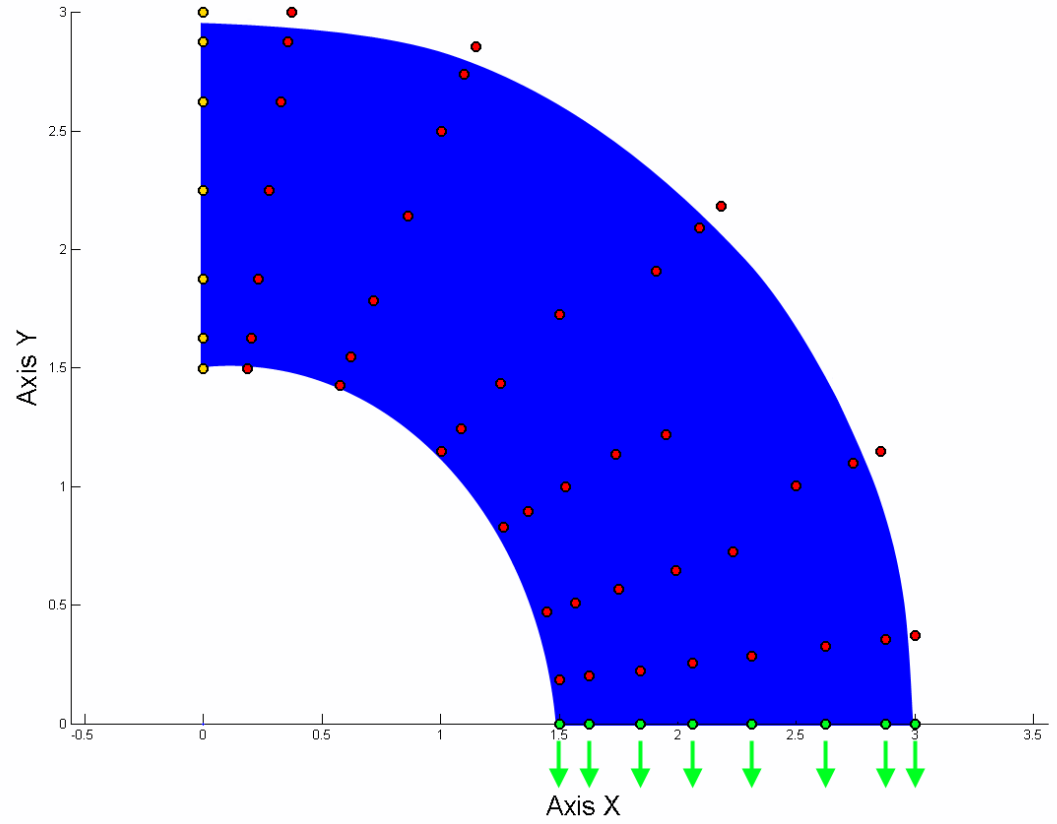


Figure 4.17

Physical space. Quarter of an annulus. 2D Analysis.
 Red color refers to free control points and yellow to the supported ones.
 Concentrated loads have been acted at green control points.
 (Created with Geomiso)

4.7 Boundary Conditions

A crucial step, that allows analysis to be done, is the enforcement of the boundary conditions, as structures cannot be analyzed when they are not stable. This means that some degrees of freedom will be free and some have to be fixed, i.e. their values of pressure and velocity will be zero. These degrees of freedom are called stationary and their corresponding rows and columns are deleted from the stiffness matrix and the load vector.

The stiffness matrix and the load vector having only free degrees of freedom are $[K_{ff}]$ and $\{F_f\}$ respectively. The solution of the equation is the final step in analysis:

$$\{F_f\} = [K_{ff}] \cdot \{D_f\} \Rightarrow \{D_f\} = [K_{ff}]^{-1} \cdot \{F_f\}$$

The (zero) values for the stationary degrees of freedom are added back to the result creating the pressure and velocity vector $\{D\}$.

The necessity of applying boundary conditions and the inability to apply strong formulation leads to the application of a weak one. The weak formulation of such boundary conditions demands that they are applicable on a finite number of points. The enforcement of the boundary conditions takes place at the control points of the structure. Each control point has one, two or three pressure degrees of freedom and two, four or six velocity degrees of freedom for 1D, 2D and 3D analysis respectively. In this reference, we deal with the enforcement of 2D boundary conditions, which are enforced at the corners of the domain's boundaries. At these points, basis functions have C-1 continuity and one component of them refers to corner control point. We aim to these control points' commitment only when their corresponding basis function has non-zero value. Having set zero corner control point's pressure, we ensure that all the material points of the specific boundary side have zero pressure values, too. For example, on parametric axis ξ :

$$\sum_{i=1}^{n+p+1} N_i D_i = 0 \Rightarrow N_1 D_1 + \sum_{i=2}^{n+p} N_i D_i + N_{n+p+1} D_{n+p+1} = 0 \Rightarrow \sum_{i=2}^{n+p} N_i D_i = 0$$

The procedure of the boundary condition enforcement is getting complicated, because the domain of influence of each control point overlaps the domains of its adjoining control points. Compared with finite element analysis, in which control points are simultaneously material points, in isogeometric analysis control points may be points out of the structure's body. So, another difficulty is ahead, concerning the enforcement of boundary conditions in IGA. Enforcing boundary conditions in this way, we do not deal with a general case of mixed conditions on a boundary domain. Every researcher should give special attention to its implementation and dare with all the above difficulties.

5. Human Circulatory System

5.1 Real geometry of aorta

The aorta originates from the left ventricle with the aortic root and ends in the abdomen with the iliac bifurcation. Its purpose is to provide oxygenated blood from the left ventricle to all organs of the human body through the systemic circulation. It can be divided on four main segments: the ascending aorta, the aortic arch, the descending aorta and the abdominal aorta.

The aorta can be simulated as a wind turbine. It stores kinetic energy during systole, which is delivered during the diastole so that the aortic pressure is maintained on the same level.

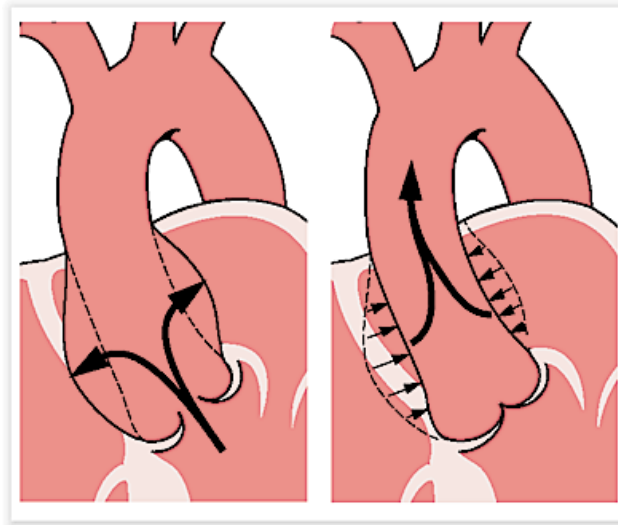


Figure 5.1
How diastole and systole works
(www.gesundheit.de)

5.1.1 Thoracic aorta

The size of the thoracic aorta follows the shape of a cone. The size of the aorta depends on various parameters such as: age, sex, body surface area (height and weight), and daily workload.

The thoracic aorta consists of the following six segments:

- **Annulus**
Annulus is the formation of a virtual ring at the base of the aortic root. The shape of this ring is elliptical. It is also known as the area of the three folds. The annulus opens during the systole of the heart and closes during the diastole. In figure 5.2 this part of thoracic aorta is shown as the bottom formation of a ring in the annulus.
- **Aortic root**
Aortic root is actually the aortic valve. This term contains the sinuses of Valsalva and the valve leaflets. The two limits are the annulus and the sinotubular junction. Figure 5.2 shows in color the parts that substitute the aortic root.

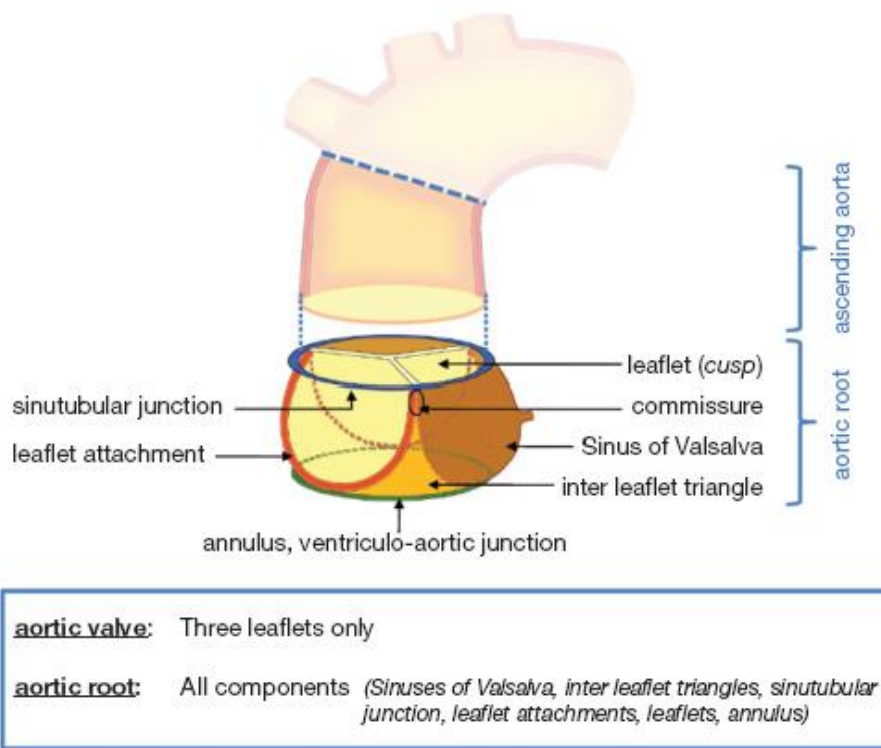


Figure 5.2

Thoracic aorta.

Ascending aorta and aortic root with its parts are depicted in color.

The components of aorta are leaflet, commissure, sinus of Valsalva, inter leaflet triangle, sinotubular junction and leaflets attachment.

(<http://www.annalscts.com>)

- **Sinotubular Junction**
It is where the normal tubular of the aorta is attained. The normal diameter for this ring is around 2.8 cm. In figure 5.2 this part of thoracic aorta is shown as the top formation of a ring in the annulus.

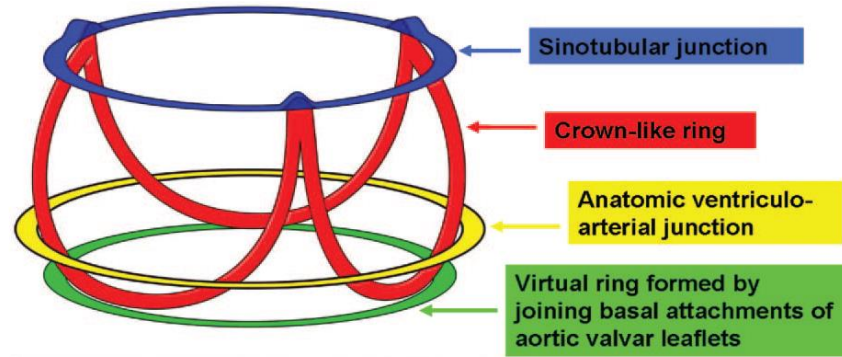


Figure 5.3

Depiction of the sinotubular junction (blue ring) and the annulus (green ring)
(Anatomy and Function of Normal Aortic Valvular Complex)

- Ascending Thoracic Aorta**
The ascending aorta is the initial part of the aorta. It rises superiorly from the left ventricle and it has a length of approximately 5 cm. The normal value of the diameter of the ascending aorta is lower than 2.1 cm/m^2 .
- Aortic Arch**
The aortic arch is the segment that links the ascending and descending aorta.
- Descending Thoracic Aorta**
The descending aorta contains a thoracic part and an abdominal part. The size of the descending aorta is lower than 1.6 cm/m^2 .

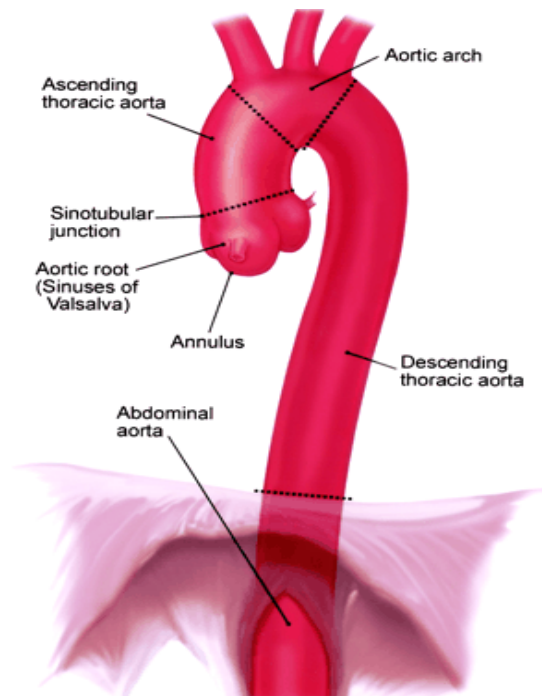


Figure 5.4

The geometry of thoracic aorta
(Contemporary Reviews in Cardiovascular Medicine)

5.1.2 Abdominal Aorta

The abdominal aorta has a diameter lower than 3cm/m2. It is a direct continuation of the thoracic descending aorta. Through the length of the aorta there are six paired branches, where the most of them are in the abdominal part. These six paired branches are:

- bronchial arteries
- mediastinal arteries
- esophageal arteries,
- pericardial arteries
- super phrenic artery
- intercostal arteries

The intercostal branches are in fact nine. The right branches are longer than the left (the descending aorta is placed on left side of the vertebrae). All this branches have a purpose: they provide blood to several organs and areas, such as the lungs, esophagus and chest area.

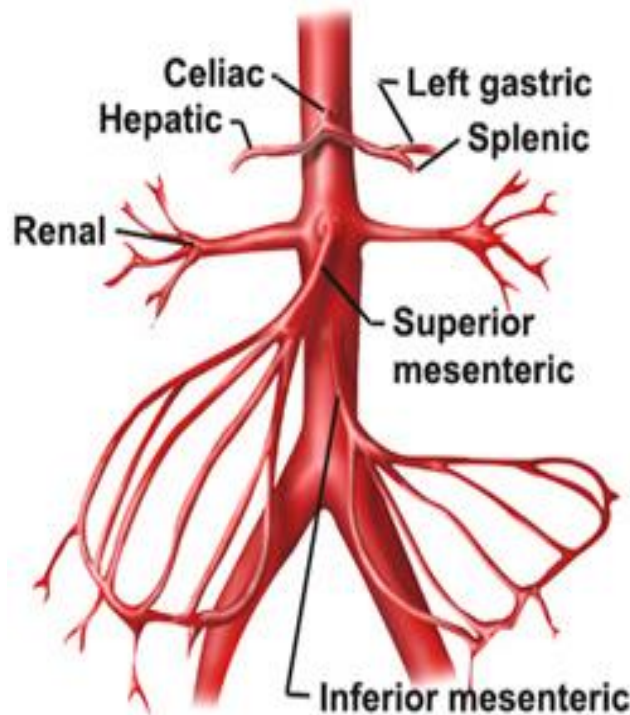


Figure 5.5
Abdominal aorta with its branches.
(www.uwhealth.org)

The definition of all these seven areas (six areas of thoracic aorta and one of abdominal aorta) is important, because each area defines a patch. Patches are segments of the entire geometry of an object. This segmentation happens due to different materials or alteration of geometry. The border between two patches is where the continuity stops.

5.2 Aneurysms

Aneurysm is a local permanent non reversible dilatation of the aorta by at least 50% of its normal size (according to the patient's height weight and sex). Aneurysms are classified as abdominal or thoracic (the thoracic aneurysm grow faster than abdominal ones, on old patients). The majority of them are abdominal. An abdominal aneurysm is any area in the abdominal aorta with diameter over 3cm and they usually appear in the area below the renal arteries. The thoracic aneurysms can be in the ascending aorta (between aortic annulus and innominate artery), aortic arch, descending aorta (in the area of the left subclavian artery) and thoracoabdominal aorta. A real aneurysm is in fact the case of dilatation of all three layers of the aortic wall.

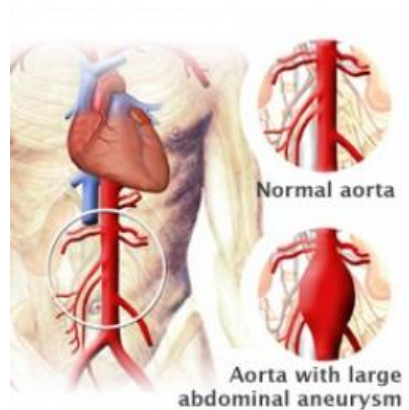


Figure 5.6

Comparison of a healthy aorta and an aorta with aneurysm
(www.aggeia.com)

The aneurysm happens in three phases. First, as an aftermath of the degradation of the elastin and the high production of collagen, the aneurysm expands (from 2cm to 3cm). Next, on the second stage the collagen degenerates and the diameter reaches at 5 cm. finally on the third phase the degeneration of collagen accelerates and in combination with the continuous increase of diameter the result is the rupture of aorta.

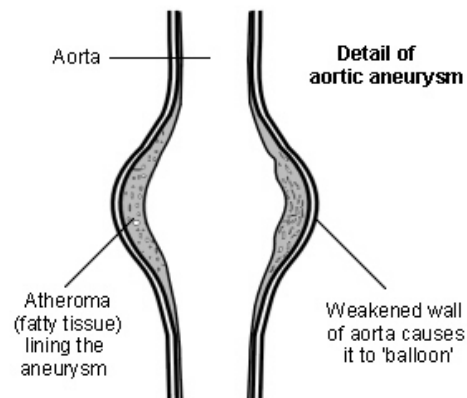


Figure 5.7

Detail of aortic aneurysm
(<http://patient.info/health/abdominal-aortic-aneurysm>)

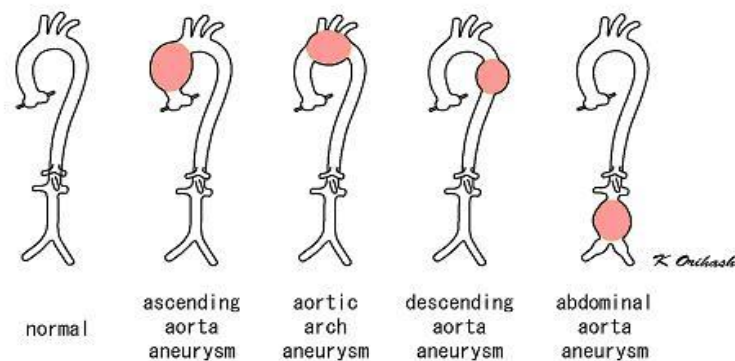
A patient that suffers from aortic rupture usually dies within 6 hour from the moment of rupture. A doctor can predict if there is a high risk of rupture from the size of the aneurysm. On the time of rupture there is acute pain and the patient collapses, gets in shock or dies.

A cause of aneurysm may be a trauma. Also, after an inflammation of the aortic wall or because of a dissection of aorta (this case has a higher rate of diameter's increase)

Whether a patient with a traumatic rupture of an aneurysm will survive, is depended on the period of time since the rupture, the rest injuries and the medication. The causes of the traumatic rupture are that the body decelerates after the crash with an immobile body and the immediate damage on thorax after the crash. So the real causes of damage are the forces on the body of the patient that create strain, rupture, bending and explosion on the wall of aorta due to the high stent pressure.

An aneurysm due to acute dissection of the aorta must be treated surgically immediately. The kinds of the aortic dissections are categorized as type I, II or III. During the dissection the aorta is torn in the media (the middle layer). Then, blood flows through the various “holes” from the lumen to the media. Due to this fact, a false lumen is created in the area of the half diameter. The rupture is often transverse and “covers” the intima and almost all the media. As to the diameter, the disorder happens in more than the half diameter of the aorta. The causes of dissection are high blood pressure and the degeneration of the media layer. The pain of the dissection is sharp and intense. Another feature of the pain of aortic dissection is that it continually migrates. Patients often describe the pain as if their internal organs are torn. The best way to face this disorder (after it is diagnosed) is with medication, so that the pain is reduced, the dissection stops and the risk of rupture is avoided. If the doctor decides on surgery, the reason is that the dissection is near a “risky” area or that the danger of rupture is high. During the surgery the problematic length of the aorta is replaced with a tubular graft.

The aneurysms of aortic root are usually ruptured on the side of the right atrium or free (in no specific direction). Similar behaviors show the aneurysms of the ascending aorta.



Various aortic aneurysms

Figure 5.8

Several cases of aortic aneurysms

(www.aorticdissection.com)

If an aneurysm has a diameter larger than 5cm, a surgical interference is required. If not, there is the risk of rupture or dissection. The critical diameters for these risks are 6cm for the ascending thoracic aorta and 7cm for the descending thoracic aorta.

Below there is a table that shows, according to the body surface area and the size of aorta how high is the risk of an aneurysm.

BSA	Aortic Size (cm)								
	3.5	4.0	4.5	5.0	5.5	6.0	6.5	7.0	7.5
1.30	2.69	3.08	3.46	3.85	4.23	4.62	5.00	5.38	5.77
1.40	2.50	2.86	3.20	3.57	3.93	4.29	4.64	5.00	5.36
1.50	2.33	2.67	3.00	3.33	3.67	4.00	4.33	4.67	5.00
1.60	2.19	2.50	2.80	3.13	3.44	3.75	4.06	4.38	4.69
1.70	2.05	2.35	2.65	2.94	3.24	3.53	3.82	4.12	4.41
1.80	1.94	2.22	2.50	2.78	3.06	3.33	3.61	3.89	4.17
1.90	1.84	2.11	2.37	2.63	2.89	3.16	3.42	3.68	3.95
2.00	1.75	2.00	2.25	2.50	2.75	3.00	3.25	3.50	3.75
2.10	1.67	1.90	2.14	2.38	2.62	2.86	3.10	3.33	3.57
2.20	1.59	1.82	2.05	2.27	2.50	2.72	2.95	3.18	3.41
2.30	1.52	1.74	1.96	2.17	2.39	2.61	2.83	3.04	3.27
2.40	1.46	1.67	1.88	2.08	2.29	2.50	2.71	2.92	3.13
2.50	1.40	1.60	1.80	2.00	2.20	2.40	2.60	2.80	3.00

low risk(~4% per year)

moderate risk(~8% per year)

severe risk(~20% per year)

Figure 5.9

The risk of an aneurysm based on the aortic size and the body surface area.
(American College of Cardiology Foundation)

The risk factors are atherosclerosis-hypercholesterolemia (are they the same??), family history, tobacco smoking, male sex, increasing age, white race, prior vascular diseases, hypertension, renal failure, previous aortic aneurysm repairs or chronic obstructive pulmonary diseases. The causes may be trauma, infections, inflammatory diseases and connective-tissue disorders, aortitis, weightlifting, amphetamines and cocaine (the three last “activities” are risky possibly due to the fact that during them a steep rise of blood pressure).

The real problem with aneurysms is that most of the thoracic aneurysms are asymptomatic and they are often misdiagnosed. So, they are usually located by luck or too late (after they are ruptured).

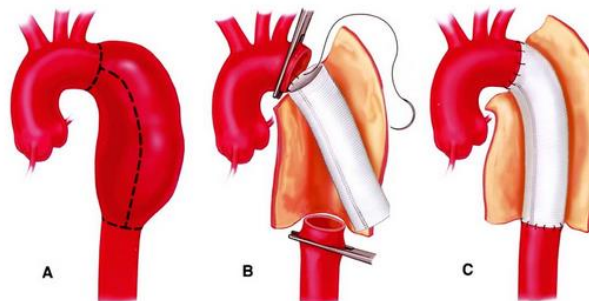


Figure 5.10

Repair of a descending thoracic aortic aneurysm with a stent
(<http://www.cardiachealth.org/thoracic-aortic-aneurysm>)

5.3 Medical Imaging

Medical imaging is a procedure for creating visual representations of human parts. It shows internal structures that are surrounded by skin and bones, without arising the problem of superimposition. They are widely used as it is a noninvasive way for detection of diseases, pre-surgical planning or for after-surgical follow-up.

There are several technologies of medical imaging being used in medicine, but in every case the doctor chooses the appropriate one, that will give the best results.

These technologies are:

- Magnetic resonance imaging
- Ultrasonography
- Endoscopy
- X-ray radiography
- Elastography
- Tactile imaging
- Thermography
- Medical photography
- Positron emission tomography
- Fluoroscopy
-

Medical imaging and equipment are used often in Biomechanics for the procedure of geometry processing. Usually a combination of apparatus is needed, as the results are not clear or missing information. This kind of apparatus often have low contrast and their results are often incomplete. Therefore the data from the patient need some analysis and clean-up, before using them for the solution of the problem.

In medical procedure, imaging is critical. The results of imaging are used for diagnosing and after surgery monitoring. Doctors are interested in watching the area of the heart and aorta during the phase of systole and diastole.



Figure 5.11

Cross section of an abdominal aneurysm
(<http://emedicine.medscape.com>)

5.3.1 Axial Tomography

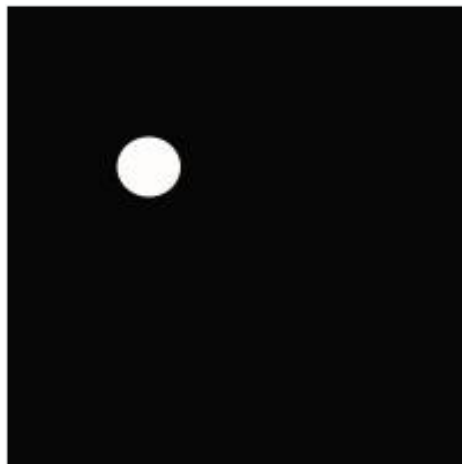
Computerized Axial Tomography Scan (CAT scan) is a medical imaging technique that gives results from combinations of many X-Ray images from different angles. The user can see any cross sectional image from the spot that he is interested without actually cutting the object. It is also known as X-Ray computed tomography (X-Ray CT). The machine takes two dimensional radiographic images around an axis of rotation. The result is a three dimensional picture of the object. The interesting fact about CT scan is that it is not used only for medical imaging but for industrial reasons too. Medical imaging is the most common application and it helps with diagnosing and decisions making for the healing process.

In some cases contrast materials are used, that highlight objects that are difficult to delineate from their surroundings (e.g. blood vessels). These materials can also provide useful information about tissues.

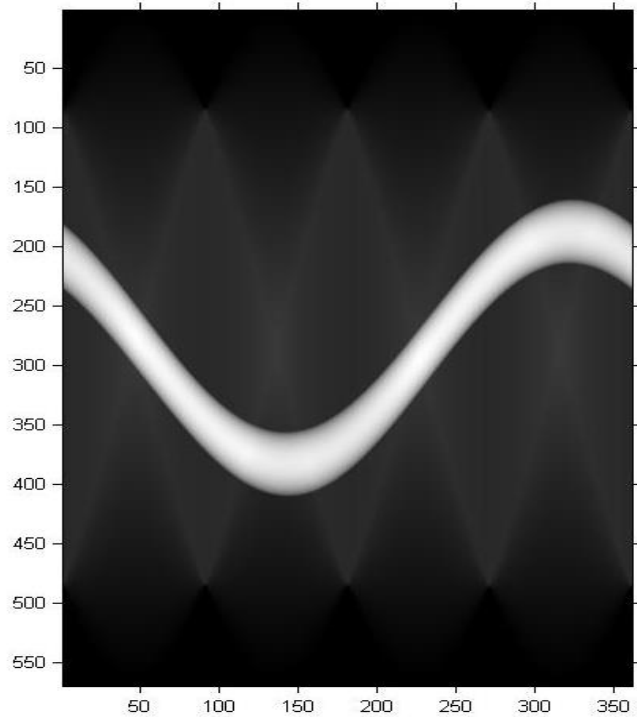
Procedure

The object investigated is surrounded by an X-ray source and X-ray sensors in opposite sides. There is continuous rotation of the source and sensors while the object slowly and smoothly slides through the ring. Due to this rotation, the machines are called helical or spiral CT machines. Some machines have multiple rows of sensors, which are capturing multiple cross-sections on the same time.

A sinogram is a visual representation of the raw data, that it is not sufficient for interpretation. The raw data are actually projections of the object being scan. With Radon transformation, the raw data create the structure of the object.



(a) Image of an off-centered disk in the (x,y) space



(b) Image of a sinogram. Radon transformation X-axis: angle, Y-axis: parameter t

Figure 5.12

Depiction of real geometry and produced raw data
(oftankonyv.reak.bme.hu)

Two-dimensional CT images are conventionally rendered so that the view is as though looking up at it from the patient's feet. Hence, the left side of the image is to the patient's right and vice versa, while anterior in the image also is the patient's anterior and vice versa. This left-right interchange corresponds to the view that physicians generally have in reality when positioned in front of patients.

Advantages

- The results are in high contrast resolution
- Every difference between tissues that differ in physical density by less than 1% is distinguished
- There is no problem with the superimposition of surrounding objects
- Data from a single CT imaging procedure consisting of either multiple contiguous or one helical scan can be viewed as images in the axial, coronal, or sagittal planes, depending on the diagnostic task

Disadvantages

- The patient is exposed to a moderate to high radiation that can even lead to cancer. As a result, doctors try to avoid using this scan, especially in the case of children. When an MRI can be used, it is preferred.
- The procedure involves injected radiocontrast agents. These agents have some side effects, such as nausea, vomiting, or an itching rash. In rarer case anaphylaxis may occur, which is an effect that can lead to death when the patient is of poor health.
- It shows only an image and not data like flow velocity or wall shear stress



Figure 5.13
CT scan machine
(www3.gehealthcare.in)

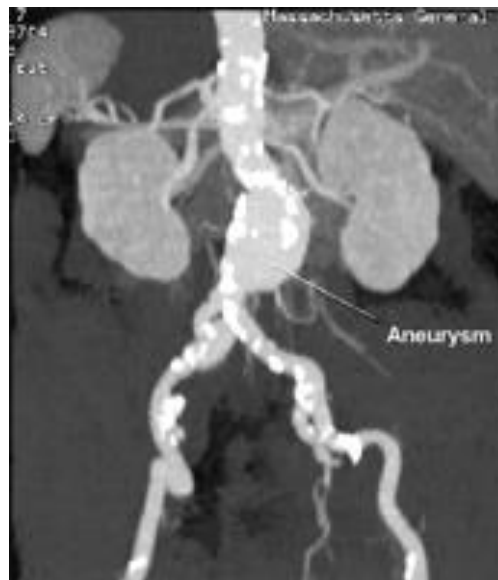


Figure 5.14
CT scan of an abdominal aneurysm. The aneurysm is right before rupture
(circ.ahajournals.org)

5.3.2 Magnetic Tomography

Magnetic Resonance Tomography (MRT) is a medical imaging technique used in radiology for investigation of the patient's anatomy and physiology. It is also known as Magnetic Resonance Imaging (MRI) and Nuclear Magnetic Resonance Imaging (NMRI). It works with magnetic fields and radio waves in order to formulate images of parts of the body. Subsequent pictures are taken with a difference of mere milliseconds, so the object of research is depicted at different times. In case of cardiovascular diseases, MRI is used in combination with other imaging techniques, as the movement of the heart is too fast. Nowadays it is widely used in hospitals for diagnosing, pre-surgical planning and follow up. Furthermore, the kinematic sequences and volumetric areas are given

Procedure

A strong magnetic field is created around the investigated object. This magnetic field must be strong and uniform, with a magnetic strength of 0.2-7 Tesla. Protons (hydrogen atoms) in tissues that contain water molecules are used to create a signal. This signal is processed to form an image of the body. Energy from an oscillating magnetic field is temporarily applied to the patient at the appropriate resonance frequency. The excited hydrogen atoms emit a radio frequency signal which is measured by a receiving coil. The radio signal can encode position information by varying the main magnetic field using gradient coils. As these coils are rapidly switched on and off, they produce the characteristic repetitive noise of an MRI scan. The contrast between different tissues is determined by the rate at which excited atoms return to the equilibrium state. Exogenous contrast agents may be given intravenously, orally or intra-articularly for more clear images.

Advantages (bullets)

- the patient is not exposed to any radiation
- more sensitive than a CT and thus used for exposing small geometries

Disadvantages

- Expensive
- time consuming
- causes claustrophobia in some cases
- not suitable for patients with cochlear implants or cardiac pacemakers

5.3.3 Geomiso Bio

Geomiso Bio is working with MRI images, as MRI is the only available medical machine in Greek hospitals that can give the necessary data, such as velocity flow. In cooperation with the Greek hospital “Hygeia” and its cardiology unit, real data from patients’ MRI will be compared with the results of Geomiso Bio. Doctors were especially interested in features like finding the value of pressure in specific areas of aorta, or simulation of treatment in complex geometries.

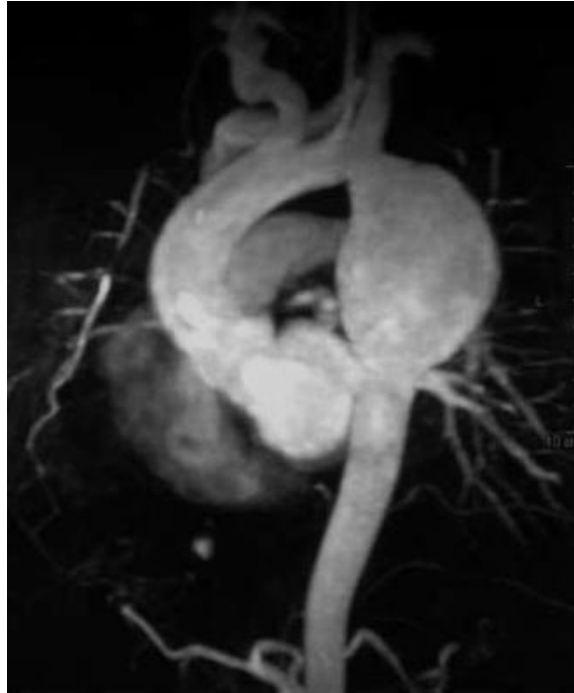
Most medical imaging files are CAD files, meaning they only show an image and they lack in analyzing the case (CAE). Geomiso Bio will solve this problem, as it will both creating an exact model of the aorta’s geometry and simultaneously analyzing it in short time. It will give more results for the geometry than any medical technology can give today,

The majority of files from medical imaging apparatus are in DICOM format (.dci). DICOM means Digital Imaging and Communications in Medicine. A file of a medical image, also contains the patient’s information so that the image can never be separated from this data. In order to process the data, a special software is needed or the creation of a plugin for the connection of MRI machine and Geomiso. Special software programs are offered free online, while there is also a huge database of DICOM files from several cases and machines.



Figure 5.15

MRI apparatus. It is a rather large machine, which requires space and also soundproofing, as the magnets produce a humming sound.
(www.universitymri.com)



(a) a large aneurysm on the origin of the left subclavian artery



(b) after the procedure.

The diameter of aorta went back to normal after the placement of a stent

Figure 5.16

MRI images of a patient with an aneurysm in the left subclavian artery and after the surgery. The case was critical as the aneurysm was in danger of rupture.

(<http://www.revespcardiol.org>)

5.4 Constitutive Law

5.4.1 Introduction

In order to achieve an analysis that corresponds to the actual behavior of the used material, its properties and constitutional law have to be defined. Properties deal with elasticity modulus, Poisson's ratio and specific weight. The constitutive law defines the response of the material under the action of external forces, depending on whether it is elastic-inelastic, isotropic-anisotropic, homogenous- no homogenous and includes equations which describe this reaction. Elastic materials tend to recover completely from deformation and return to their initial shape after the external load is removed. Isotropic materials have identical properties in all directions and the homogenous ones have identical properties at all points in their body.

So, the constitutive law of the material plays a major role on the analysis type that will be performed. Many types of analysis can be applied to a structure, varying from linear (stress proportional to strain) to nonlinear and static to dynamic. Linear and nonlinear analyses are types imposed by material properties, as explained above. The choice between static and dynamic analysis depends on the acceleration of the applied load in comparison to the natural frequency of the structure. When the load is applied slowly enough, static analysis can be performed. Otherwise, inertia forces should be taken into consideration and the suitable analysis type is the dynamic one.

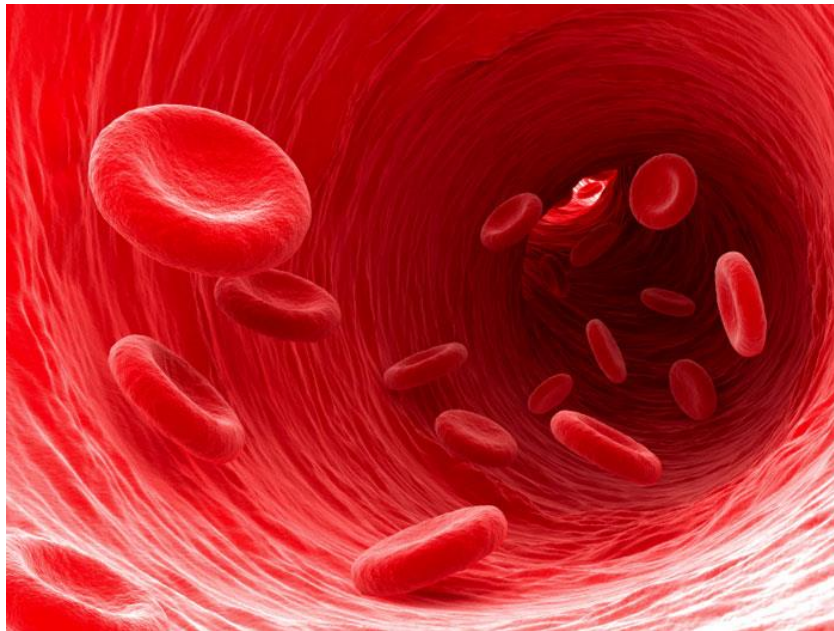


Figure 5.17
Blood cells moving through an artery
(www.sciencedaily.com)

5.4.2 Aortic wall

The aortic wall has three layers:

1. intima
2. media
3. adventitia.

The intima is the inner thin layer and the media provides the strength of the lumen through the formation of a spiral layer of tissue that consists of elastic fibers and smooth muscle cells. Finally the adventitia is the outermost connective tissue that provides the nutrition from the arterial and venous vasa vasorum. The thickness of the aortic wall is lower than 4mm.

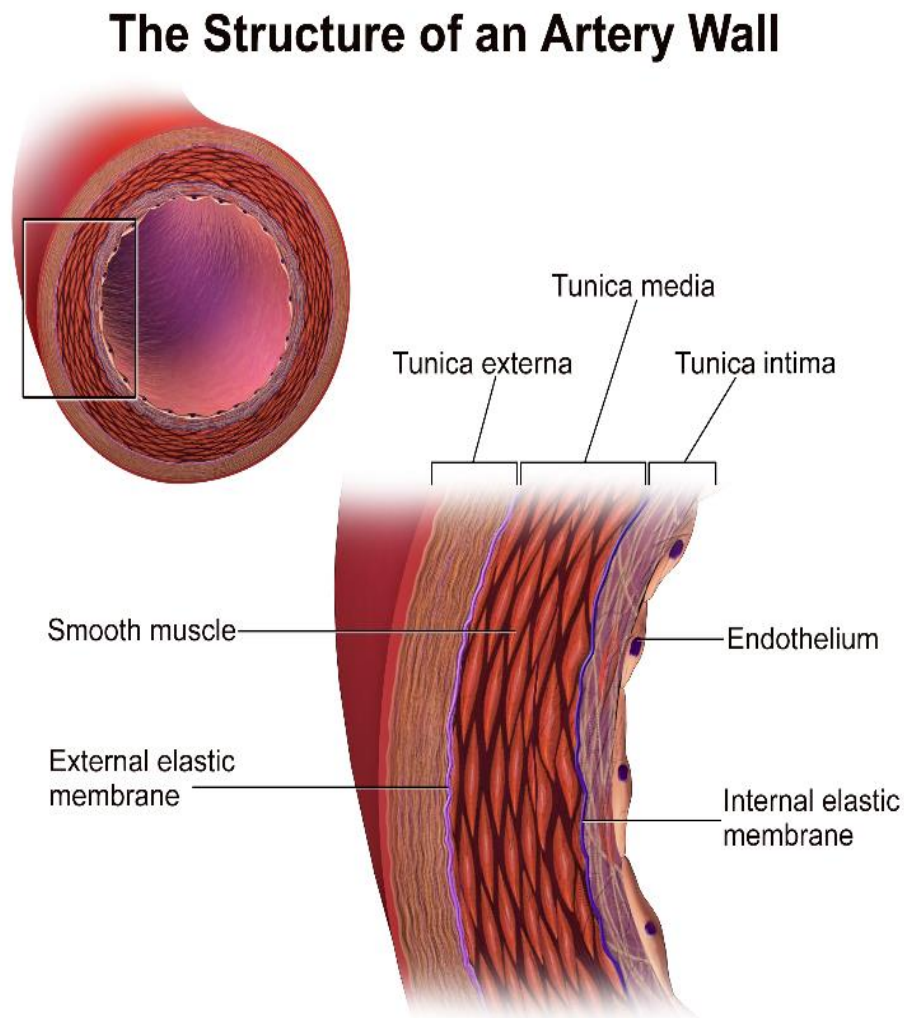


Figure 5.18

The cross section and detail of aortic wall.
(<http://biology.about.com>)

An aorta has a thick wall to carry blood at high pressure. The wall of aorta works as an elastic tube that has the ability to expand during a pressure pulse and to store elastic energy. Because of this specification of the aortic wall the blood can flow smoothly through the arteries to the human body. The tissue of the wall is similar with skin. It contains elastin to give the ability to expand and collagen to set limits to this expansion. A section of the aorta can be seen in figure 5.18.

The components of an aortic wall are:

- endothelium
- internal elastic membrane
- smooth muscle
- external elastic membrane

Figure 5.19 shows the image of the aortic wall's structure from a microscope. Collagen strands, because of their "fiber" nature, create an elastic mesh that allows the wall to stretch and deform. Collagen is a protein that provides stiffness and strength and play a major role in the properties.

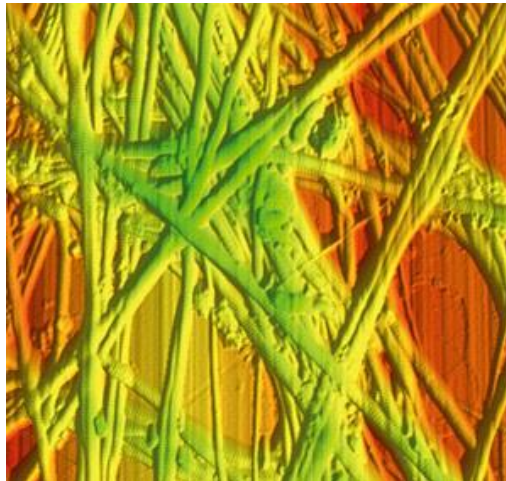


Figure 5.19

Collagen strands imaged by atomic force microscopy.

(Image generated with an Asylum Research MFP-3D Atomic Force Microscope, image courtesy of Asylum Research UK)
(CES database)

The mechanical characteristics of the wall of aorta vary from person to person. They also change through the years. They lose their tensile strength and in case of high blood pressure, the strain of the wall increases.

The following diagrams shows the relationship between stress-strain and modulus-pressure. Both pairs are rising exponentially. These quantities don't have a constant value through the length of aorta.

Specifically on the first graph, the modulus of artery and vein increases with strain in a manner designed to prevent bursting.

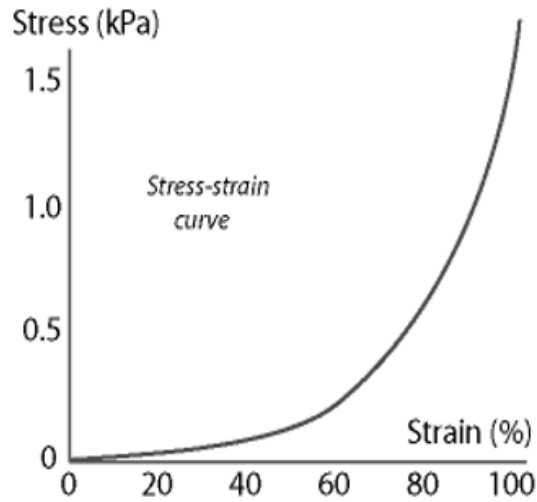


Figure 5.20
Stress-strain curve for human elastic arterial tissue
(CES database)

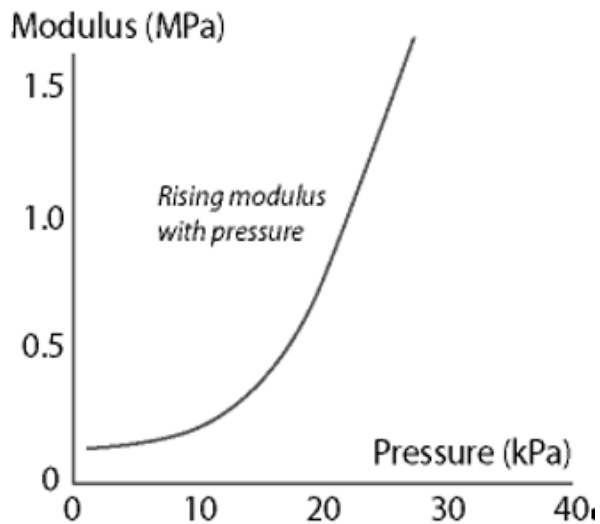


Figure 5.21
Modulus-density curve for human elastic arterial tissue
(CES database)

Some of the mechanical properties of the wall are:

- Density: $1,3e3-1,35e3$ kg/m³
- Young's modulus: $8e-4-0,0015$ GPa
- Elongation strain: 74-104%
- Mechanical loss coefficient (tan delta): 0,1-0,15

The modulus of the wall increases with strain, in order to prevent bursting. Also, the loss coefficient has a low value, so that at least 85% of the elastic energy is provided to pump blood between expansion pulses.

In order to describe an elastic material, the elastic modulus is needed. In our case, aortic tissue is a non linear material, so a single value of the elastic modulus cannot describe the aortic wall. Some assumptions are made, such as that the aortic wall is an incompressible material. These characteristics can vary from person to person. Doctors can determine the range of these values through tests and enter an average value in Geomiso Bio.

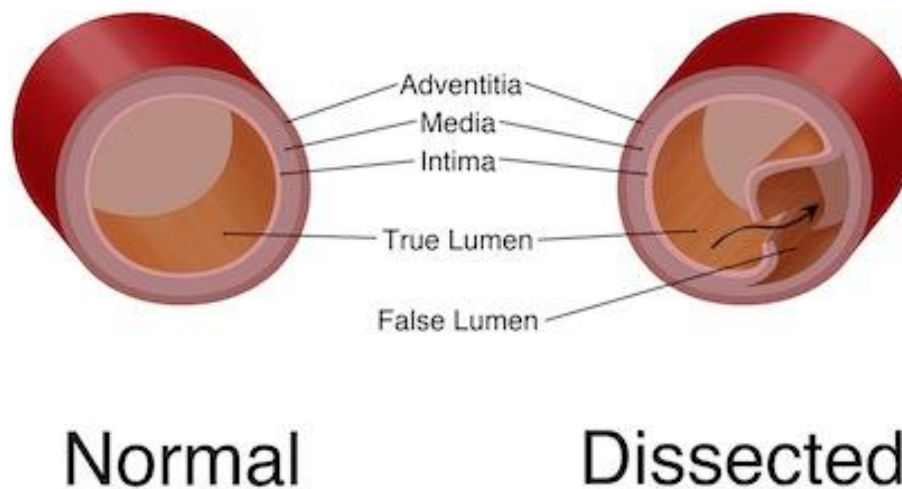


Figure 5.22

When mechanical properties of aorta are decreasing, danger of aortic dissection shows up. Dissection is a tear in the inner layer of the wall. After dissection blood flows into the wall and the layers separate, with danger of rupture.

(<https://ufhealth.org/uf-health-aorta-center/aortic-dissection>)

5.4.3 Blood Properties

An assumption of a rigid wall means exclusion of pressure wave propagation and it overestimates the shear stress. In order to take in consideration the movement of the wall a computing method is needed, such as the Lagrangian-Eulerian approach (How ALE works: The arterial wall is treated as a nonlinear elastic solid in the Lagrangian description governed by the equations of elastodynamics.)

As a simplification of the problem, the fluid that interacts with the solid wall is considered to be a Newtonian viscous fluid governed by the incompressible Navier-Stokes equations. Only in a very small scale blood behaves as elastic.

The purpose of the blood is to carry the essential to the cells of the body and to carry waste away from them. An average adult has 5 liters of blood in his body, which consist 8% of his total weight. Blood is circulated around the body through blood vessels by the pumping action of the heart. The process of systole and diastole “pushes” the blood and through arteries and veins, it goes to the body.

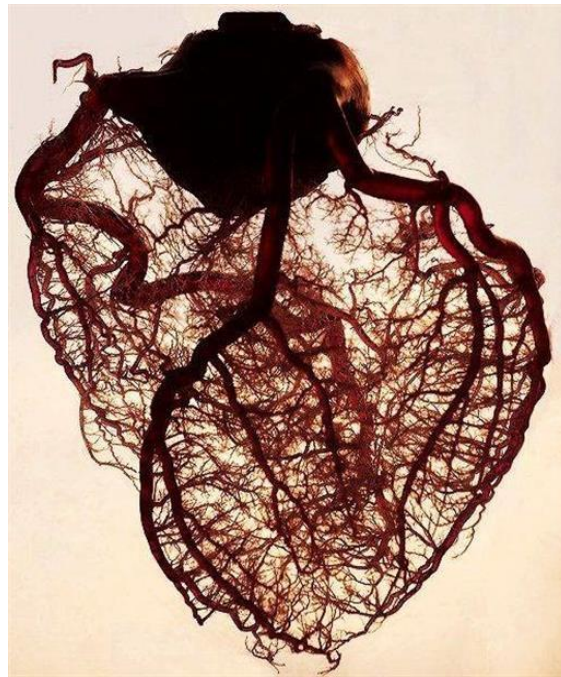


Figure 5.23
A real human heart with the arteries.
(www.nickbouboulis.4ty.gr)

Red blood cells are disc-shaped cells containing hemoglobin, which enables the cells to pick up and deliver oxygen to all parts of the body, then pick up carbon dioxide and remove it from tissues.

The blood flows through the human body with the help of the heart that works as a pump. The velocity of the blood in the aorta is 40 cm/s. The velocity is higher during the systole than during the diastole.

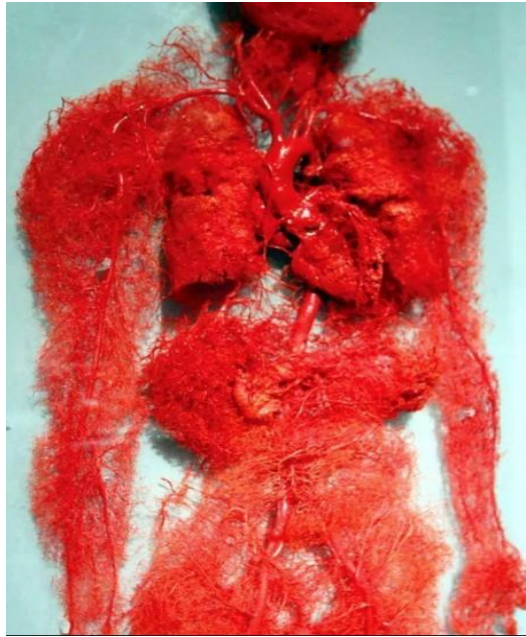


Figure 5.24

The blood vessels of the human body
(<http://www.innerbody.com/>)

The blood contains 55% of plasma and 45% of cells. The plasma is consisted of 92% water and 8% proteins and other solutes. The cells that are contained in the blood are the red and white blood cells and the platelets.

The blood cannot be described as a Newtonian fluid, due to the interaction of plasma and cells. Therefore the classic hydrodynamics cannot express the behavior of the blood. There is a special scientific branch for this purpose; the hemodynamics. Also, the blood is a shear-thinning fluid, which is it has lower viscosity at high shear rates.

Viscosity is a property of fluids, which shows the resistance of the substance to deform. The velocity of deformation is connected with the shear stress.

The blood viscosity is affected from many factors, such as:

- Hematocrit
- Plasma viscosity
- Mechanical properties of red blood cells
- Temperature

The normal value of blood viscosity at 37°C is $3 \cdot 10^{-3}$ Pa s.

Even though, the blood is not a Newtonian fluid, the plasma can be described as such. The viscosity of plasma at 37°C is 1.2 Ns/m². An increase of the temperature causes a decrease of the viscosity.

6. Applications

6.1 Bent Pipe

The bent pipe was first presented in *Isogeometric Analysis: Toward Integration of CAD and FEA* - J. Austin Cottrell, Thomas J. R. Hughes, Yuri Bazilevs - Wiley, 2009. It consists of a straight and a circular section, joined together. Parametric direction ξ represents the longitudinal direction of the pipe. Parametric direction η represents the pipe thickness and ζ the creation of the circular shape.

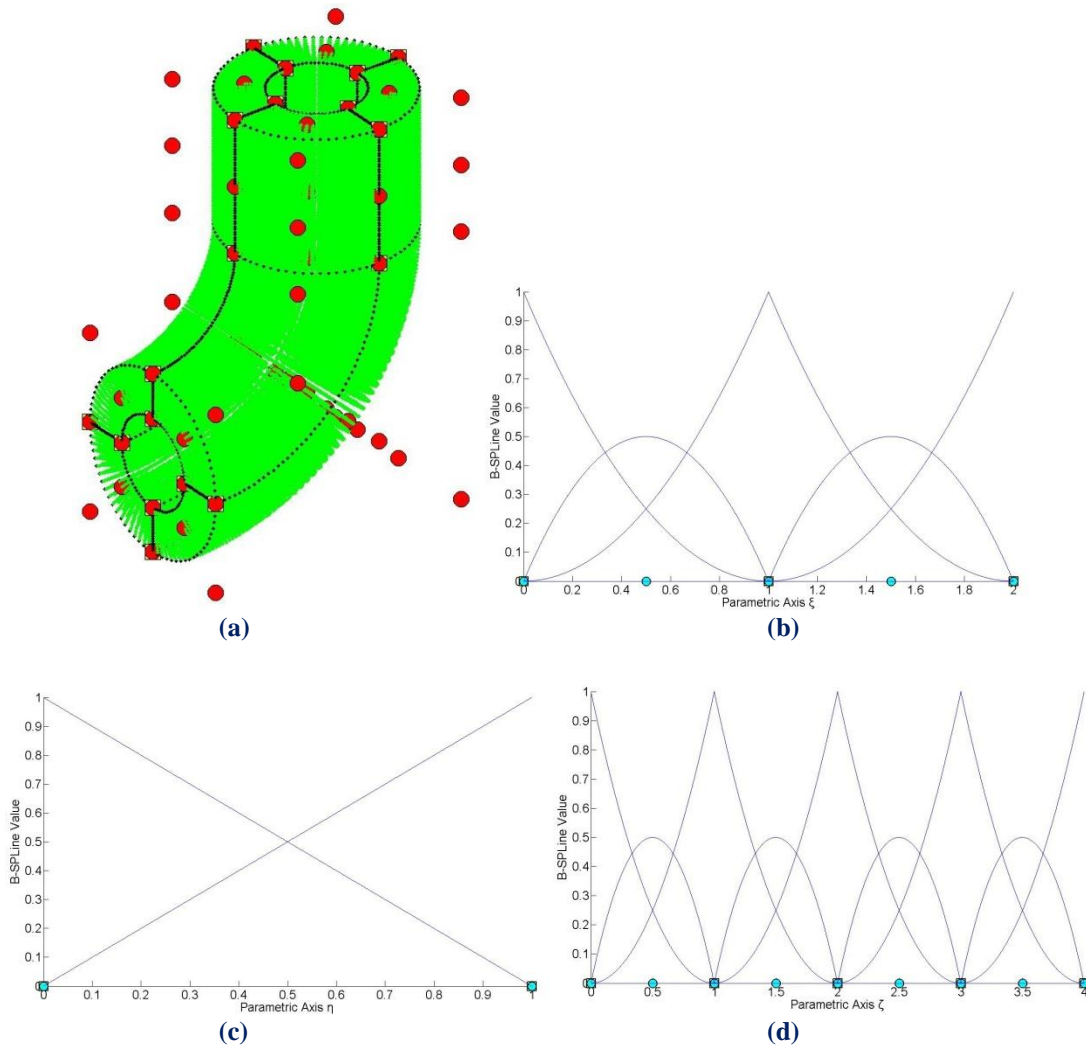
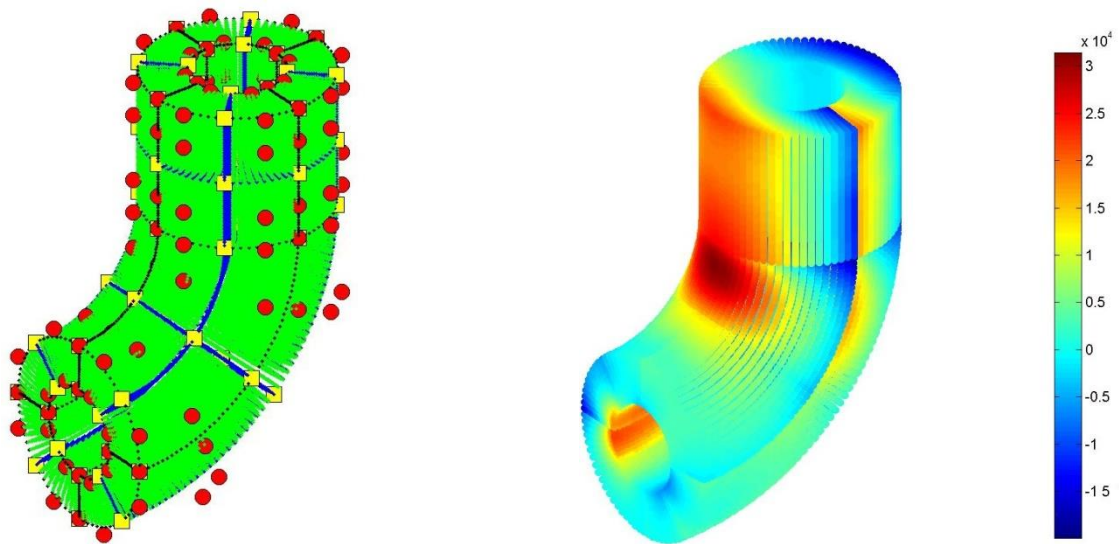


Figure 6.1.
 (a) Physical Space and (b), (c), (d) basis functions for bent pipe.

There are four patches across ζ , as required for the representation of a circle, and one patch across η , necessary for the transition from straight to circular section of the pipe.

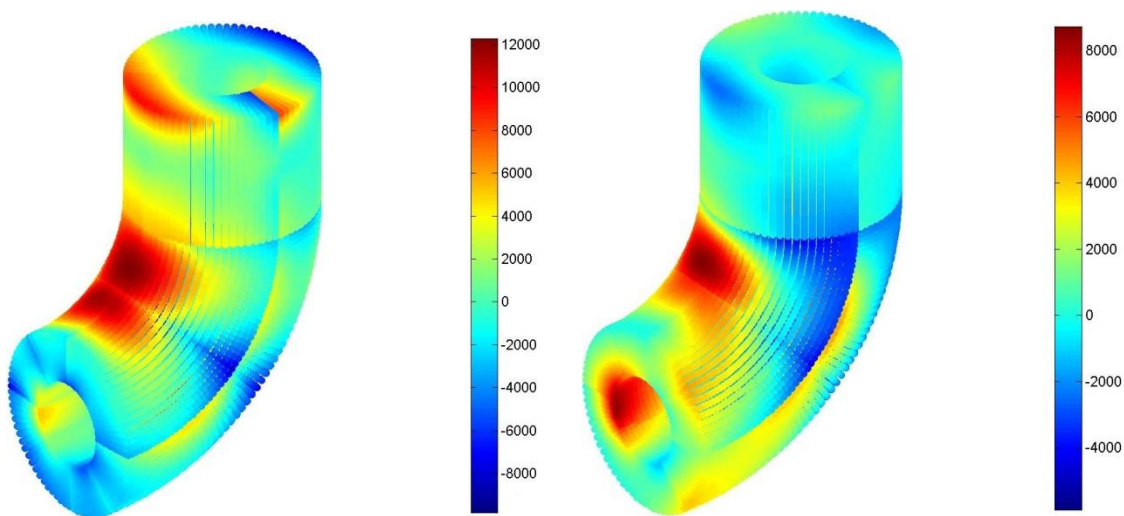
This coarse mesh cannot produce accurate results. These are achieved, as usual, by Refinement. h- and k- Refinement are applied on the bent pipe. The corresponding basis functions on ξ, ζ are represented in Figures 6.33 (e),(f) and 6.34 (e),(f).

Refinements lead to increased continuity and element interconnectivity. The stress discontinuity across patch boundary on ξ is visible as well.



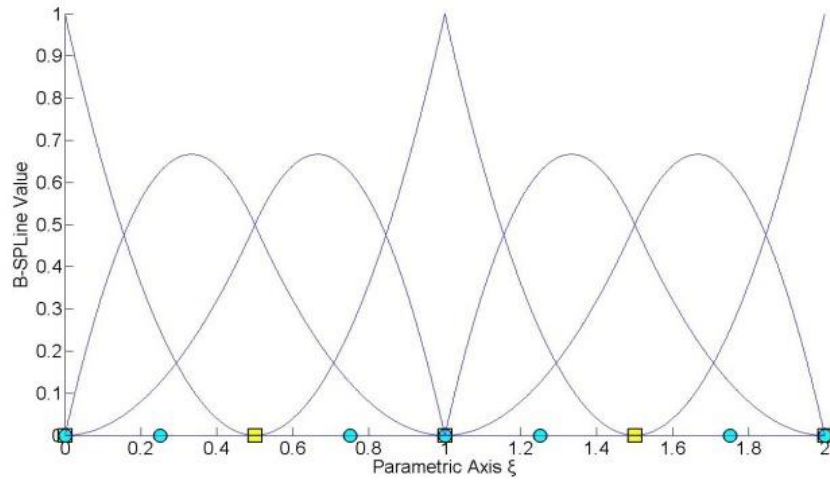
(a) Physical Space

(b) σ_{zz} contour

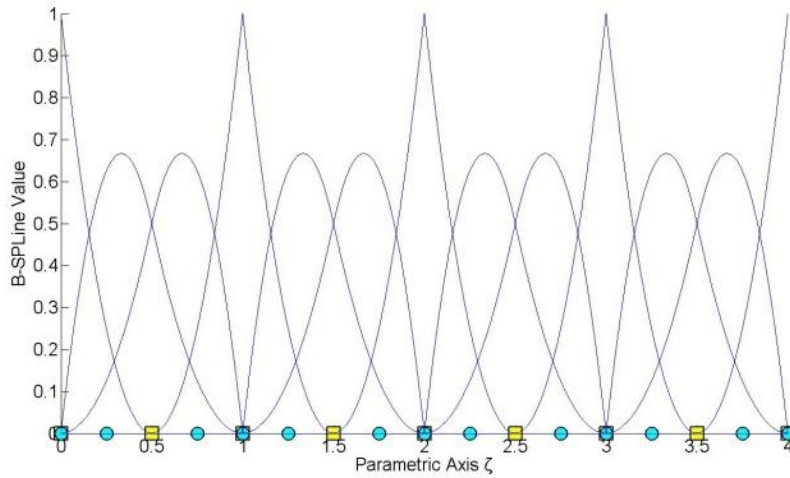


(c) σ_{xx} contour

(d) τ_{zx} contour



(e) B-Spline basis function ξ

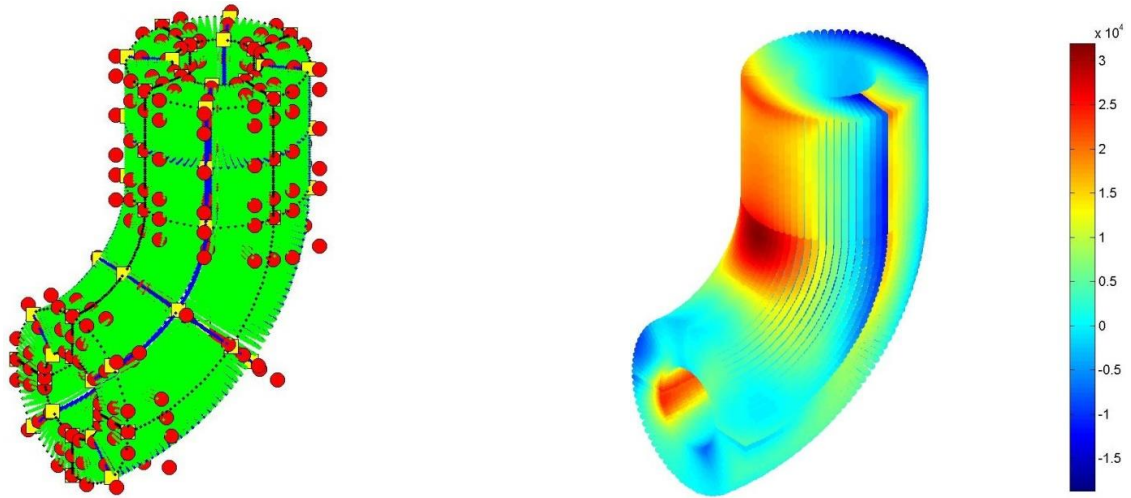


(f) B-Spline basis function η

Figure 6.2

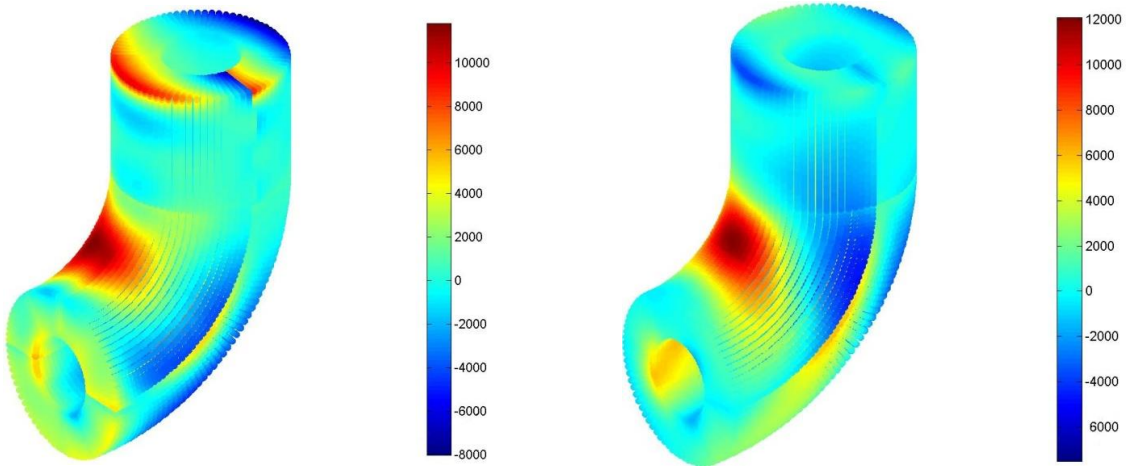
h-Refinement for Bent Pipe

Simulation of Human Aorta and Isogeometric Fluid Analysis



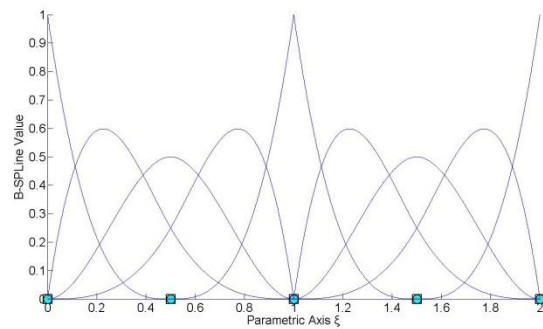
(a) Physical Space

(b) σ_{zz} contour

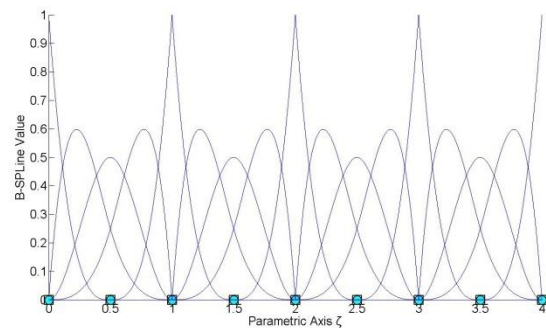


(c) σ_{xx} contour

(d) τ_{zx} contour



(e) B-Spline basis function ξ



(f) B-Spline basis function η

Figure 6.3
k-Refinement for Bent Pipe

6.2 Annulus

It is one of the most important applications as it simulates a section of aorta. Only a quarter of the annulus has to be analyzed as there is symmetry on both axis. There is a comparison of exact solution and the computed solution with the Geomiso software. The required results are velocity and pressure.

The first representation shows a NURBS geometrical model. The coarse mesh is shown with the minimum required number of control points, which is nine (shown in red color in figure 6.4). For the time only the 2D case is investigated.

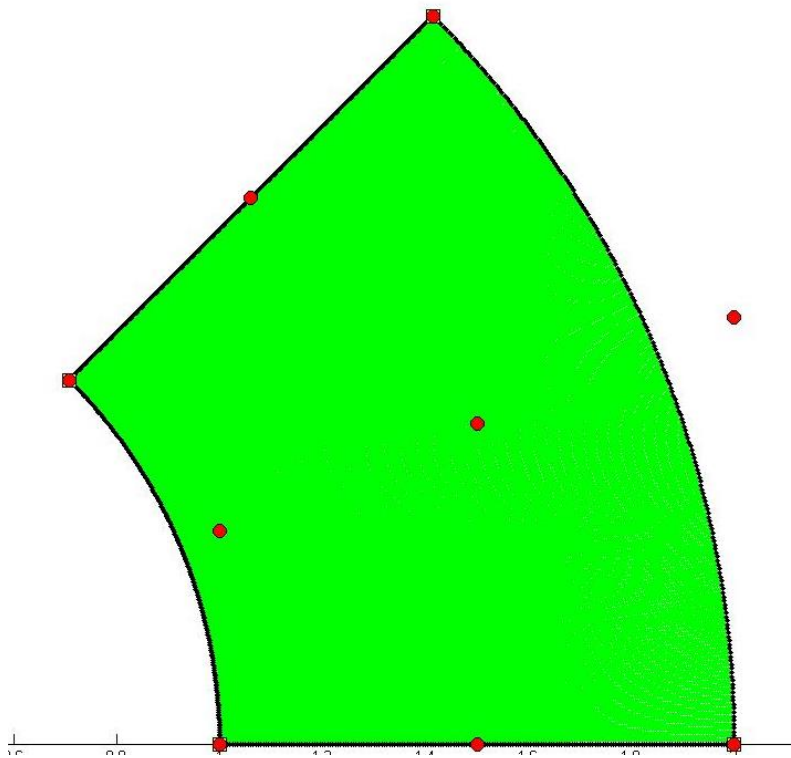
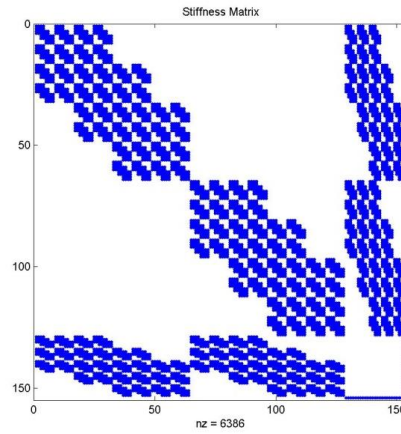


Figure 6.4

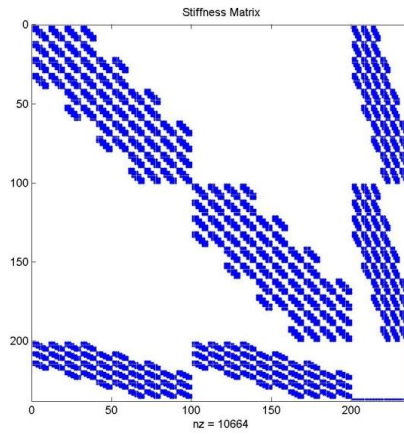
NURBS Geometrical Representation

A parametric investigation was made in all three elements (Taylor Hood, Nedelec, Raviart Thomas) with different degrees and continuities. Keeping constant the pressure degree (first at 2 and then at 3), the knot spans are increasing per ξ and η . Below there are the stiffness matrices from this investigation, as produced by Geomiso Bio.

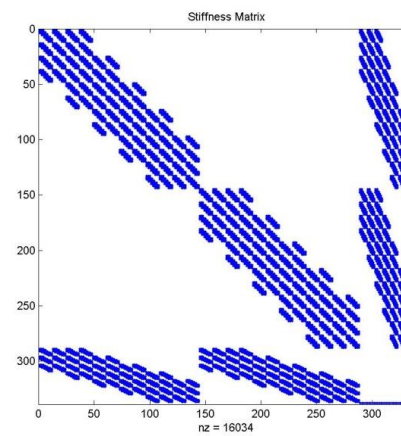
Simulation of Human Aorta and Isogeometric Fluid Analysis



(a) Knot Span=3



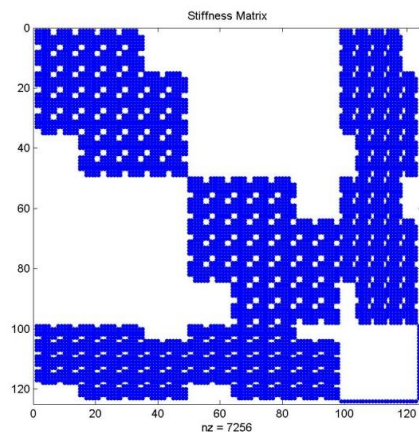
(b) Knot Span=4



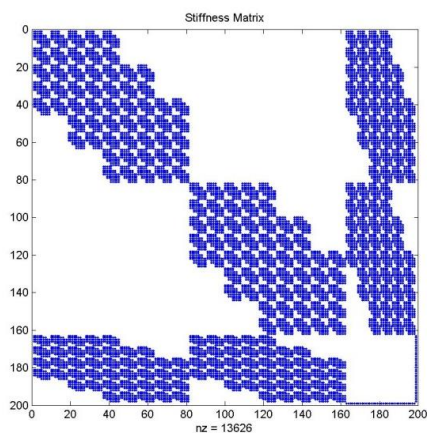
(c) Knot Span=5

Figure 6.5

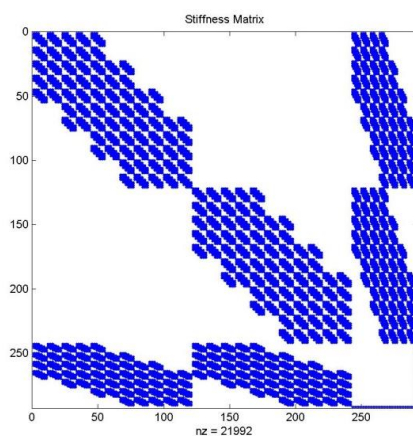
Taylor Hood stiffness matrix, Degree=2



(a) Knot Span=2

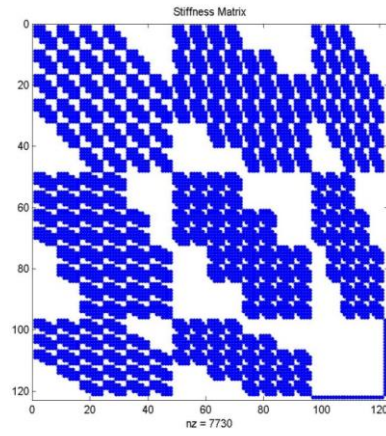


(b) Knot Span=3

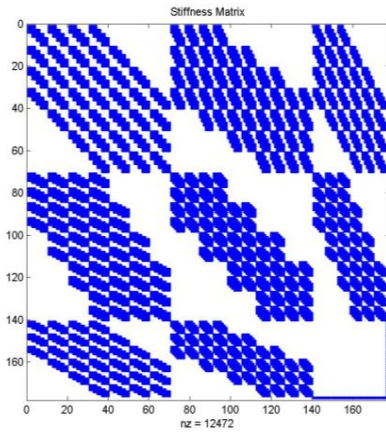


(c) Knot Span=4

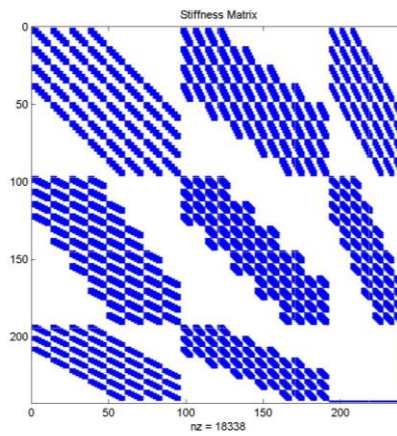
Figure 6.6
Taylor Hood stiffness matrix, Degree=3



(a) Knot Span=3

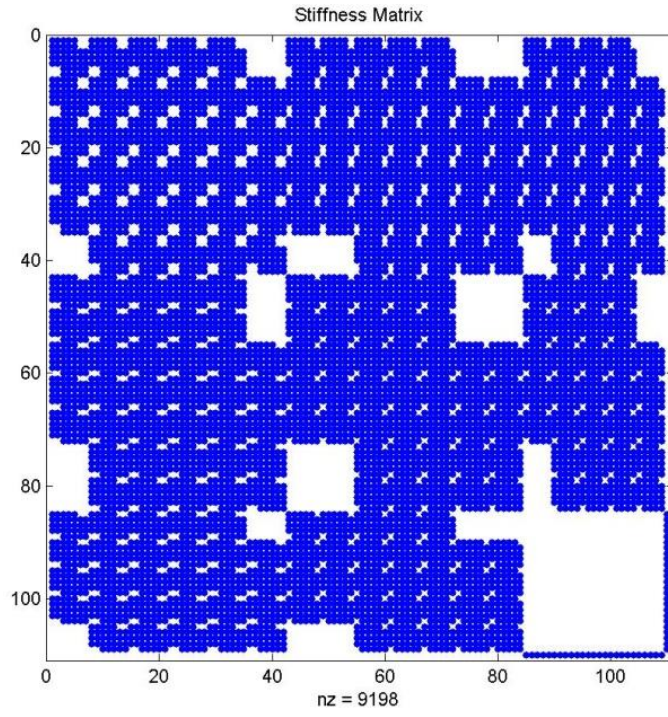


(b) Knot Span=4

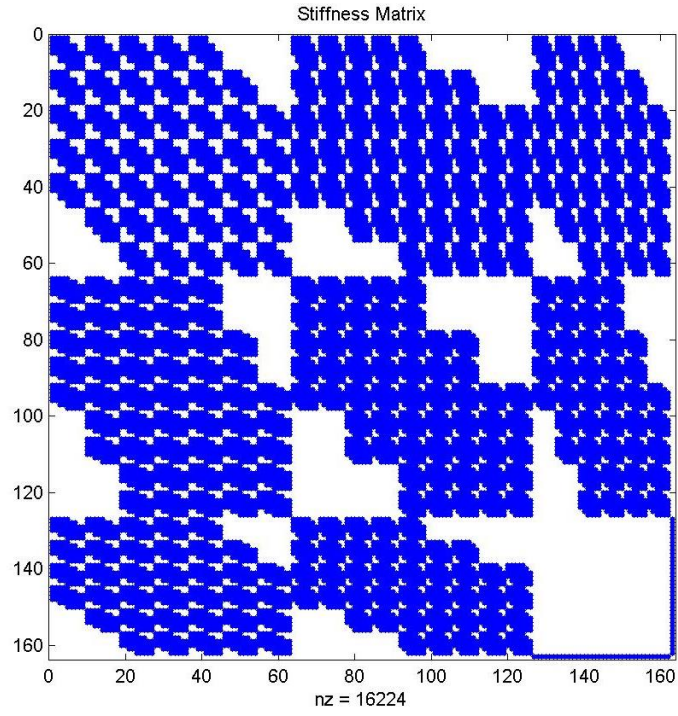


(c) Knot Span=5

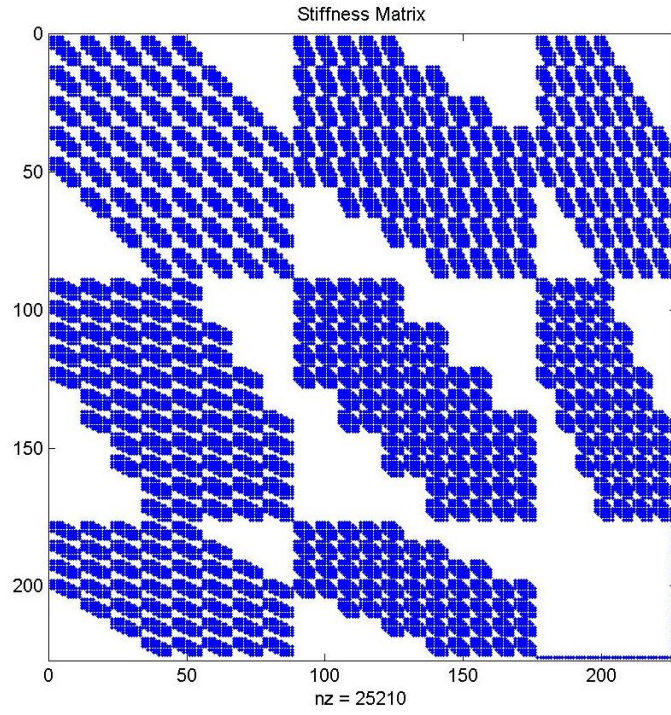
Figure 6.7
Nedelec stiffness matrix, Degree=2



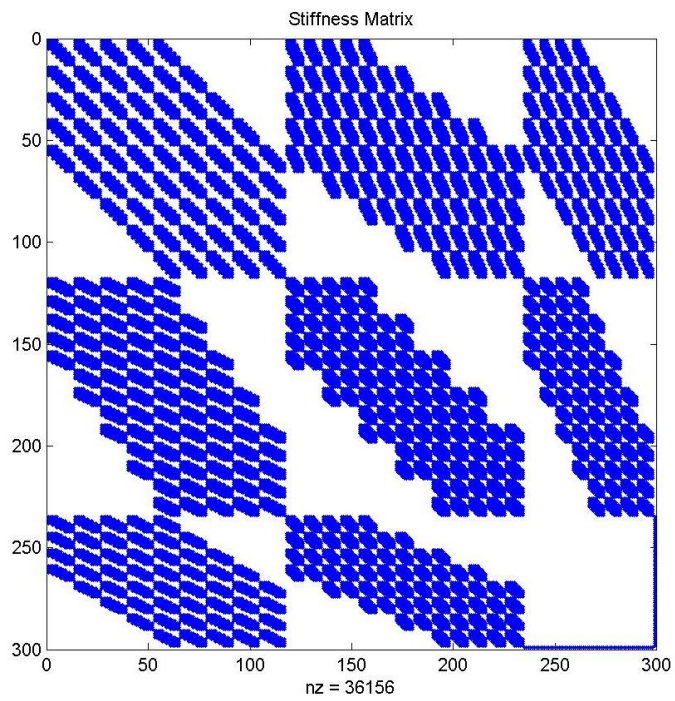
(a) Knot Span=2



(b) Knot Span=3

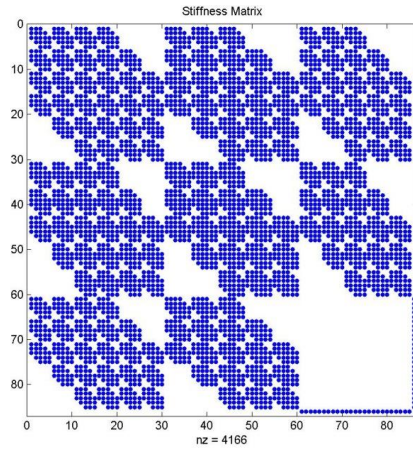


(c) Knot Span=4

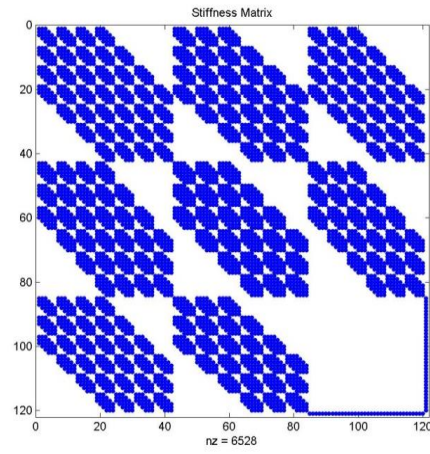


(d) Knot Span=5

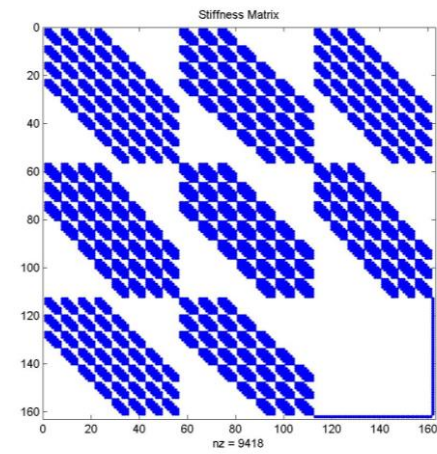
Figure 6.8
Nedelec stiffness matrix, Degree=3



(a) Knot Span=3



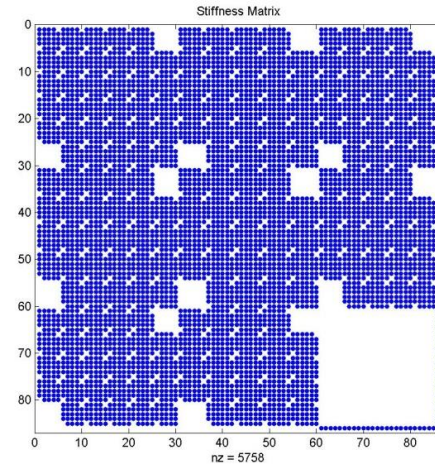
(b) Knot Span=4



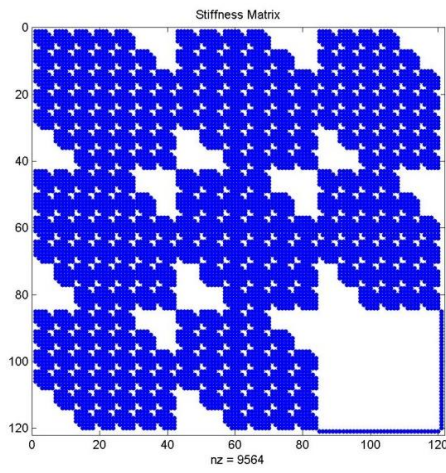
(c) Knot Span=5

Figure 6.9
Raviart Thomas stiffness matrix, Degree=2

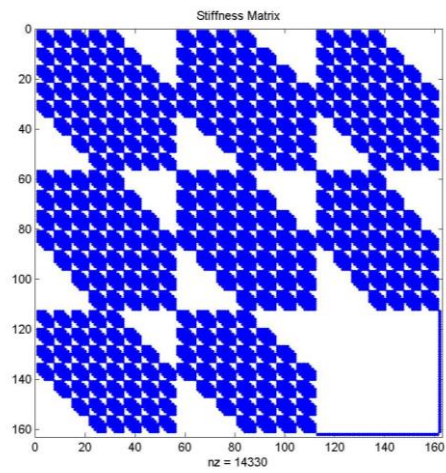
Simulation of Human Aorta and Isogeometric Fluid Analysis



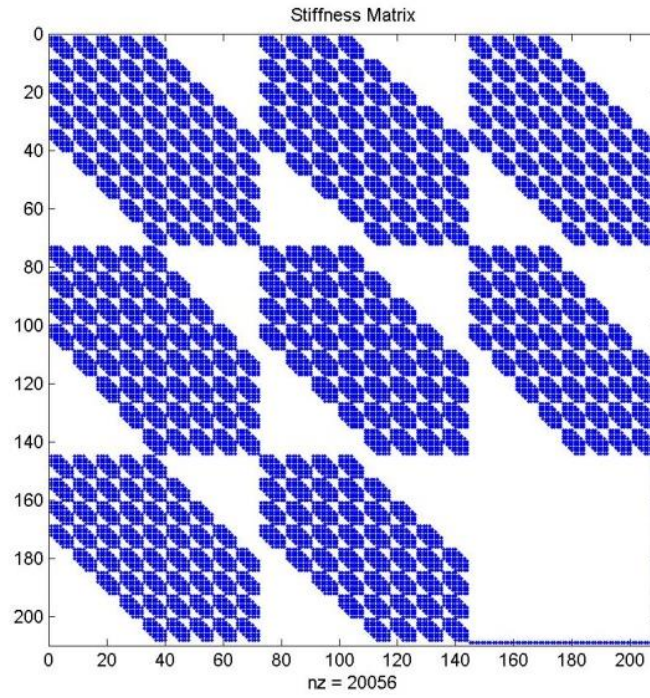
(a) Knot Span=2



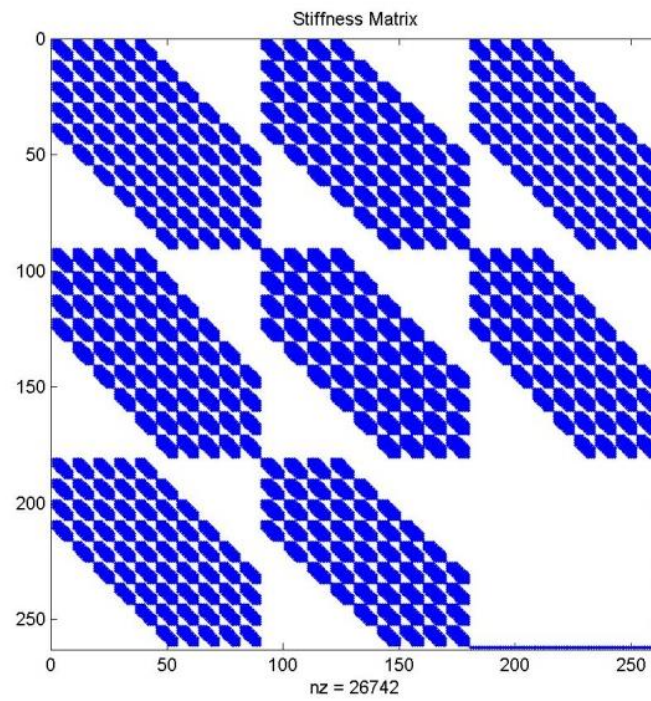
(b) Knot Span=3



(c) Knot Span=4



(d) Knot Span=5



(e) Knot Span=6

Figure 6.10
Raviart Thomas stiffness matrix, Degree=3

The following diagrams are showing the comparison of results' errors (for pressure and velocity) between the second and third degree of pressure for every element type.

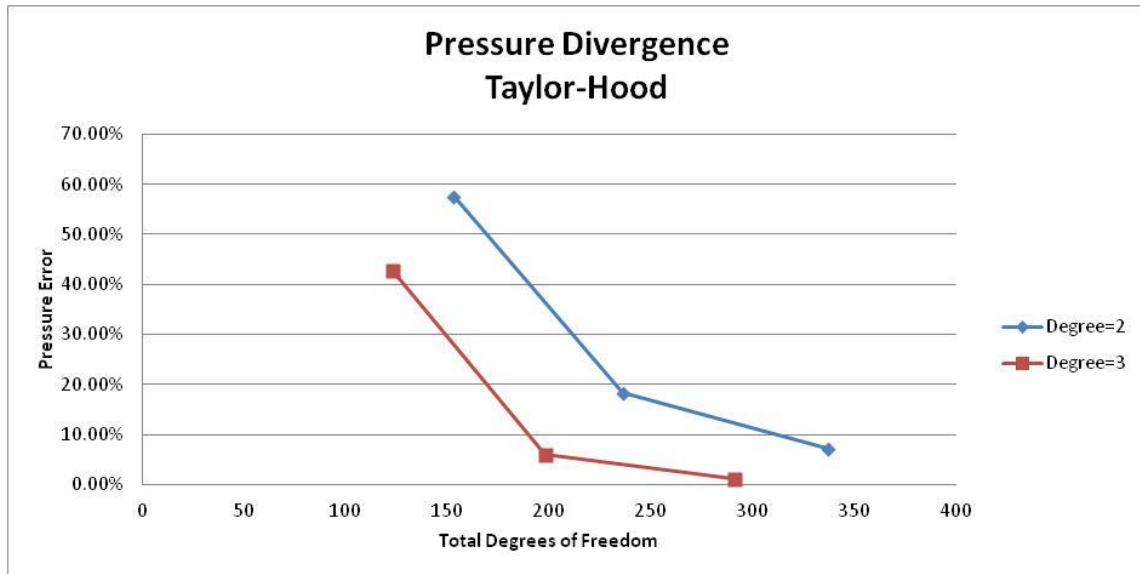


Figure 6.11
Taylor Hood pressure divergence.
Comparison of pressure error between second and third degree

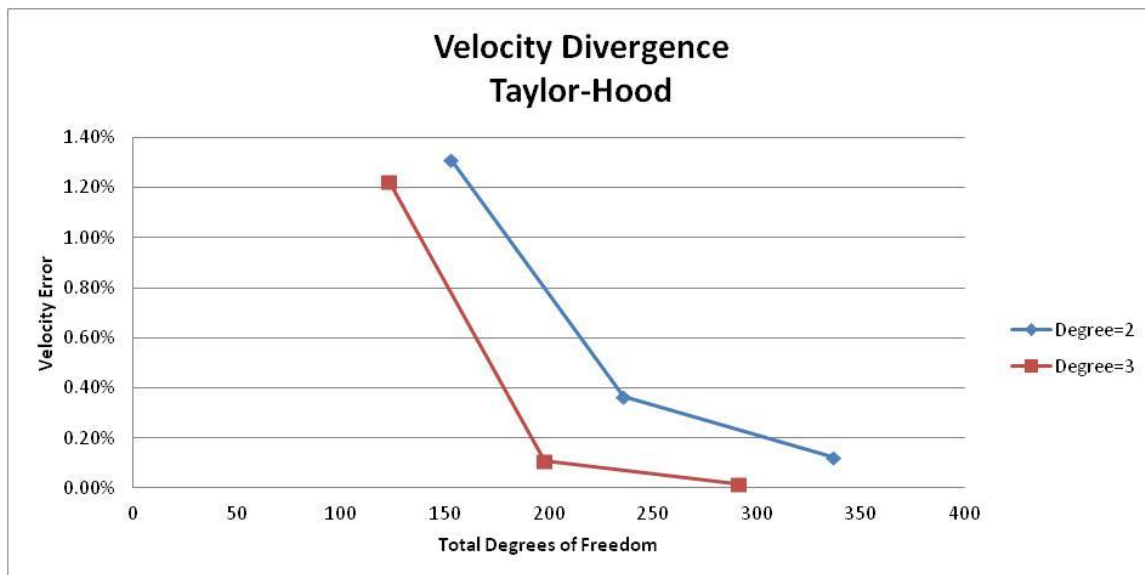


Figure 6.12
Taylor Hood velocity divergence.
Comparison of velocity error between second and third degree

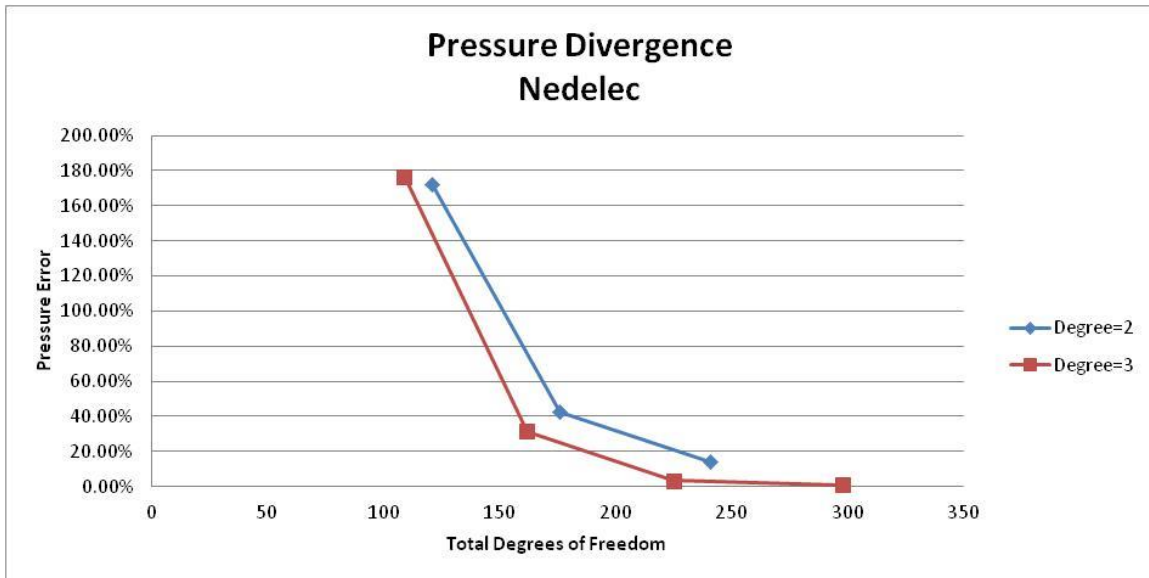


Figure 6.13
Nedelec pressure divergence.
Comparison of pressure error between second and third degree

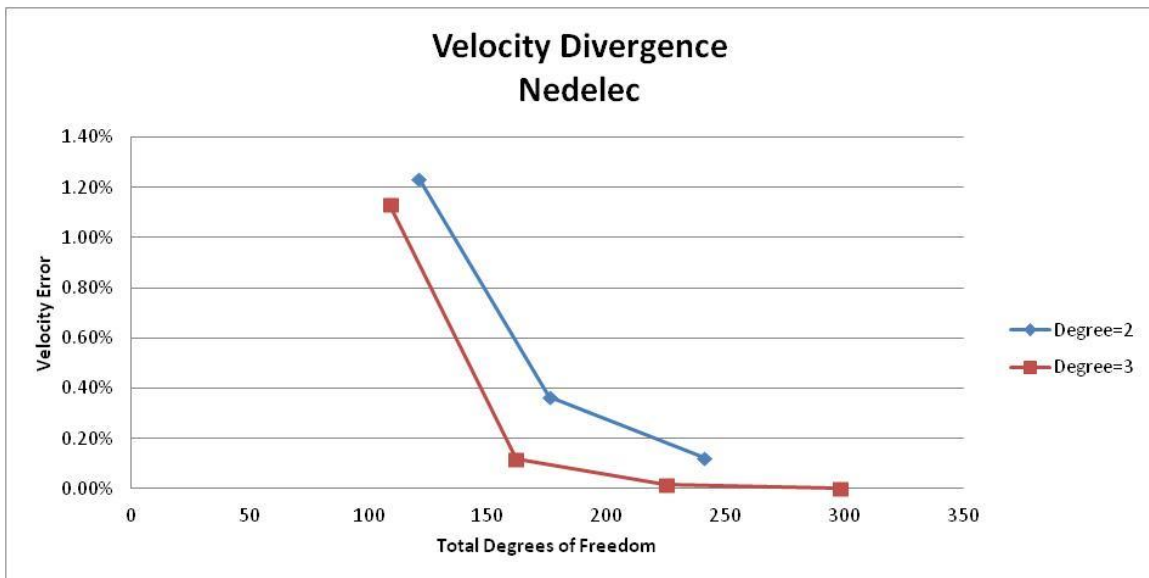


Figure 6.14
Nedelec velocity divergence.
Comparison of velocity error between second and third degree

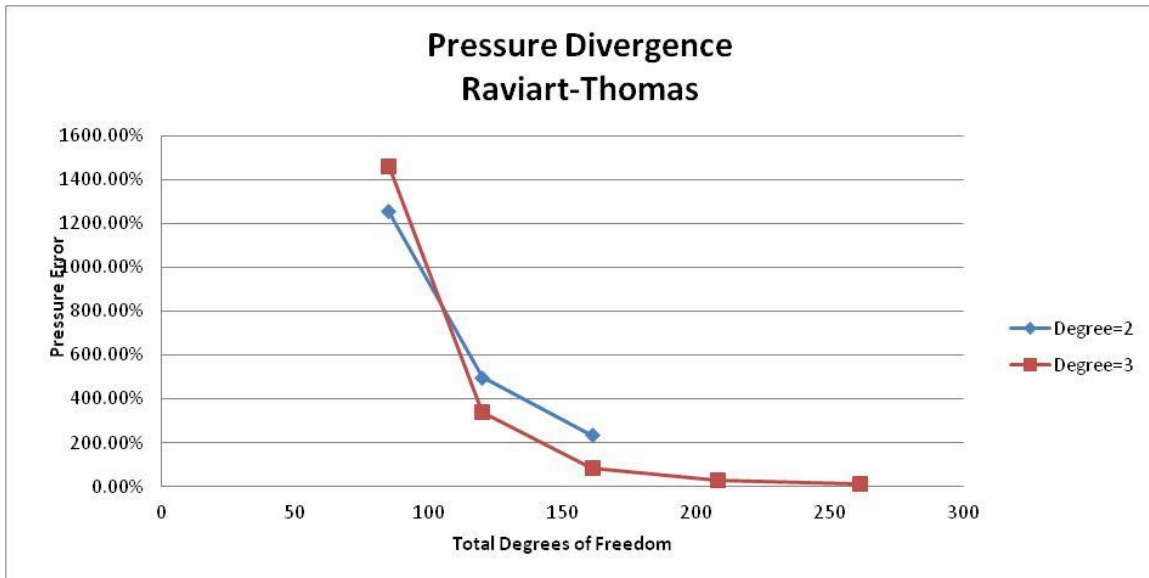


Figure 6.15
Raviart Thomas pressure divergence.
Comparison of pressure error between second and third degree

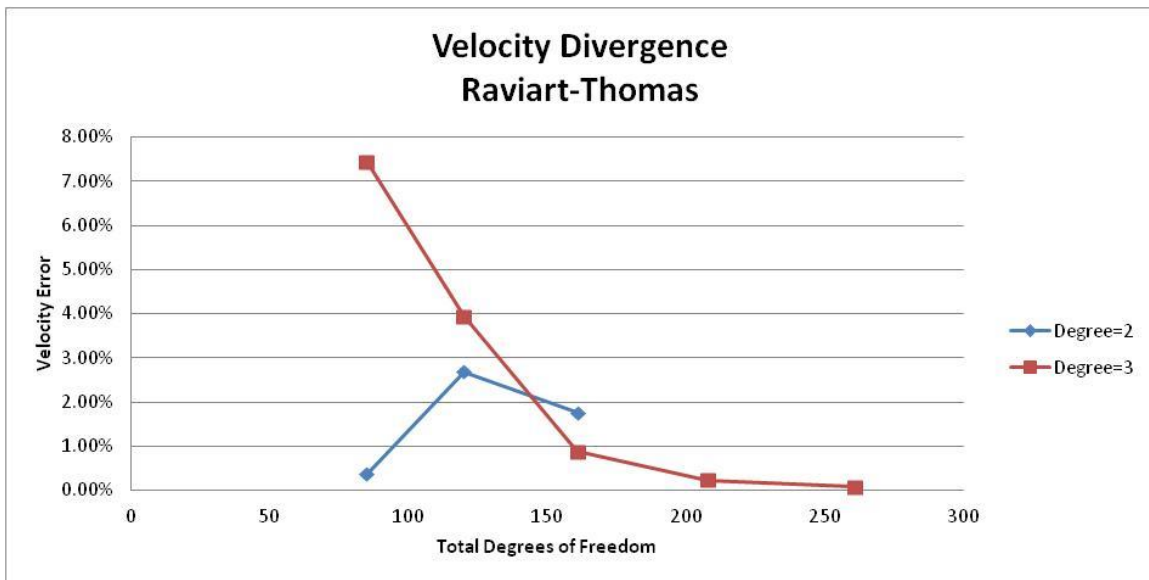


Figure 6.16
Raviart Thomas velocity divergence.
Comparison of velocity error between second and third degree

A comparison between all three element types, based on the degree was also depicted. The following diagrams are showing the results of comparison for pressure and velocity respectively.

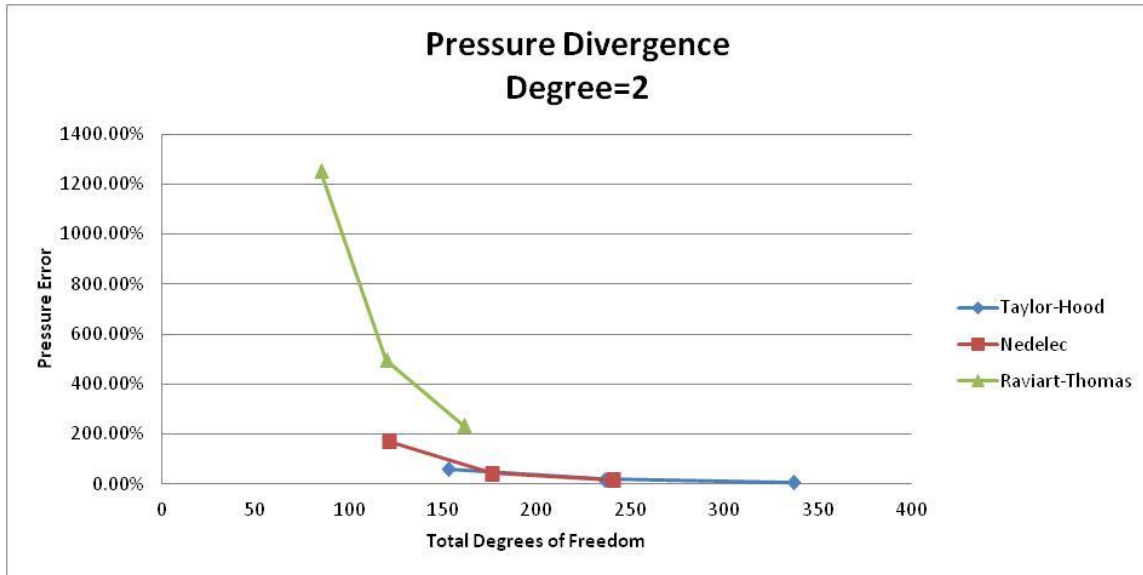


Figure 6.17
 Pressure divergence, degree=2.
 Comparison of velocity error between the three element types

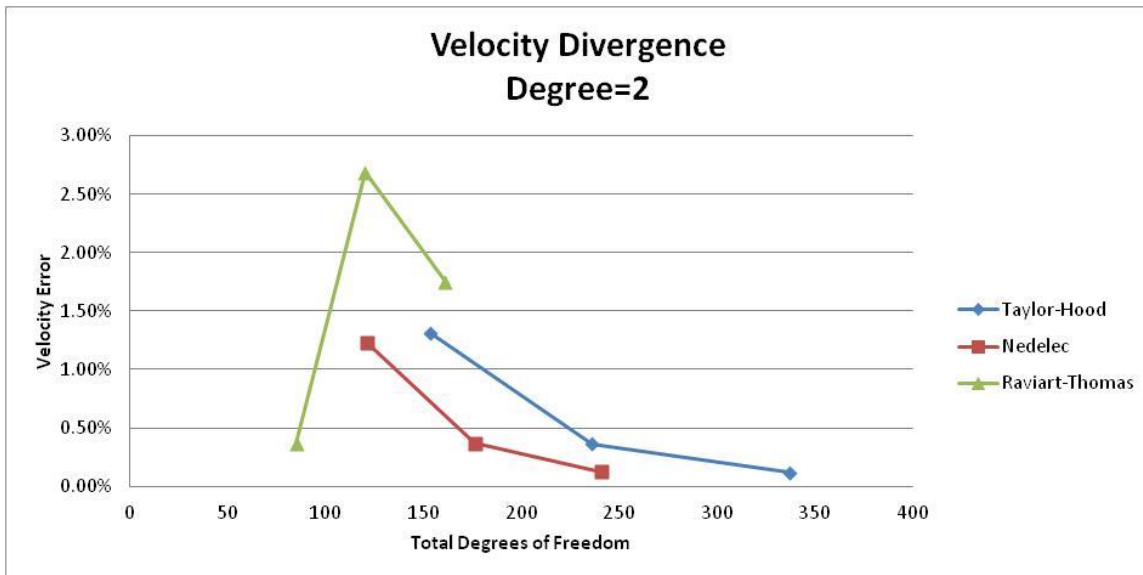


Figure 6.18
 Velocity divergence, degree=2.
 Comparison of velocity error between the three element types

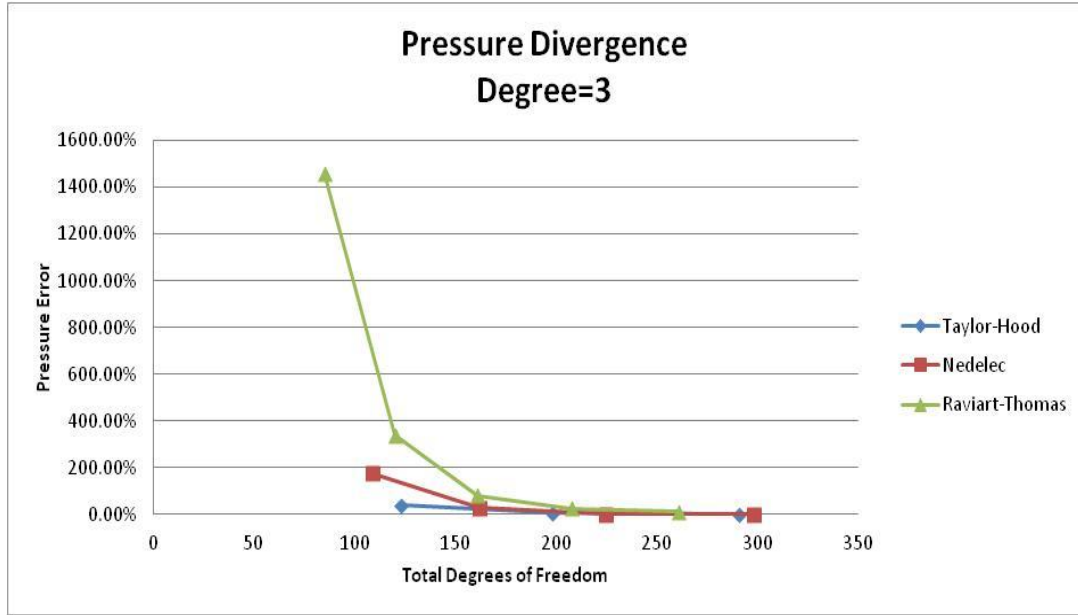


Figure 6.19
Pressure divergence, degree=3.
Comparison of velocity error between the three element types

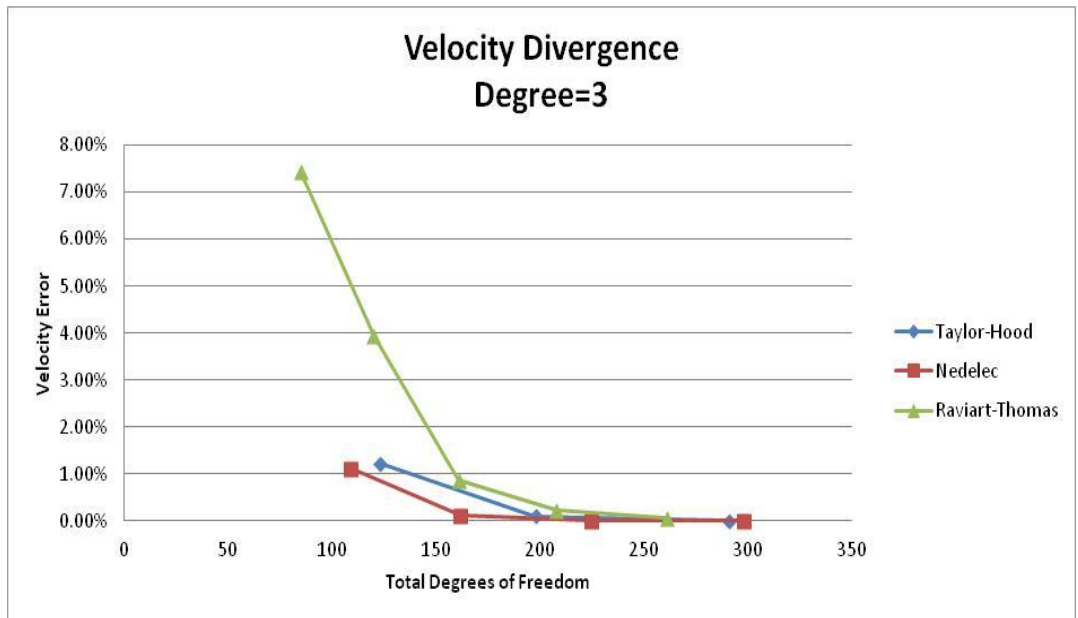
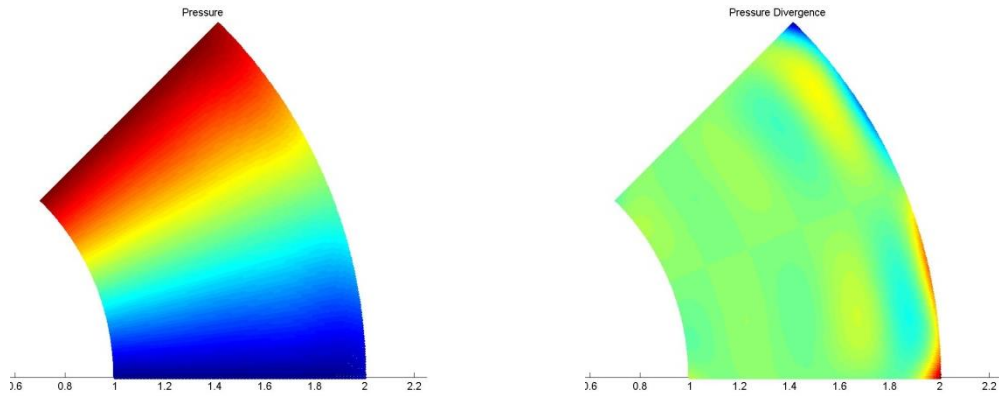
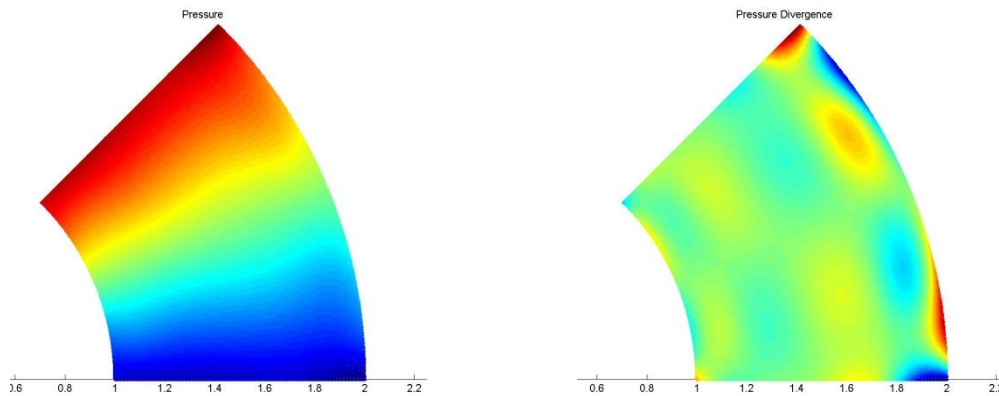


Figure 6.20
Pressure divergence, degree=3.
Comparison of velocity error between the three element types

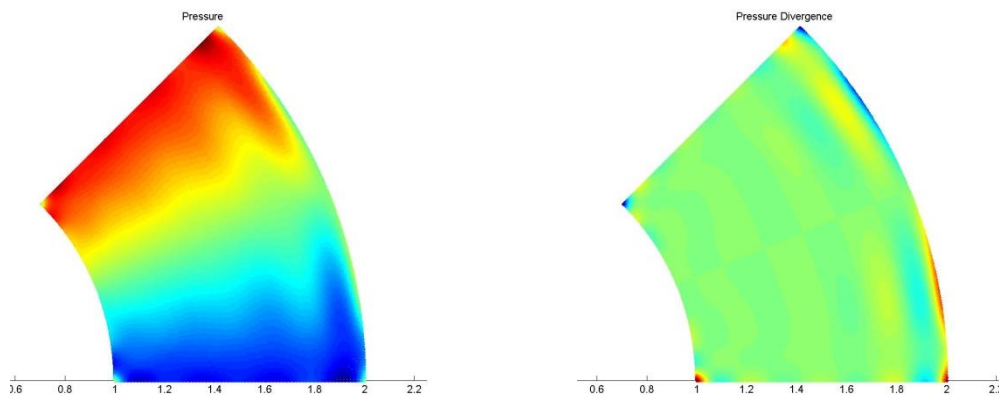
The following set of figures is showing graphically the values of pressure and their divergence from the exact solutions.



(a) Taylor Hood



(b) Nedelec

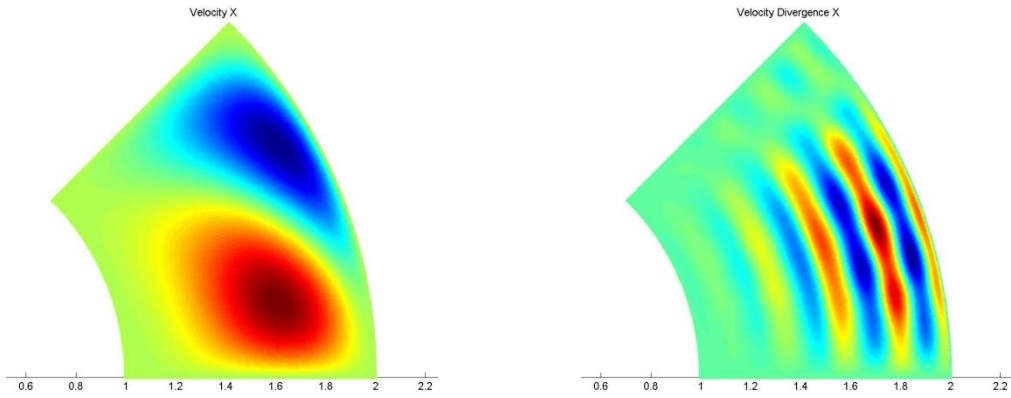


(c) Raviart Thomas

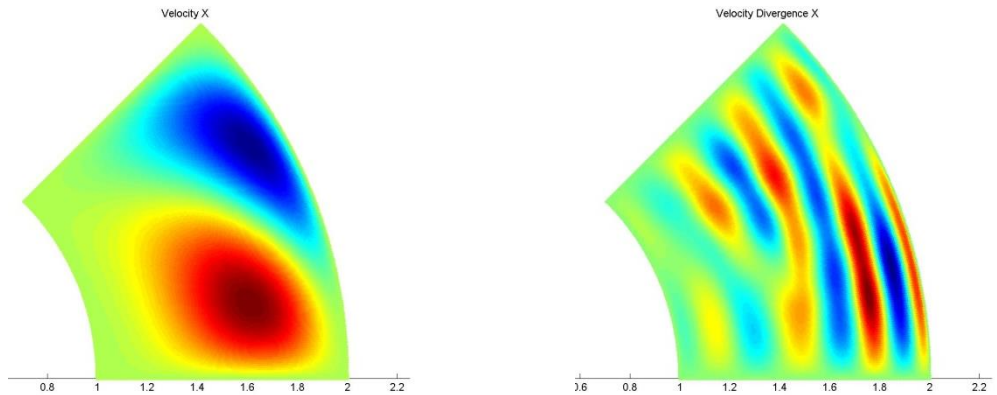
Figure 6.22

Graphical presentation of pressure values (left) and their divergence from the exact solution (right) for every element type

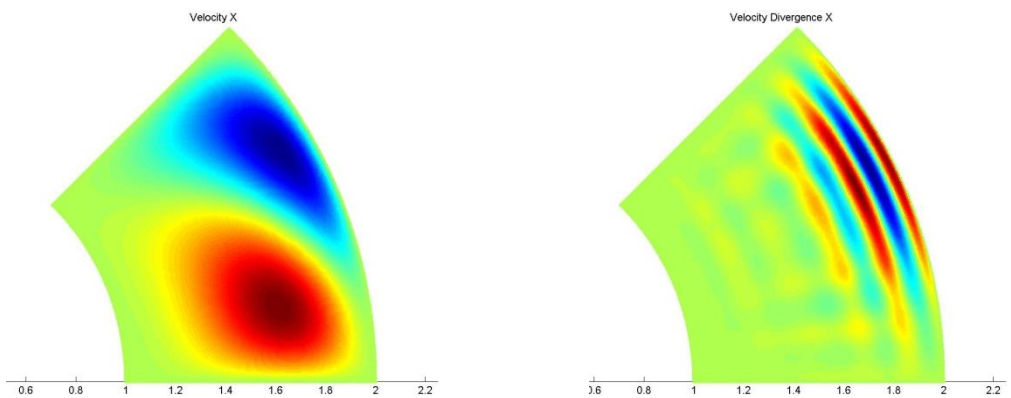
The following set of figures is showing graphically the values of velocity along the axis x and their divergence from the exact solutions.



(a) Taylor Hood



(b) Nedgelec

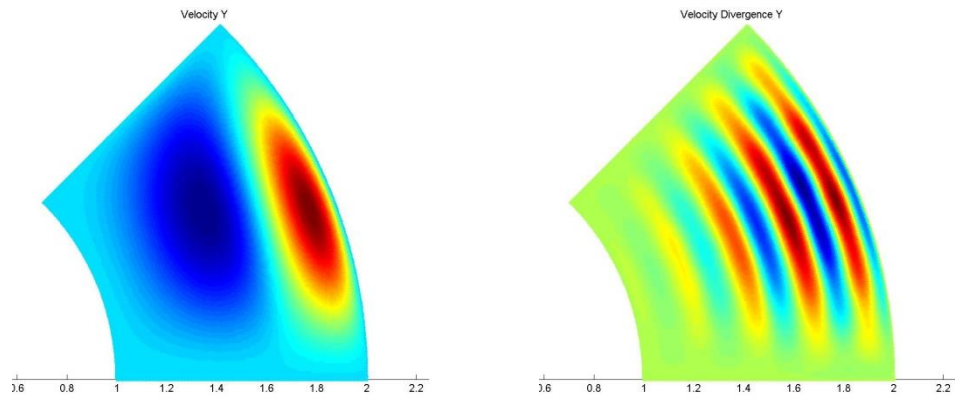


(c) Raviart Thomas

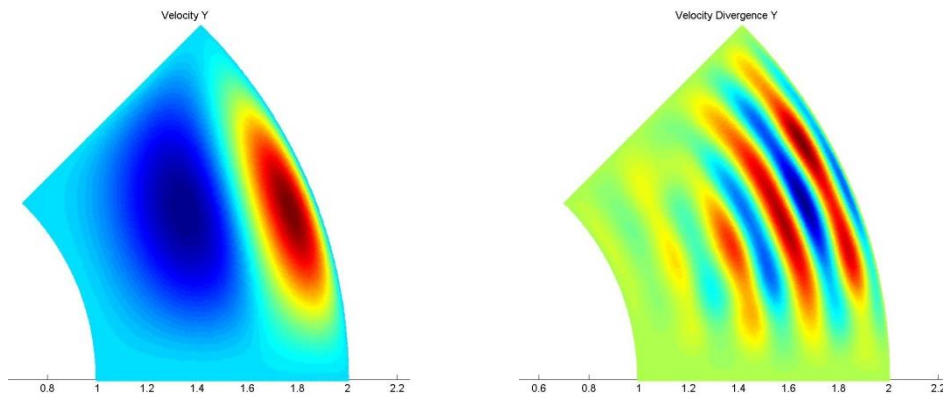
Figure 6.23

Graphical presentation of **velocity** x values (left) and their divergence from the exact solution (right) for every element type

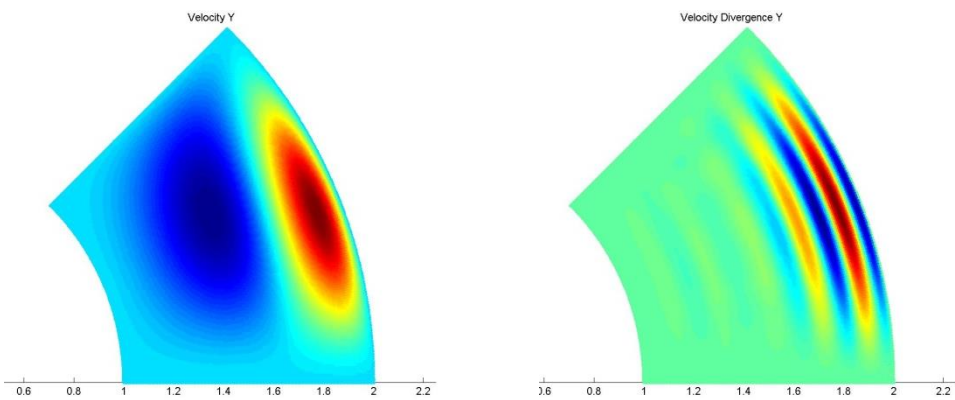
In a similar way, the next set of figures shows graphically the values of velocity along the axis y and their divergence from the exact solutions.



(a) Taylor Hood



(b) Nedelec



(c) Raviart Thomas

Figure 6.24

Graphical presentation of velocity y values (left) and their divergence from the exact solution (right) for every element type

6.2.1 Conclusions

According to the previous graphs, there is acceptable convergence even for a limited number of knot spans. Also, as expected, the lower order pressure approximation gives poorer results, while for velocity space the results were competent.

The fluid element types require different number of control points, due to the fact that every type has different continuities, even for the same number of knot spans.

Finally, from all three element types, Nedelec, with enhanced Continuity, produces the optimum results. Raviart-Thomas though is the most promising, but due to problems with boundary conditions, for the time it does not give the best results.

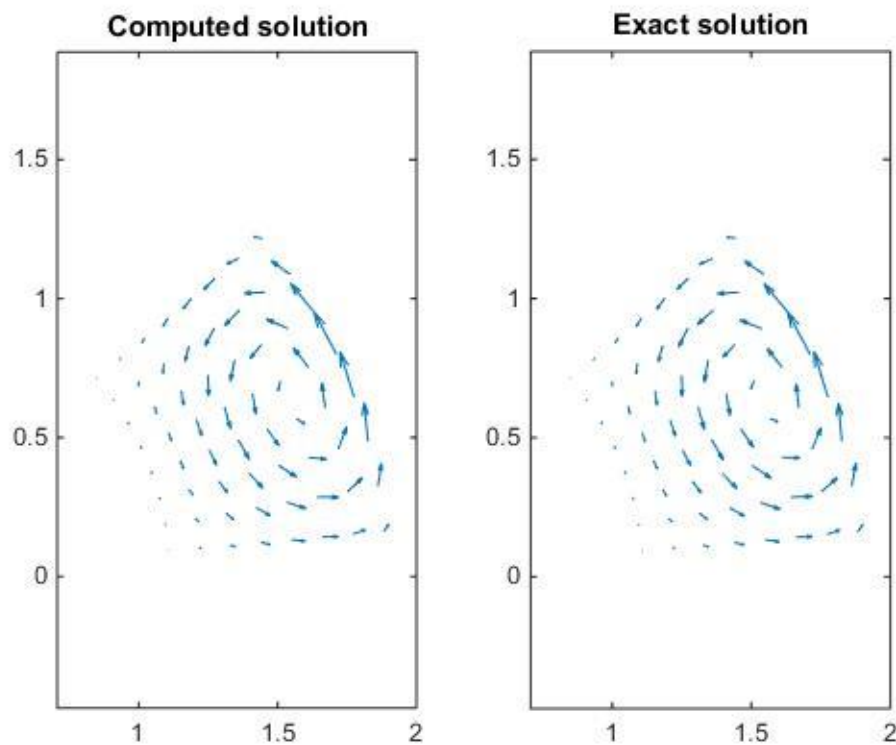


Figure 6.25

Graphical depiction of the vectors of velocity. On the left is the computed results (as given by the isogeometric software Geopdes) and the exact solution

Appendix

Point Inversion

Introduction

Definition:

Having the Cartesian coordinates of a point of the NURBS-model, we want to find the corresponding parametric coordinates of this point.

We investigate the second method that is referred in NURBS Book (page 230), as it is more simple (and equally effective). The first method depends on the solution of a (linear?) system of equations. This method uses the Newton iteration with the form:

$$\xi_{i+1} = \xi_i - \frac{f(\xi_i)}{f'(\xi_i)} = u_i - \frac{C'(\xi_i) \cdot (C(\xi_i) - X)}{C''(\xi_i) \cdot (C(\xi_i) - X) + |C'(\xi_i)|^2}$$

where:

- ξ_i : the point's parametric coordinate of iteration i
- X : the point's physical coordinate
- $C(\xi)$: the equation of the curve

At first we have to set the initial value u_0 . According to NURBS Book, the selection criteria are:

- If we know that the point is on the curve, we use the Convex Hull Property and we define the candidate spans.
- We split the candidate span in (n-1) parts using n parameter values. We calculate the Cartesian coordinates of those parameter values. Then, we calculate the distance of each parametric value in Physical Space (whose coordinate we just got) from the given point $P(X,Y,Z)$. We choose the point (parametric value) which has the minimum distance.

Actually an initial value was chosen from the corresponding Knot Value Vector.

After we apply the Newton iteration type, we have to check if the new value converges. Previously, I have set two zero tolerances (as data entry in Excel):

ε_1 : a measure of Euclidean distance

ε_2 : a zero cosine measure

We have to check the first two criteria.

1. Point Coincidence

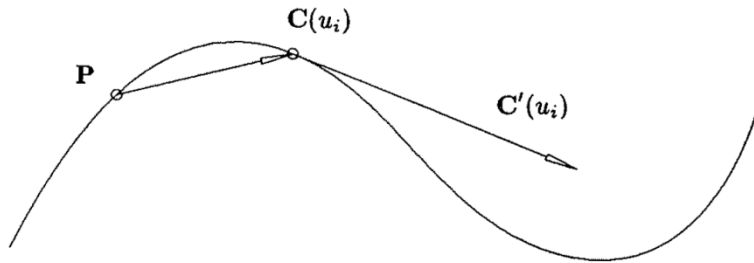
$$|C(\xi_i) - X| \leq \varepsilon_1$$

The points must be close together, that is they must almost coincide.

2. Zero Cosine

$$\frac{|C'(\xi_i) \cdot (C(\xi_i) - X)|}{|C'(\xi_i)| \cdot |C(\xi_i) - X|} \leq \varepsilon_2$$

The difference of the two points must be vertical on the direction of the derivative (see NURBS Book fig6.1b page 231)



If at least one of the two criteria is not satisfied, a new value is calculated. Otherwise, we continue.

3. The parameter stays within the range of the curve $\xi_{i+1} \in [\xi_1, \xi_{n+p+1}]$.

We consider that the curve is open.

$$\xi_{i+1} < \xi_1 \Rightarrow \xi_{i+1} = \xi_1$$

$$\xi_{i+1} > \xi_{n+p+1} \Rightarrow \xi_{i+1} = \xi_{n+p+1}$$

4. The parameter does not change significantly.

$$|(\xi_{i+1} - \xi_i) \cdot C'(\xi_i)| \leq \varepsilon_1$$

If the criteria (1), (2) or (4) are satisfied, the process is halted.

2D Application

In case of 2D

$$r(\xi, \eta) = S(\xi, \eta) - P$$

$$f(\xi, \eta) = \mathbf{r}(\xi, \eta) \cdot \mathbf{S}_\xi(\xi, \eta)$$

$$g(\xi, \eta) = \mathbf{r}(\xi, \eta) \cdot \mathbf{S}_\eta(\xi, \eta)$$

$$\delta_i = \begin{bmatrix} \Delta \xi \\ \Delta \eta \end{bmatrix} = \begin{bmatrix} \xi_{i+1} - \xi_i \\ \eta_{i+1} - \eta_i \end{bmatrix}$$

$$\mathbf{J}_i = \begin{bmatrix} f_\xi & f_\eta \\ g_\xi & g_\eta \end{bmatrix} = \begin{bmatrix} |\mathbf{S}_\xi|^2 + r \cdot S_{\xi\xi} & \mathbf{S}_\xi \cdot \mathbf{S}_\eta + r \cdot S_{\xi\eta} \\ \mathbf{S}_\xi \cdot \mathbf{S}_\eta + r \cdot S_{\eta\xi} & |\mathbf{S}_\eta|^2 + r \cdot S_{\eta\eta} \end{bmatrix}$$

$$\kappa_i = - \begin{bmatrix} f(\xi_i, \eta_i) \\ g(\xi_i, \eta_i) \end{bmatrix}$$

The system $\mathbf{J}_i \cdot \delta_i = \kappa_i$ is solved as to δ and using the next two equations the two new parametric values are determined:

$$\xi_{i+1} = \Delta \xi + \xi_i$$

$$\eta_{i+1} = \Delta \eta + \eta_i$$

The convergence criteria have to be applied, with the same process as in 1D.

1. Point Coincidence

$$|S(\xi_i, \eta_i) - P| \leq \varepsilon_1$$

2. Zero Cosine

$$\frac{|S_\xi(\xi_i, \eta_i) \cdot (S(\xi_i, \eta_i) - P)|}{|S_\xi(\xi_i, \eta_i)| |S(\xi_i, \eta_i) - P|} \leq \varepsilon_2$$

3. Two variables are defined now, one as to ξ and one as to η . The surface is considered open in the two dimensions, so this is the only case investigated.

Open as to ξ

- If ($\xi_{i+1} < a$) $\xi_{i+1} = a$
- If ($\xi_{i+1} > b$) $\xi_{i+1} = b$

Open as to η

- If ($\eta_{i+1} < c$) $\eta_{i+1} = c$
- If ($\eta_{i+1} > d$) $\eta_{i+1} = d$

4. This criterion checks that there is no significant difference between the initial parametric value and the final.

$$|(\xi_{i+1} - \xi_i)S_\xi(\xi_i, \eta_i) + (\eta_{i+1} - \eta_i)S_\eta(\xi_i, \eta_i)| \leq \varepsilon_1$$

3D Application

In case of 3D

$$r(\xi, \eta, \zeta) = S(\xi, \eta, \zeta) - P$$

$$f(\xi, \eta, \zeta) = \mathbf{r}(\xi, \eta, \zeta) \cdot \mathbf{S}_\xi(\xi, \eta, \zeta)$$

$$g(\xi, \eta, \zeta) = \mathbf{r}(\xi, \eta, \zeta) \cdot \mathbf{S}_\eta(\xi, \eta, \zeta)$$

$$h(\xi, \eta, \zeta) = \mathbf{r}(\xi, \eta, \zeta) \cdot \mathbf{S}_\zeta(\xi, \eta, \zeta)$$

$$\delta_i = \begin{bmatrix} \Delta\xi \\ \Delta\eta \\ \Delta\zeta \end{bmatrix} = \begin{bmatrix} \xi_{i+1} - \xi_i \\ \eta_{i+1} - \eta_i \\ \zeta_{i+1} - \zeta_i \end{bmatrix}$$

$$J_i = \begin{bmatrix} f_\xi & f_\eta & f_\zeta \\ g_\xi & g_\eta & g_\zeta \\ h_\xi & h_\eta & h_\zeta \end{bmatrix} = \begin{bmatrix} |S_\xi|^2 + r \cdot S_{\xi\xi} & S_\xi \cdot S_\eta + r \cdot S_{\xi\eta} & S_\xi \cdot S_\zeta + r \cdot S_{\xi\zeta} \\ S_\xi \cdot S_\eta + r \cdot S_{\eta\xi} & |S_\eta|^2 + r \cdot S_{\eta\eta} & S_\eta \cdot S_\zeta + r \cdot S_{\eta\zeta} \\ S_\xi \cdot S_\zeta + r \cdot S_{\xi\zeta} & S_\eta \cdot S_\zeta + r \cdot S_{\eta\zeta} & |S_\zeta|^2 + r \cdot S_{\zeta\zeta} \end{bmatrix}$$

$$\kappa_i = - \begin{bmatrix} f(\xi_i, \eta_i, \zeta_i) \\ g(\xi_i, \eta_i, \zeta_i) \\ h(\xi_i, \eta_i, \zeta_i) \end{bmatrix}$$

The system $\mathbf{J}_i \cdot \delta_i = \kappa_i$ is solved as to δ and using the next two equations the two new parametric values are determined:

$$\xi_{i+1} = \Delta\xi + \xi_i$$

$$\eta_{i+1} = \Delta\eta + \eta_i$$

$$\zeta_{i+1} = \Delta\zeta + \zeta_i$$

The convergence criteria have to be applied, with the same process as in the previous dimensions.

1. Point Coincidence

$$|S(\xi_i, \eta_i, \zeta_i) - P| \leq \varepsilon_1$$

2. Zero Cosine

$$\frac{|S_\xi(\xi_i, \eta_i, \zeta_i) \cdot (S(\xi_i, \eta_i, \zeta_i) - P)|}{|S_\xi(\xi_i, \eta_i, \zeta_i)| |S(\xi_i, \eta_i, \zeta_i) - P|} \leq \varepsilon_2 \qquad \frac{|S_\eta(\xi_i, \eta_i, \zeta_i) \cdot (S(\xi_i, \eta_i, \zeta_i) - P)|}{|S_\eta(\xi_i, \eta_i, \zeta_i)| |S(\xi_i, \eta_i, \zeta_i) - P|} \leq \varepsilon_2$$

$$\frac{|S_\zeta(\xi_i, \eta_i, \zeta_i) \cdot (S(\xi_i, \eta_i, \zeta_i) - P)|}{|S_\zeta(\xi_i, \eta_i, \zeta_i)| |S(\xi_i, \eta_i, \zeta_i) - P|} \leq \varepsilon_2$$

3. Three variables are defined now, one as to ξ , one as to η and one as to ζ . The surface is considered open in the three dimensions, so this is the only case investigated.

Open as to ξ

- If ($\xi_{i+1} < a$) $\xi_{i+1} = a$
- If ($\xi_{i+1} > b$) $\xi_{i+1} = b$

Open as to η

- If ($\eta_{i+1} < c$) $\eta_{i+1} = c$
- If ($\eta_{i+1} > d$) $\eta_{i+1} = d$

Open as to ζ

- If ($\zeta_{i+1} < e$) $\zeta_{i+1} = e$
- If ($\zeta_{i+1} > f$) $\zeta_{i+1} = f$

4. This criterion checks that there is no significant difference between the initial parametric value and the final.

$$|(\xi_{i+1} - \xi_i)S_\xi(\xi_i, \eta_i, \zeta_i) + (\eta_{i+1} - \eta_i)S_\eta(\xi_i, \eta_i, \zeta_i) + (\zeta_{i+1} - \zeta_i)S_\zeta(\xi_i, \eta_i, \zeta_i)| \leq \varepsilon_1$$

References

- J. A. Cottrell., T. J. R. Hughes, and Y. Bazilevs, (2009). *Isogeometric Analysis Toward Integration of CAD And FEA*, Wiley
- Y. Bazilevs, V. M. Calo, Y. Zhang and T. J. R. Hughes (2006). *Isogeometric Fluid-Structure Interaction Analysis with Applications to Arterial Blood Flow*, *Computational Mechanics* September 2006, Volume 38, Issue 4-5, pp 310-322
- J. F. Gerbeau, M. Vidrascu and P. Frey (2006). *Fluid Structure Interaction in Blood Flows on Geometries coming from Medical Imaging*, [Research Report] RR-5052, 2003
- C. de Falco et al. (2011). *GeoPDEs: A research tool for Isogeometric Analysis of PDEs*. *Adv Eng Softw*.
- G. A. Holzapfel (2004). *Computational Biomechanics of Soft Biological Tissue*, *Encyclopedia of Computational Mechanics*, Vol.2, pp. 605–635
- A. Duprey (2008). *Mechanical Properties of the Aorta*, *Annual Report to the European Society for Vascular Surgery*
- N. K. Melas (2010). *Endovascular Repair of Abdominal Aortic Aneurysms*
- A. Stamatis (2013). *Isogeometric Linear Static Analysis with NURBS*, National technical University of Athens
- D. Tsapetis (2014). *Isogeometric Static Analysis with T-SPLines*, National technical University of Athens
- T. Xing, S. Bhushan and F. Stern (2010). *Introduction to Computational Fluid Dynamics*, IHR—Hydroscience & Engineering, C. Maxwell Stanley Hydraulics Laboratory, The University of Iowa
- S. Morganti, F. Auricchio, D. Benson, F.I. Gambarin, S. Hartmann, T.J.R. Hughes, and A. Real, (2014). *Patient-specific isogeometric structural analysis of aortic valve closure*, ICES REPORT 14-10, The Institute for Computational Engineering and Sciences, The University of Texas at Austin

Y. Zhang, Y. Bazilevs, S. Goswami, C. L. Bajaj, and T. J. R. Hughes (2007). Patient-Specific Vascular NURBS Modeling for Isogeometric Analysis of Blood Flow, *Computer Methods in Applied Mechanics and Engineering*, Volume 196, Issues 29–30, pp. 2943–2959

C. Bajaj, S. Goswami, Z. Yu, Y. Zhang, Y. Bazilevs and T. J. R. Hughes (Patient Specific Heart Models from High Resolution CT

A. Buffa, C. de Falco and G. Sangalli (2002). Isogeometric Analysis new stable elements for the Stokes equation, *International Journal for Numerical Methods in Fluids*, *Int. J. Numer. Meth. Fluids* 2000;00:1–6

Y. Bazilevs, Y. Zhang, V. M. Calo, S. Goswami, C. L. Bajaj, and T. J.R. Hughes. Isogeometric Analysis of Blood Flow: a NURBS-based Approach

F. Auricchio, M. Conti, A. Ferrara, S. Morganti and A. Reali (2012). Patient-specific simulation of a stentless aortic valve implant: the impact of fibres on leaflet performance, *Computer Methods in Biomechanics and Biomedical Engineering*, DOI:10.1080/10255842.2012.681645

F. Auricchio, M. Conti, A. Ferrara, S. Morganti and A. Reali (2012). Patient-specific finite element analysis of carotid artery stenting: a focus on vessel modeling, *International Journal for Numerical Methods in Biomedical Engineering*, *Int. J. Numer. Meth. Biomed. Engng.* (2012) Published online in Wiley Online Library (wileyonlinelibrary.com). DOI: 10.1002/cnm.2511

F. Auricchio, et al. (2013). Patient-specific aortic endografting simulation: From diagnosis to prediction, *Comput. Biol. Med*

P. N. Nielsen, A. R. Gersborg, J. Gravesen and N. L. Pedersen (2011). Discretizations in IGA of Navier Stokes Flow, *Comput. Methods Appl. Mech. Engrg.* 200 3242-3253

L. Piegl, W. Tiller (1995). *The NURBS Book*, Springer

CES EduPack Database, Granta Design

D. Kuzmin. *Introduction to Computational Fluid Dynamics*, Institute of Applied Mathematics University of Dortmund

- M. Papadrakakis (2001). Analysis of Structures with the Finite Element Method, Papasotiriou
- T. J. R. Hughes, A. Realli and G. Sangalli (2008). Efficient quadrature for NURBS- based Isogeometric Analysis
- F. Auricchio, L.B. da Veiga, A. Buffa, Lovadina, A. Reali and G. Sangalli (2007). A fully “locking-free” isogeometric approach for plane linear elasticity problems
- C. de Boor (2001) A Practical Guide to Splines - - 1st Revised Edition, Springer
- P. V. Nguyen, R. N. Simpson, S. Bordas and T. Rabczuk (2012). An introduction to IGA with Matlab implementation, FEM and XFEM Formulations
- D. F. Rogers (2000). An Introduction to NURBS with Historical Perspective - The Morgan Kaufmann Series in Computer Graphics
- D. Rypl and B.Patzak (2011). Comparison of Numerical Quadrature Schemes in IGA -
- G. Farin (2001). Curves and Surfaces for CAGD, A Practical Guide - - 5th Edition 2001
- T. J. R. Hughes, A. Reali and G. Sangalli (2008). Efficient quadrature for NURBS-based IGA - Elsevier
- S. Kleiss, B. Jüttler and W. Zulehner (2011). Enhancing IGA by a FEA-based local refinement strategy
- T. J. R. Hughes, J. A. Cottrell and Y. Bazilevs (2004). Isogeometric Analysis, CAD, finite elements, NURBS, exact geometry and mesh refinement
- N. Collier, D. Pardo, L. Dalcin, M. Paszynski and J. M. Calo (2011). The cost of continuity, Performance of using direct solvers in IGA
- <http://www.medicalimaging.org>
- <http://medical.nema.org/dicom/geninfo/Brochure.pdf>
- <http://www.dicomlibrary.com/>
- <http://www.americasblood.org/about-blood/what-is-blood.aspx>

